2023

MANCOZEB EXPOSURE RESULTS IN OXIDATIVE STRESS AND DISRUPTION OF MITOCHONDRIAL COMPLEXES III & IV IN TRANSFORMED HUMAN COLON CELLS

Amanda Dhaneshwar

MANCOZEB EXPOSURE RESULTS IN OXIDATIVE STRESS AND DISRUPTION OF MITOCHONDRIAL COMPLEXES III & IV IN TRANSFORMED HUMAN COLON CELLS

A dissertation submitted in partial fulfillment
of the requirement for the degree of

DOCTOR OF PHILOSOPHY

to the faculty of the

DEPARTMENT OF PHARMACEUTICAL SCIENCES

of

COLLEGE OF PHARMACY AND HEALTH SCIENCES

at

ST. JOHN'S UNIVERISTY
New York
by
Amanda Dhaneshwar

Date Submitted: _____ Date Approved: _____

_____ _____

Amanda Dhaneshwar Diane Hardej, Ph.D.

ABSTRACT

MANCOZEB EXPOSURE RESULTS IN OXIDATIVE STRESS AND DISRUPTION OF MITOCHONDRIAL COMPLEXES III AND IV IN TRANSFORMED HUMAN COLON CELLS

Amanda Dhaneshwar

The ethylene bisdithiocarbamate pesticides, a subclass of the dithiocarbamate pesticides, are broad spectrum organometallic fungicides used on a variety of crops. The fungicide Mancozeb is comprised of an ethylene bisdithiocarbamate backbone complexed to the metals manganese and zinc. Ingestion of food containing pesticide residue and occupational exposure are common routes of Mancozeb exposure. Previous work demonstrated that Mancozeb exposure to HT-29 colon cancer cells resulted in cytotoxicity, apoptosis, and disruption of mitochondrial complex I, II, and V activity. The current study investigated the effect of Mancozeb exposure on mitochondrial complex III and IV activity and oxidative stress parameters in the HT-29 cell line. Kinetic assays were used to evaluate and compare the effect of Mancozeb exposure on the activity of complexes III and IV. Complex III showed a significant decrease in activity at 60 µM and 100 µM Mancozeb. Activity of complex IV showed significant decreases at 60 µM, 100 µM, and 140 µM Mancozeb. Further mitochondrial disruption was seen in transmission electron micrographs that showed severe mitochondrial distortions at 100 µM Mancozeb. Significant loss of mitochondrial membrane potential (60 µM, 100 µM, and 140 µM Mancozeb) measured with use of a fluorescent mitochondrial potential dye, further confirmed mitochondrial disruption and induction of apoptosis. Scanning electron

micrographs demonstrated cellular blebbing at concentrations of 80-140 μM Mancozeb. Quantification of cell blebbing from SEM micrographs revealed a significant increase in the mean percentage of blebbed cells at 100 μM Mancozeb. Oxidative stress parameters were measured to determine the role in mitochondrial dysfunction following Mancozeb exposure. Cellular reactive oxygen species, mitochondrial superoxide, and superoxide dismutase 2 levels were all significantly increased at concentrations of 100 μM and 140 μM Mancozeb. The antioxidant capacity of the cells was significantly decreased at 100 μM and 140 μM Mancozeb. Antioxidant pre-treatment and co-treatment with butylated hydroxy toluene and MitoQ failed to increase cell viability of cells exposed to 100 μM Mancozeb. The results indicate that the underlying mechanism of Mancozeb toxicity that contributes to mitochondrial dysfunction is oxidative stress in HT-29 cells.

DEDICATION

This thesis is dedicated

to the loving memory of my grandfather

whose unconditional love has kept me going.

This journey would not have been possible without you.

ACKNOWGLEDGEMENTS

My deepest and most sincere gratitude goes to my mentor, Dr. Diane Hardej, for her guidance, encouragement, and support throughout this journey. Her expertise and advice have made this dissertation possible.

I would like to extend my deepest appreciation to Dr. Louis Trombetta, who provided support, guidance, and invaluable expertise in the completion of this work.

I would like to thank the members of my committee, Dr. Cerreta, Dr. Cheng, and Dr. Mantell, who have generously given their time and expertise to better my work.

Special thanks to my lab mates, Lisa, Puneet, Ben, Jeff, and Saif for their friendship, advice, and encouragement throughout this process.

I would also like to thank my friends in the Graduate Program for their encouragement and support.

Thank you to the PHS department for all their support.

I would like to thank my parents for always supporting me in my academic career. I would also like to thank my brother, aunt, and grandma for always being there for me.

Finally, I would like to thank my fiancé Alex for his unwavering patience, support, and understanding. He has shared the ups and downs of my research and guided me through them. I would not have made it this far without your love and encouragement.

TABLE OF CONTENTS

LIST OF TABLES

LIST OF FIGURES

1. INTRODUCTION

1.1 Ethylene Bisdithiocarbamate Pesticides

Pesticide toxicity studies are important due to the widespread use of pesticides on a global scale. Pesticides are used in agriculture to reduce or eliminate crop loss and maintain high product quality by preventing or controlling pests, disease, weeds, or other plant pathogens. Substances such as herbicides, insecticides, fumigants, and fungicides are pesticides. According to the Environmental Protection Agency's Pesticide Industry Sales and Usage (2008-2012), in both 2011 and 2012 the worldwide annual pesticide usage was nearly 6 billion pounds and over 1.1 billion pounds in the United States (Atwood and Paisley-Jones, 2017). Ideally, pesticides should be highly specific for the target organism and innocuous to non-target organisms. However, the lack of specificity presents a risk to non-target organisms such as humans, beneficial organisms, and the environment. Occupational workers and the general population are both exposed to pesticides. Individuals can be exposed to pesticides occupationally through the production, application, and spreading of these agents. Non-occupational exposure can occur in individuals of the general population through domestic use, run-off from farms and fields, and consumption of contaminated food and water. The widespread use of pesticides and effects on non-target organisms makes the effects of pesticides on human health a great concern (Roede and Miller, 2014; Maroni et al., 2000; Damalas and Eleftherohorinos, 2011).

In agriculture, dithiocarbamate (DTC) pesticides are used mainly as fungicides and insecticides and to a lesser extent herbicides (Maroni et al., 2000). Since the 1940s, dithiocarbamate fungicides have been used to control several hundred fungal pathogens on a variety of crops. Generally, most fungicides are applied to plants or crops prior to

infection by fungal spores. However, other fungicides can be used therapeutically to cure plants after an infestation has occurred (Costa and Aschner, 2014). The DTCs are a class of organosulfur fungicides, which can be classified according to their chemical structure in various groups including: thiurams, methyldithiocarbamates, dimethyldithiocarbamates, diethyldithiocarbamates, ethylene bisdithiocarbamates, and propylene bisdithiocarbamates (Janz, 2014; Maroni et al., 2000).

The ethylene bisdithiocarbamates have a metal atom coordinated with the ethylene bisdithiocarbamate (EBDC) backbone. These organometallic fungicides, promote fungicide resistance by inactivating the sulfhydryl groups of amino acids in enzymes found in fungal cells resulting in disruption of lipid metabolism, respiration, and ATP production. Furthermore, they can act as chelating agents allowing them to interfere with enzymes that contain metals essential for activity. Maneb, Zineb, and Mancozeb are all members of the EBDC fungicides and have an ethylene bisdithiocarbamate backbone complexed with different transition metals associated with the individual compounds. Maneb is complexed with the metal manganese (Figure 1) and Zineb is complexed to the metal zinc (Figure 2). Mancozeb (MZ) is a combination of Maneb and Zineb and is complexed with both manganese and zinc in a 9:1 ratio of manganese to zinc (Figure 3) (Costa and Aschner, 2014; Janz, 2014; Roede and Miller, 2014).

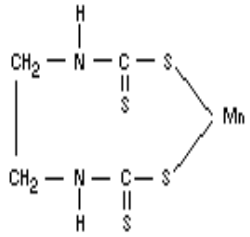

Figure 1: The chemical structure of Maneb.

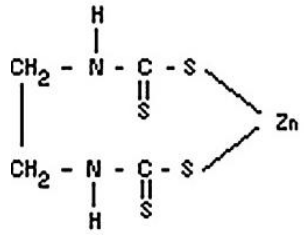

Figure 2: The chemical structure of Zineb.

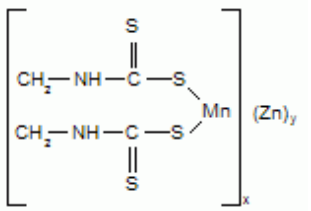

Figure 3: The chemical structure of Mancozeb.

1.2 Mancozeb

Mancozeb was first registered in the United States in 1948 as a broad-spectrum fungicide for use in agriculture, professional turf management, and horticulture. Furthermore, Mancozeb is registered for use in both home gardens and residential turf. Mancozeb is used on a wide variety of food and crops including grapes, onions, pears, tomatoes, squash, and melons. However, it is used in greatest amount on potatoes and apples (Environmental Protection Agency, 2005). According to the United States Geological Survey, an estimated 7 million pounds of Mancozeb was used in 2018 mainly on fruit and vegetable crop (United States Geological Survey, 2021). Although Mancozeb is widely used, there has been no reported environmental levels in water or soil (Roede and Miller, 2014). The EPA (Environmental Protection Agency) states that the acceptable daily intake (ADI) for Mancozeb is 0.029 mg/kg/day for oral exposure (Environmental Protection Agency, 2005; Maroni et al., 2000). Other exposure standards and guidelines

for Mancozeb include a value of 5mg/m^3 from the United States Occupational Safety and Health Administration (OSHA) (Roede and Miller, 2014).

The wide global use of EBDCs, such as Mancozeb is due to their good follicular protection, low environmental persistence, and presumed low acute toxicity in humans (Environmental Protection Agency, 2005; Roede and Miller, 2014). However, due to the possible health risks associated with Mancozeb, many global agencies have reviewed it for reregistration of use. In 2020, the European Union (EU) banned the use of Mancozeb while citing it as a potential endocrine disruptor. India, the world's largest producer of Mancozeb, drafted a notification in 2020 stating that it is presently reviewing the compound to ban its manufacture, sale, and import. Mancozeb was approved for reregistration for use in Canada in 2020 and will undergo reregistration for use in the United States by the EPA in 2023 (Saha et al., 2022).

1.3 Mancozeb Toxicity

Mancozeb is a known endocrine disruptor and toxic to reproduction as the primary target organ for repeated Mancozeb exposure is the thyroid gland (Roede and Miller, 2014; Maranghi et al., 2013). The thyroid is an important regulator of metabolic activities in addition to endocrine mechanisms pertaining to reproduction (Pandey and Mohanty, 2015). The DTCs are purported to have low acute human toxicity following exposure via the dermal, oral, and respiratory routes (Costa and Aschner, 2014; Environmental Protection Agency, 2005). DTCs are mainly metabolized to carbon disulfide (CS_2) and measurement of urine levels for this metabolite is used as a biomarker for high-level DTC exposure. CS_2 can be further metabolized to thiourea, which is an antithyroid substance. Both CS_2 and the metabolite ethylene thiourea (ETU) can be used

as biomarkers for EBDC exposure. ETU is a metabolite of EBDC biotransformation in mammals, but EBDC in residues in food may be partly transformed to ETU during the cooking process of contaminated food. ETU is a probable human carcinogen and potent teratogen. ETU is metabolized to ethylene urea with the release of atomic sulfur (Janz, 2014; Maranghi et al., 2013; Maroni et al., 2000). Mancozeb exposure has been demonstrated to disrupt the pituitary-thyroid axis of the wildlife bird, Red Munia (*Amandava amandava)*, through alteration of plasma levels of T3, T4, and TSH (Pandey and Mohanty, 2015). Additionally, rat dams exposed to Mancozeb exhibited thyroid hormone disruption (Axelstad et al., 2014). Ksheerasagar and Kaliwal (2003) demonstrated that the testes and accessory reproductive organs in male albino mice were affected by Mancozeb exposure. Mancozeb toxicity has also been documented in female reproductive organs causing damage to ovarian structure and impairment of embryo implantation (Akthar et al., 2020; Baligar and Kaliwal, 2001; Bao et al., 2022; Bindali and Kaliwal, 2002).

Occupational workers have the highest risk of Mancozeb exposure and adverse effects. Biological indicators of occupational exposure to Mancozeb include measuring urinary concentrations of CS_2, ETU, and manganese (Costa and Aschner, 2014; Dallagnol et al., 2021; Maroni et al., 2000). Workers exposed to Mancozeb have been reported to have increased urinary excretion of manganese and ETU, hemoglobin-ETU adducts, and altered thyroid function (Canossa et al., 1993; Colosio et al., 1996; Gowers and Gordon, 1980; Kurttio and Savolainen, 1990). Additionally, immunomodulatory effects, specifically an increase in T-cell function and inhibition of NF-κB activation, in agriculture workers that handle Mancozeb have also been reported (Corsini et al., 2005).

Mancozeb exposure has also been documented to be strongly associated with both an increased incidence of thyroid disease in female spouses of pesticide applicators and neural tube defects in newborns of farmers (Goldner et al., 2010; Norby et al., 2005).

Studies have also shown that Mancozeb can affect other organ systems. Mancozeb has been documented to elevate serum levels of alanine amino transferase (ALT), aspartate amino transferase (AST), and alkaline phosphatase activities and exacerbate fatty acid-induced steatosis in the liver. In addition, decreased liver and kidney weight and altered protein, lipid, glycogen, metal homeostasis, and status of the glutathione system in the liver and kidney have been reported (Kistinger and Hardej, 2022; Ksheerasagar and Kaliwal, 2003; Pirozzi et al., 2016; Saber et al., 2019; Sakr, 2007). Neurotoxic effects of Mancozeb include cytotoxicity and accumulation of manganese in astrocytes, toxic effects to both dopaminergic and GABAergic neurons, and neurochemical and morphological alterations to the hypothalamus (Domico et al., 2006, 2007; Morales-Ovalles et al., 2018; Tsang and Trombetta, 2007). The gastrointestinal (GI) tract is of particular importance when evaluating the toxicity of Mancozeb exposure as ingestion is a common route of exposure.

Inhalation and dermal exposure are the primary routes of Mancozeb exposure. However, ingestion can cause Mancozeb to be absorbed via the gastrointestinal tract of not only the workers, but also the general population that consumes food that has been treated with the compound. Various studies have revealed that the residues from pesticides can still reach the consumer and be ingested. Detectable levels of CS_2 (≥ 0.10 mg/kg) were found on produce collected in Federal District, Brazil, however, the levels were under the ADI (Caldas et al., 2004). A study conducted on several fresh fruit and

vegetables, including apples, wine grapes, lettuce, peppers, tomatoes, and strawberries, collected from small and large food chains in Galicia, Spain found DTC residues in all products except strawberries. The main contributors to the total pesticide load of the DTC residue were EBDCs. Furthermore, it was found that DTC residue concentrations in 6% of the samples exceeded the Maximum Residue Limit (MRL), specifically lettuce and pepper samples (López-Fernández et al., 2012). Furthermore, a study conducted in five selected districts of Central Uganda tested tomatoes from markets and farms for Mancozeb residue. Mancozeb residue was detected in all samples that were analyzed and there was a higher concentration in farm samples than market samples (Kaye et al., 2015). Although pesticide residue has been documented on produce in various studies, the residues are influenced by processing or household preparation such as storage, washing, peeling, and cooking (Naman et al., 2022).

Previous studies in our laboratory have investigated the mechanisms of toxicity of EBDC pesticides on the gastrointestinal tract. The work of Hoffman and Hardej (2012) showed that Mancozeb exposure caused increased lipid peroxidation, decreased ratio of reduced glutathione to glutathione disulfide, and increased caspase 3/7, 8, & 9 activity in both transformed and non-transformed human colon cells. Further investigation revealed in a later study, both the backbone and metal moiety of ethylene bisdithiocarbamate pesticides contribute to their toxicity. ICP-OES data demonstrated that exposure to Mancozeb caused a significant accumulation of manganese, zinc, and copper within cells. This suggests that the common organic backbone of ethylene bisdithiocarbamates can complex with copper facilitating its accumulation within the cell. This increase in metal

concentrations, within the cell, alters metal homeostasis leading to oxidative insult (Hoffman et al., 2016).

Various studies have established Mancozeb as a mitochondrial toxicant causing oxidative stress leading to mitochondrial dysfunction (Bailey et al., 2016; Domico et al., 2006, 2007; Iorio et al., 2015; Kumar et al., 2019; Todt et al., 2016). Mancozeb may be able to compromise the mitochondria and potentially lead to apoptosis by reacting with the sulfhydryl groups of mitochondrial complex enzymes. Previous work has shown that Mancozeb inhibits the activity of mitochondrial complexes I, II, and V leading to apoptosis in transformed human colon cells.

1.4 Mitochondria

Mitochondria are cellular organelles that are responsible for the production of energy. Mitochondria generate energy for the cell through a process called oxidative phosphorylation, which involves the synthesis of ATP (adenosine triphosphate) from ADP (adenosine diphosphate) and inorganic phosphate. In addition, mitochondria play a role in metabolic cell signaling pathways, regulation of cellular morphology, mobility, multiplication, and apoptosis (Wallace and Starkov, 2000). Mitochondria are also able to function when they are isolated from the cell. Isolated mitochondria maintain their membrane composition, organization, membrane potential, ability to fuse and import proteins, and are still competent for respiration and ATP synthase (Kühlbrandt, 2015).

It is believed that mitochondria are derived from bacteria that were engulfed by primitive eukaryotes 1.6 billion years ago. The possession of mitochondria and a cell wall are significant differences between prokaryotes and eukaryotes. Mitochondria, also, have their own genetic system, that uses a distinct DNA code that differs from both their

eukaryotic hosts and bacterial ancestors (Kühlbrandt, 2015; Perkins and Frey, 2000). Each human cell, except mature erythrocytes, contains between 5 and 2,000 mitochondria, with the size and shape depending on the cell type. They can be spherical with a diameter of 0.5-5 μm or cylindrical with a diameter of at least 0.2 μm and up to 20 μm long. Furthermore, mitochondria can be branched and exhibit specialized shapes such as annuli, discs, or cup shapes. These shapes may enhance the exchange of metabolites between mitochondria and the cytosol by increasing the surface area to volume ratio (Perkins and Frey, 2000; Wallace and Starkov, 2000). Mitochondrial consumption of oxygen and production of ATP differ greatly in different tissue types. For example, heart mitochondria have a high-energy demand due to continuous pumping of blood. As a result, they consume 50 times the oxygen of liver mitochondria, which are specialized to detoxify ammonia. Mitochondria in various tissues also utilize different fuels. Heart mitochondria meet their energy needs using fatty acids, while liver mitochondria are dependent on sugars and fats (Perkins and Frey, 2000).

All mitochondria are bound by two lipid bilayer membranes. The outer mitochondrial membrane encloses the organelle and separates it from the cytoplasm. Additionally, the outer membrane is rich in cholesterol and permeable to small molecules and ions up to 14 kDa. These molecules travel through porins, which are pore-forming membrane proteins. Proteins and larger molecules are imported by special translocases. There is no membrane potential across the outer membrane because of its porosity. Furthermore, the outer membrane surrounds the inner membrane, which separates the intermembrane space from the matrix. The intermembrane space is a gap, approximately 20 nm, between the outer and inner membrane. The inner membrane consists of

invaginations called cristae, which increases the membrane surface area within the same volume. The cristae extend deeply into the matrix which is enclosed by the inner membrane. The matrix, a water-containing compartment, is the site of mitochondrial DNA replication, transcription, protein biosynthesis, and numerous enzymatic reactions. The matrix has a negative charge and a slightly alkaline pH ~ 8 compared to the intermembrane space with has a pH ~ 6.9. These characteristics of the matrix are due to the protons pumped across the inner membrane, associated with oxidative phosphorylation. Compared to the outer membrane, the inner membrane is a tight diffusion barrier as it is impermeable to protons while small molecules have specific transporters. An electrochemical membrane potential, of about 180 mV (interior negative), builds up across the inner membrane due to its ion selectivity. The complex enzymes involved in the electron transport chain (ETC) are located on the inner membrane and oxidative phosphorylation occurs here. The electrochemical gradient across the inner membrane is created by the complex enzymes, which use it for ATP synthesis. The inner membrane is the most common target for mitochondrial toxicants. Mitochondria may be damaged by foreign chemicals that either increase the permeability of the inner membrane or inhibit the transport proteins that are embedded within it. In addition, the inner membrane contains large amounts of cardiolipin and virtually no cholesterol. Many drugs have a high affinity for cardiolipin and thus they bind to and concentrate in the inner mitochondrial membrane (Kühlbrandt, 2015; Meyer et al., 2013; Navarro and Boveris, 2007; Wallace and Starkov, 2000).

Oxidative phosphorylation is the metabolic pathway that takes place on the inner mitochondrial membrane and uses enzymes to oxidize nutrients and release energy to

form ATP. Over ninety percent of cellular energy is produced by oxidative phosphorylation. There are five membrane bound enzyme complexes that are involved in electron transfer, proton pumping, generation of an electrochemical proton gradient across the inner membrane, and formation of ATP. Electrons are transferred from electron donors to electron acceptors and finally to oxygen, the final electron acceptor, during this process. Energy is released through the passage of electrons between donors and acceptors and the energy is used to generate a proton gradient by pumping protons into the intermembrane space. The proton gradient is largely responsible for the mitochondrial membrane potential. The ETC is comprised of complex enzymes I-IV, which are electron transfer or respiratory complexes that catalyze electron transfer via redox reactions. Complex I, III, and IV, function as proton pumps, creating a proton gradient. This proton gradient creates potential energy. The protons flow back across the membrane and down the gradient through complex V (ATP synthase) which generates ATP (Navarro and Boveris, 2007). Figure 4 shows the process of oxidative phosphorylation, with the solid black arrows showing proton movement across the membrane and the dashed black arrows showing the flow of electrons along the respiratory chain.

Figure 4: Model of Oxidative Phosphorylation.

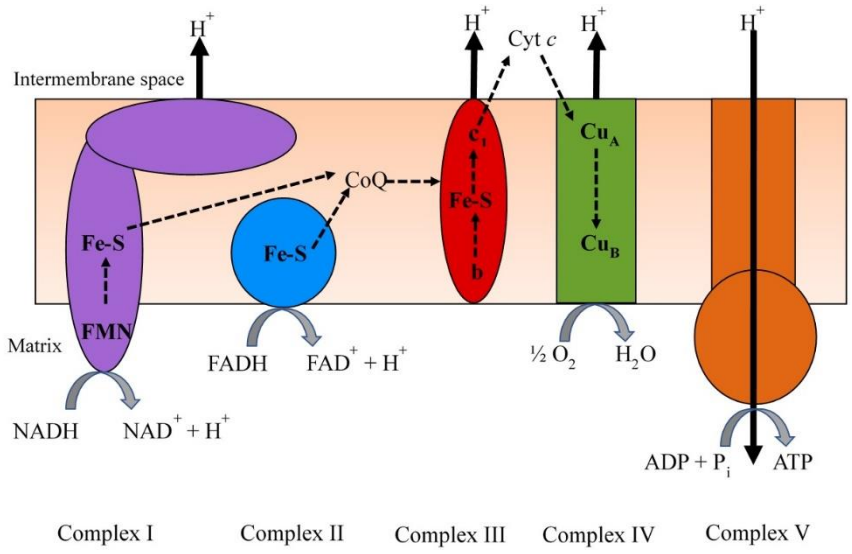

Drawn based on Shoubridge, 2001.

The pathway of oxidative phosphorylation starts at complex I (NADH-ubiquinone oxidoreductase; NADH dehydrogenase), which is composed of 42-43 different polypeptides, which include a FMN-containing flavoprotein. The L-shaped complex has 6 iron-sulfur centers, which catalyze electron transfer. The long arm is a hydrophobic integral membrane protein and the short, hydrophilic arm extends into the matrix and contains the FMN and NADH active center. NADH can donate a pair of electrons along with protons to this complex. The complex releases the protons into the intermembrane space and transfers its electrons to ubiquinone (Coenzyme Q) resulting in the formation of the fully reduced species ubiquinol (Kühlbrandt, 2015; Navarro and Boveris, 2007).

Complex II (succinate dehydrogenase; succinate-ubiquinone reductase) is part of both the ETC and Krebs cycle. Unlike the other four complexes of the ETC it does not act as a proton pump. Additionally, complex II is composed of a covalently bound FAD and iron-sulfur center that catalyzes the electron transfer to ubiquinone (Coenzyme Q).

During oxidative phosphorylation, electrons from succinate enter complex II and leave as ubiquinol. Ubiquinone (Coenzyme Q) can be thought of as the electron collector of complex I and complex II. The ability of Coenzyme Q to act as an electron carrier allows it to act as a free-radical scavenging antioxidant (Kühlbrandt, 2015; Navarro and Boveris, 2007).

Ubiquinol donates its electrons to complex III (cytochrome bc_1 complex; ubiquinol-cytochrome *c* oxidoreductase) and releases protons from the matrix to the intermembrane space, further contributing to the proton gradient. This complex is composed of 9-10 polypeptides, of which 3 are associated with redox centers (b_{562}, b_{566}, c_1 hemes, and an iron sulfur cluster). Half of the electrons donated to complex III reduces cytochrome *c*, which moves freely in the intermembrane space to transfer electrons from complex III to complex IV. The other half moves through the Q cycle, which is involved in the formation of the proton gradient (Navarro and Boveris, 2007).

Complex IV (cytochrome *c* oxidase, cytochrome oxidase; cytochrome *c*-O_2 oxidoreductase) acts as the final catalyst of the electron transport chain. Unlike the previous complexes which have iron-sulfur centers, complex IV has two copper centers (Cu_A and Cu_B). Electrons that enter complex IV react with oxygen to form water. Complex IV dysfunction is common in both aging and neurological diseases. The inhibition of complex III or complex IV blocks all mitochondrial energy production (Navarro and Boveris, 2007; Wallace and Starkov, 2000).

Complex V (F_1F_oATP synthase) catalyzes the movement of protons down the gradient and has an active site for the synthesis of ATP. The F_1 (factor one) portion of the complex binds to adenine nucleotides and is responsible for ATP synthesis and the F_o

(oligomycin sensitive factor) which conducts protons through the membrane (Navarro and Boveris, 2007).

Although oxidative phosphorylation is a vital part of metabolism, it also produces reactive oxygen species (ROS) and reactive nitrogen species (RNS). The propagation of free radicals can damage cellular lipids, proteins, oxidative phosphorylation enzymes, and DNA contributing to aging and disease. Electrons can escape from the ETC primarily at complex I and III, leading to the production of superoxide anion radical. Superoxide radicals are effectively detoxified to hydrogen peroxide by superoxide dismutase (SOD) enzymes. In mammals three forms of SOD exist including CuZnSOD (SOD1), MnSOD (SOD2), and extracellular SOD (SOD3). CuZnSOD is mainly localized to the cytosol with some expression in the inner mitochondrial membrane. MnSOD is present in the mitochondrial matrix. As the name implies extracellular SOD is found in the extracellular space of the cell. Hydrogen peroxide is further degraded to water by catalase (CAT), glutathione peroxidase (GPX), and peroxiredoxin III (TRX III). Glutathione (GSH) is regenerated from glutathione disulfide (GSSG) by glutathione reductase (GR). Hydrogen peroxide in turn can be converted to hydroxyl radical, the most reactive species, by the electron transfer from reduced transition metals via Fenton and/or Haber-Weiss reactions. Peroxynitrite, a powerful oxidant and nitrating agent, forms when superoxide anion radical reacts with nitric oxide. In response to oxidative stress and damage mitochondria can undergo fission, fusion, or mitophagy (Circu and Aw, 2010; Halliwell, 1966; Navarro and Boveris, 2007; Pieczenik and Neustadt, 2007; Wallace and Starkov, 2000).

1.5 Oxidative Stress

ROS/RNS are products of normal metabolism and xenobiotic exposure. They can be beneficial or harmful to cells and tissues depending on their concentration. At physiological low levels ROS/RNS can function as “redox messengers” in intracellular signaling and regulation. However, when these species are present in excess they inhibit protein function, induce oxidative modification of cellular macromolecules, and promote cell death (Circu and Aw, 2010). Oxidative stress is a term used to describe an imbalance between excessive ROS/RNS and limited antioxidant defenses. Cellular ROS/RNS levels are maintained at levels that prevent excess oxidation of cellular molecules by cellular antioxidant defenses. Antioxidant defense systems within an organism include both endogenous (glutathione peroxidase, catalase, and superoxide dismutase) and dietary (ascorbic acid, α-tocopherol, and β-carotene) (Halliwell, 1966; Nicolson, 2014; Turrens, 2003).

A major component of ethylene bisdithiocarbamate pesticide induced toxicity is the generation ROS and RNS resulting in oxidative stress. As metal containing pesticides, these compounds have the ability to induce oxidative stress through the production of reactive oxygen species particularly via Fenton-like reactions (Fitsanakis et al., 2002). Manganese, zinc, and copper are essential metals important in maintaining homeostasis in living systems. In particular, they can protect against reactive oxygen species by acting as cofactors to enzymes such as MnSOD and CuZnSOD (Aschner and Aschner, 2005; Turrens, 2003). These metals also have the potential to exert toxic effects within the body. Zinc can cause alterations in glutathione levels and mitochondrial function. Copper can form DNA lesions and reduce glutathione levels. All these effects can contribute to

oxidative stress. In addition, it has been documented that mutations in CuZnSOD are involved in neurodegenerative diseases related to motor neurons, such as Parkinson's Disease and amyotrophic lateral sclerosis (ALS) (Halliwell, 1966; Nzengue et al., 2011). Manganese concentrations are highest in tissues that are rich with mitochondria. Furthermore, manganese has been shown to exert toxicity by impeding mitochondrial respiration and generating reactive oxygen species (Erikson and Aschner, 2003; Prabhakaran et al., 2009). Inhibition of mitochondrial function and the formation of reactive oxygen species may also be linked to neurological effects such as Parkinson's Disease (Domico et al., 2007; Zhang et al., 2003). Chronic manganese toxicity (manganism) can exhibit symptoms similar to those associated with Parkinson's Disease (Erikson and Aschner, 2003).

Various studies have demonstrated that Mancozeb exposure induces oxidative stress. Studies done by Domico et al. (2006, 2007) have shown that exposure to Mancozeb can produce toxic effects to both dopaminergic and GABAergic neurons, cause cellular damage through the generation of reactive oxygen species, uncouple the mitochondrial electron transport chain, and inhibit mitochondrial respiration. In addition, mouse granulosa cells exposed to Mancozeb have been documented to have low p53 content, depolarized mitochondrial membrane potential, and low ATP and reduced GSH levels associated with increased ROS generation (Iorio et al., 2015). Oxidative stress following Mancozeb exposure in human and rat spleen lymphocytes has also been reported, specifically, changes in intracellular levels of reduced GSH, hydroperoxides (markers of lipid peroxidation), and carbonyl proteins (markers of protein oxidation) and activities of CAT and SOD (Medjdoub et al., 2011).

1.6 HT-29 cells: *In Vitro* Model for Gastrointestinal Toxicity

The current study utilizes the HT-29 cell line as a model for the gastrointestinal toxicity of Mancozeb. The advantage of using an *in vitro* model, such as HT-29 cells, over an *in vivo* model is the ability to investigate mechanistic processes of toxicity. The mechanistic findings can then be applied to *in vivo* models reducing the number of animals used for subsequent studies. Furthermore, *in vitro* studies generally produce consistent, reproducible results. The cell line was first isolated by Dr. Jorgen Fogh of Memorial Sloan Kettering Cancer Center in 1964 from a primary colorectal adenocarcinoma tumor of a 44-year-old Caucasian woman (Fogh et al., 1977).

The human intestinal epithelium is composed of two major cell phenotypes. These cells are enterocytes and goblet cells. Enterocytes or intestinal absorptive cells are simple columnar epithelial cells that line the inner surface of the small and large intestines. Microvilli are present on the apical surface of the enterocyte. Additionally, microvilli increase the surface area of the enterocyte and facilitate the transport of small molecules into the enterocyte from the intestinal lumen. Furthermore, the enterocytes are interspersed by goblet cells. Goblet cells make, store, and secret mucin glycoproteins, which are responsible for the production of mucus. Mucus can protect the epithelial cells. In addition, mucus provides nutrients for bacterial growth which promotes intestinal colonization (Gagnon et al., 2013; Pelaseyed et al., 2014). In culture the HT-29 cells are epithelial-like cells that grow in a rounded cobblestone shape that are essentially undifferentiated. Furthermore, they are heterogeneous because they contain both columnar absorptive cells and a small portion (<5%) of goblet cells (Huet et al., 1995).

The HT-29 cell line can be used as a model for colorectal cancer on an *in vitro* model to study the absorption, transport, secretion, and toxicity of intestinal cells. Studies have used the cell line for a variety of reasons. For example, HT-29 cells can be used to test the efficacy of natural products such as curcumin, quercetin, and apple flavonoids as a treatment against colon cancer (Goel et al., 2001; Kim et al., 2005; Li et al., 2022; Supruniuk et al., 2022; Veeriah et al., 2006). The cell line has also been used to study the effects of environmental toxicants such as metals and pesticide residues on the gastrointestinal tract (Baysal and Atlı-Eklioğlu, 2021; Dhaneshwar and Hardej, 2021; Hoffman et al., 2016; Hoffman and Hardej, 2012; Vázquez et al., 2013; Vij and Hardej, 2012, 2016). The efficacy of antioxidant to alleviate oxidative stress from toxic insult to the gastrointestinal tract has also been explored (Guo et al., 2014; Kalaiselvi et al., 2013; Mahmoud et al., 2020).

1.7 Purpose of Study

The purpose of the current study was to investigate the effect of Mancozeb on mitochondrial activity in a transformed human colon cancer cell line, HT-29. Previous work has demonstrated that Mancozeb exposure results in the disruption of mitochondrial complex enzymes (I, II, and V) resulting in apoptosis in the HT-29 cell line. The goal of this study was to determine how oxidative stress contributes to Mancozeb toxicity in the cell line leading to cytotoxic effects such as mitochondrial dysfunction and apoptotic cell death. For the present study, mitochondria were isolated from cells treated with Mancozeb and the activity of complex III and complex IV were evaluated. Various parameters including cellular ROS, mitochondrial superoxide, superoxide dismutase 2, and total antioxidant capacity were explored to investigate the role of oxidative stress in Mancozeb induced cytotoxicity. Mitochondrial membrane potential was evaluated, as a marker of mitochondrial dysfunction leading to apoptosis. Cytotoxic changes in cellular morphology and ultracellular changes, specifically mitochondrial, were investigated. Finally, the effect of mitoquinol (MitoQ) and butylated hydroxytoluene (BHT) as a mitochondrial and cellular antioxidant respectively were evaluated for their protective effects against cytotoxicity of Mancozeb in the cell line.

1.8 Hypotheses

1) Exposure of HT-29 cells to Mancozeb will inhibit mitochondrial respiration by decreasing the activities of complex III and complex IV.

2) Mancozeb treatment will alter cellular and mitochondrial morphology of HT-29 cells.

3) Mancozeb exposure will cause mitochondrial dysfunction due to oxidative stress in HT-29 cells.

4) Antioxidant pre-treatment or co-treatment will protect against Mancozeb cytotoxicity in HT-29 cells.

1.9 Specific Aims

1) Confirm previously established HT-29 cell viability by exposing cells to various purities of Mancozeb for 24 hours using the MTT assay.

2) Evaluate the activity of mitochondrial enzymes, complex III and complex IV, to determine if exposure to Mancozeb for 24 hours alters mitochondrial function.

3) Observe topographical changes in HT-29 cells treated with Mancozeb for 24 hours using scanning electron microscopy (SEM).

4) Observe ultrastructural changes in HT-29 cells treated with Mancozeb for 24 hours using transmission electron microscopy (TEM).

5) Determine if exposure of HT-29 cells to Mancozeb for 24 hours results in mitochondrial dysfunction by measuring mitochondrial membrane potential.

6) Determine if mitochondrial dysfunction in HT-29 cells following exposure to Mancozeb for 24 hours is a result of oxidative stress by measuring cellular ROS levels, mitochondrial superoxide levels, superoxide dismutase 2 levels, and total antioxidant capacity.

7) Determine the protective effect of Mitoquinol pre-treatment or co-treatment as a mitochondrial antioxidant in HT-29 cells exposed to Mancozeb for 24 hours by the MTT assay.

8) Determine the protective effect of butylated hydroxytoluene pre-treatment or co-treatment as a cellular antioxidant in HT-29 cells exposed to Mancozeb for 24 hours by the MTT assay.

2. MATERIALS AND METHODS

2.1 Materials

Mancozeb (MZ; MW: 266.31 g/mol) was purchased from Sigma Aldrich (St. Louis, MO). Butylated hydroxytoluene (2,6-Di-tert-butyl-p-cresol; BHT; MW: 220.36 g/mol) was obtained from Spectrum Chemical MFG. Corporation (New Brunswick, NJ). Mitoquinol ([10-(2,5-dihydroxy-3,4-dimethoxy-6-methylphenyl)decyl]triphenyl-phosphonium, monomethanesulfonate; MW: 680.8 g/mol) was purchased from Cayman Chemical Company (Ann Arbor, MI). McCoy's 5A Media containing L-glutamine was obtained from Caisson Laboratories (North Logan, UT). Gentamicin (50 mg/mL) was acquired from Quality Biological, Inc. (Gaithersburg, MD). Premium, heat inactivated fetal bovine serum (FBS) was purchased from Atlanta Biologicals (Lawrenceville, GA). Trypsin EDTA 1X (0.25% Trypsin/2.21 mM EDTA in HBSS without sodium bicarbonate, calcium, and magnesium) and sterile black 96-well plates with clear bottoms and lids, for fluorescent experiments were obtained from Corning (Corning, New York). Dulbecco's phosphate buffered saline (PBS) without calcium and magnesium, bovine serum albumin (BSA) standards (2.0 mg/mL in a 0.9% aqueous NaCl solution containing sodium azide), and bottle top filters (150 and 500 mL) were purchased from Thermo Fisher Scientific (Waltman, MA). Thiazolyl Blue tetrazolium bromide (3-[4,5-dimethylthiazol-2-yl]-2,5-diphenyltetrazolium bromide or MTT reagent) was acquired from Alfa Aesar (Ward Hill, MA). T75 cell culture flasks and cell scrapers were obtained from Greiner Bio-One (Monroe, NC). Mammalian Protease Inhibitor Cocktail 100X was purchased from G-Biosciences (St. Louis, MO). Copper grids (200 lines/inch, square mesh) were obtained from Electron Microscopy Sciences (Hatfield, PA). Dimethyl sulfoxide (DMSO), conical tubes (15 and 50 mL), disposable serological pipettes (1, 5,

10, 25, and 50 mL), pipette tips (10, 200, and 1000 µL), glass reagent bottles (100, 250, 500, and 1000 mL), Falcon 6, 24, and 96-well plates, round 12mm glass cover slips, magnetic stir bars, weigh boats, reagent reservoirs, microcentrifuge tubes, scoopulas, and micro spoons were all purchased from VWR International (Randor, PA). Tips (200 µL and 300 µL) for Rainin Multichannel pipettor were acquired from Molecular BioProducts Inc. (San Diego, CA). All other reagents and assay materials used were purchased from reputable chemical suppliers and were of reagent grade.

2.2 Cell Culture and Treatments

HT-29 cells, a transformed human colon cancer cell line, were obtained from the American Type Culture Collection (ATCC HTB-38). The cells were grown in T75 culture flasks containing 15 mL of McCoy's 5A media with L-glutamine supplemented with 10% heat inactivated FBS and 0.1% gentamicin. The flasks were incubated at 37ºC in 5% bone dry grade carbon dioxide (CO_2) in a NAPCO 8000 water-jacketed incubator (Thermo Fisher Scientific). All experiments were performed using cells of passage numbers 170 through 190.

Mancozeb stock solution of 400 µM was prepared immediately before experiments. The solution was made in unsupplemented media (devoid of FBS or antibiotic) with the aid of DMSO <0.5% (v/v) to help with dissolving the compound. The stock solution was diluted to the experimental concentrations (40 µM, 60 µM, 80 µM, 100 µM, 120 µM, 140 µM, 160 µM, 180 µM, 200 µM) using unsupplemented media. For all studies a vehicle control was made with DMSO < 0.5% (v/v) and did not show any significant difference in viability from controls. All treatments were carried out for a period of 24 hours.

2.3 MTT Cytotoxicity Assay

The MTT assay was used to measure the viability of the cells and is based on the procedure first published by Mosmann (1983). This colorimetric assay uses the reduction of the tetrazolium salt by mitochondrial succinate dehydrogenase as a measure of cellular viability. Viable cells are able to reduce the yellow MTT reagent to a purple formazan crystal, which can be solubilized and measured spectrophotometrically.

The cells were seeded at a density of 20,000 cells per well in 24-well plates. They were grown in an incubator at 37ºC in 5% CO_2 for a minimum of five days until they reached 90% confluency. Once the cells were confluent, media were removed and the cells were treated with 1 mL of Mancozeb solution ranging from 40 µM to 200 µM. After 24 hours, the treatment media were removed and each well was washed three times with 1 mL of PBS. After the last PBS wash was removed, 300 µL of PBS were added to each well followed by 30 µL of freshly prepared MTT reagent (0.5% (w/v) 3-[4,5-dimethylthiazol-2-yl]-2,5-diphenyltetrazolium bromide in PBS). The MTT reagent is light sensitive, therefore the prepared reagent was protected from light. The plates were incubated for 3 hours in the incubator at 37ºC in 5% CO_2. After the incubation period, the formazan crystals were dissolved by adding 300 µL of solubilization solution (270 mL isopropyl alcohol, 30 mL Triton-X, 30 mL 0.1 N HCl) to each well. The plate was then placed on an orbital shaker set at 140 rpm for 30 minutes at room temperature. A micropipette was used to further solubilize the crystals mechanically. Afterward, 200 µL of the solution in each well were transferred to a 96-well plate and read at 570 nm in an iMark™ Microplate Reader, Bio-Rad Laboratories (Hercules, CA).

2.4 Scanning Electron Microscopy

Scanning electron microscopy was used to observed changes in HT-29 cell morphology after exposure to Mancozeb. The cells were seeded at a density of 80,000 cells per well in 6-well plates, containing two round 12 mm glass coverslips in each well, and incubated at 37ºC in 5% CO_2 for a minimum of five days until they reached ~90% confluency. The medium was removed and the cells were treated with 5 mL of Mancozeb ranging from 60 μM to 160 μM for 24 hours. After the treatment period, the medium was removed and each well was washed three times with 2 mL of Sorensen's Phosphate Buffer (pH 7.4). After the cells were rinsed, 2 mL of 3% (v/v) glutaraldehyde were added to each well to fix the cells. The cells were fixed for an hour and half on ice and periodically shaken every 15 min. The cells were then washed with 2 mL of Sorensen's Phosphate Buffer (pH 7.4) on ice for an hour. The coverslips were then placed into a slide holder that was submerged in Sorensen's Phosphate Buffer (pH 7.4) to prevent the cells from drying out. The cells were dehydrated, as the slide holder containing the coverslips were placed in solutions of 30%, 60%, and 90% ethanol for 15 minutes. The slide holder was then placed in 100% ethanol three times for 5 minutes. After complete dehydration, the specimens were critically point dried in the Autosamdri-815, Tousimis Research Corporation (Rockville, MD). Afterward, the coverslips were placed on aluminum stubs, cleaned with 100% acetone and lint-free cloth, using double sided sticky tape. Before sputter coating, a dot of silver paint was placed on the top and bottom of each coverslip. The coverslips were sputter coated with platinum and palladium using Cressington 108 Auto/SE Sputter Coater, Ted Pella, Inc (Redding, California). Micrographs were viewed

and captured at 20 kV using a scanning electron microscope, JEOL JSM-6010LA, (JEOL Ltd.; Tokyo, Japan).

2.5 Transmission Electron Microscopy

Transmission electron microscopy was performed on control and treated HT-29 cells to observed morphological changes, particularly in the mitochondria. Cells were seeded into T75 flasks at a density of 800,000 cells per flask and grown for minimum of 5 days until they reached ~90% confluency. At confluency, control cells were collected and cells for treatment were treated with 100 μM of Mancozeb for 24 hours then collected. During the collection, the flasks were placed flat on ice and the media were decanted. The flasks were then washed twice with 7 mL of Sorensen's Phosphate Buffer (pH 7.4). Cells were fixed by adding 5 mL of 3% glutaraldehyde to each flask. The flasks were incubated on ice for an hour and half and periodically shaken every fifteen minutes. The glutaraldehyde was decanted and the flasks were washed twice with 7 mL of Sorensen's Phosphate Buffer (pH 7.4). After the flasks were washed, 5 mL of Sorensen's Phosphate Buffer (pH 7.4) were added to each flask. The flasks were scraped and combined in to 15 mL conical tubes. The tubes were spun at 1,000 rpm for 10 minutes in a PowerSpin™ MX Centrifuge, Unico (Dayton, NJ). The supernatants were decanted and the pellets suspended in 10 mL of Sorensen's Phosphate Buffer (pH 7.4). The cells were centrifuged again at 1,000 rpm for 10 minutes. The supernatants were decanted and twice the volume of the pellets of 1% osmium tetroxide was added. The pellets were incubated on ice for 45 minutes and resuspended every 15 minutes. At the end of the incubation, the cells were centrifuged for 10 minutes at 1,000 rpm. The supernatants were aspirated off and the pellets were washed with 10 mL of Sorensen's Phosphate Buffer (pH 7.4) and the

tubes were further combined. The cells were then centrifuged at 1,000 rpm for 10 minutes and washed with 10 mL of Sorensen's Phosphate Buffer (pH 7.4) twice. After the second wash, the cells were centrifuged at 1,000 rpm for 10 minutes and the supernatant was decanted.

A series of dehydrations were performed as 10 mL of 30% acetone was added to the pellet with a glass pipette. The cells were allowed to incubate in the acetone for 10 minutes at room temperature and vortexed periodically. At the end of the incubation, the cells were centrifuged for 10 minutes at 1,000 rpm and supernatant was decanted. The cells were then resuspended in 10 mL of 60% acetone. At this point cells were left in 60% acetone, either overnight or 1-2 days, before the dehydration process was completed. The cells in 60% acetone were centrifuged for 10 minutes at 1,000 rpm and supernatant was aspirated. The pellets were resuspended in 10 mL of 90% acetone for 10 minutes and vortexed periodically. The cells were centrifuged at 1,000 rpm for 10 minutes and the supernatant was aspirated off. The pellets were then resuspended in 10 mL of 100% acetone for 5 minutes, vortexed periodically, centrifuged at 1,000 rpm for 10 minutes, and the supernatant was aspirated off. The 100% dehydration step was done a total of three times.

The cells were then infiltrated with LX112 – Araldite Mixture. To the pellets, 1 part LX112 – Araldite Mixture and 2 parts 100% acetone was added. The pellets were incubated at room temperature for 30 minutes and resuspended by vortexing periodically. The mixture was then centrifuged for 10 minutes at 1,000 rpm and the supernatant was aspirated off. Then 1 part LX112 – Araldite Mixture and 1 part 100% acetone was added to the pellets and allowed to incubate for 30 minutes at room temperature with periodic

vortexing. The mixture was then centrifuged again for 10 minutes at 1,000 rpm and the supernatant aspirated. To the pellets, 2 parts LX112 – Araldite Mixture and 1 part 100% acetone was added and allowed to incubate for 30 minutes at room temperature with periodic vortexing. The mixture was then centrifuged again for 30 minutes at 1,000 rpm and the supernatant aspirated. The LX112 – Araldite Mixture, approximately twice the volume of the pellet, was added to the pellet and resuspended with a wooden stick. The mixture was then poured into BEEM capsules until they were three quarters full. A syringe was then used to fill the rest of the BEEM capsule with the LX112 – Araldite Mixture. The BEEM capsules were placed in 15 mL conical tubes without lids and centrifuged in the Heraeus Multifuge X3R (Thermo Fisher Scientific) at 500 rcf for 4 hours. Samples, still in test tubes, were then placed in an oven at ~ 60ºC for about 4 days. The BEEM capsules were then stored at room temperature until ready for use. BEEM capsules were sectioned to ultrathin sections (40 nm) using an EM UC6 ultramicrotome, Leica (Wetzlar, Germany) and collected on 200 mesh copper grids.

The grids were stained using the following method. Grids were placed in boiled distilled water for 1 minute and then stained with uranyl acetate in a small petri dish for 30 minutes with occasional shaking. The small petri dish containing uranyl acetate was placed in a larger petri dish filled with methanol and covered. Grids were then washed in absolute methanol three times, washed in a 50% mixture of water and methanol, and washed in boiled distilled water three times. The grids were stained with lead citrate for 5 minutes in a waxed petri dish with a pellet of sodium hydroxide placed next to each drop of lead citrate. After staining with lead citrate, the grids were washed in 3 changes of boiled distilled water and placed on filter paper to dry over night before viewing.

Micrographs were viewed and captured using a transmission electron microscope (JEOL JEM-1200EX) at 80kV.

2.6 Bradford Protein Assay

The method developed by M.M. Bradford in 1976 is the basis for the Bradford protein assay. The assay was used to measure the protein concentration of samples by utilizing the binding of Coomassie Brilliant Blue G-250 dye to protein. A shift in the maximum absorption of the dye from 465 nm (red) to 595 nm (blue) occurs when the dye binds to protein. Therefore, the higher the absorbance of the sample when read in a spectrophotometer at 595 nm, the higher the protein concentration of the sample.

The protein concentration of the samples was determined using the protocol provided by Amersco® with their Bradford reagent. The protocol was modified for a 96-well plate. BSA, with a concentration of 2 mg/mL, was diluted to a final concentration of 0.5 mg/mL using PBS. The standards were made by adding increasing volumes of 0.5 mg/mL BSA (5 µL, 10 µL, 15 µL, 20 µL, 30 µL, 40 µL, 50 µL, and 60 µL) into microcentrifuge tubes to which 0.15 M sodium chloride was added to obtain a final volume of 100 µL in each microcentrifuge tube. A blank was prepared by adding 100 µL of 0.15 M sodium chloride to a microcentrifuge tube. Samples were prepared by adding 2 µL, 5 µL, and 10 µL into three separate microcentrifuge tubes to which 0.15 M sodium chloride was added to obtain a final volume of 100 µL in each tube. To each standard, sample, and blank tube, 1 mL of Bradford reagent was added. All tubes were vortexed and allowed to incubate at room temperature for 2 minutes. After incubation, 200 µL from each tube were transferred into three wells of a 96-well plate and read at 600 nm by the GloMax Multi + Detection System, Promega (Fitchburg, WI). Absorbance values

from the three wells were averaged to give an average absorbance for each sample, standard, and blank. The average blank absorbance was subtracted from each averaged absorbance. These readings were used to construct a standard curve, which was used to determine the protein concentration of the sample.

2.7 Mitochondrial Isolation

HT-29 cells were seeded into T-75 flasks at a density of 800,000 cells per flask and grown for a minimum of 5 days until they reached ~90% confluency. Media were then removed and cells were treated with 15 mL of 60 µM, 100 µM, and 140 µM Mancozeb solution. After the 24-hour treatment period, cells from the treatment groups and control groups were collected in 15 mL conical tubes by scraping and centrifuged at 5,000 rpm for 5 minutes in VWR Clinical 200. Flasks and pellets were kept on ice during this process to prevent protein degradation. Supernatant was removed and the pellets were washed in 10 mL of ice cold PBS and centrifuged for 5 minutes at 5,000 rpm. The pellets were then resuspended in 0.5 mL of PBS and the pellets were combined into one 15 mL conical tube. The samples were centrifuged at 5,000 rpm for 5 minutes and the supernatant was poured off. The pellet was resuspended in 1 mL of PBS. To determine what volume of the remaining sample contained a protein concentration of 5 mg/mL of whole cell protein, a 200 µL aliquot of cell suspension was subjected to five-freeze thaw cycles by snap-freezing in liquid nitrogen and thawing in room temperature water in order to lyse the cells. After the final thaw, lysate was centrifuged at 14,000 rpm for 20 minutes at 4ºC in an Eppendorf 5804R 15-amp refrigerated centrifuge (Hamburg, Germany). The supernatant was collected and transferred to a new microcentrifuge tube that was kept on ice for protein determination using the Bradford protein assay. The

sufficient volume of cell suspension, from original 15 mL conical tube, that was calculated to yield 5 mg/mL of protein was then transferred to a 15 mL conical tube and centrifuged at 5,000 rpm for 5 minutes. The supernatant was removed and the pellet was kept frozen at -20ºC overnight.

The remainder of the procedure was performed according to the Mitochondria Isolation Kit for Cultured Cells purchased from Abcam (Cambridge, MA). The pellets were thawed on ice to weaken the cell membranes and resuspended in 800 µL of Reagent A. The samples were transferred to microcentrifuge tubes and incubated on ice for 10 minutes. Cells were ruptured by 30 pulses of VWR Pellet Mixer. The homogenized samples were centrifuged (to remove debris and extremely large cellular organelles) at 1,000 x g for 10 minutes at 4ºC. The supernatant (supernatant #1) was saved on ice. The pellets were resuspended in 800 µL of Reagent B, homogenized using 30 pulses of the pellet mixer, and centrifuged at 1,000 x g for 10 minutes at 4ºC. The supernatant (supernatant #2) was saved on ice, and pellets were discarded. Supernatant #1 and supernatant #2 for each sample were transferred to the same 15 mL conical tube, mixed, and equally divided into two microcentrifuge tubes. Combined supernatants for each sample were then centrifuged at 12,000 x g for 15 minutes at 4ºC to isolate the mitochondria. The supernatant was discarded. The pellets in the two microcentrifuge tubes were combined and resuspended in a total of 500 µL of Reagent C that was supplemented with 5 µL of protease inhibitors. Aliquots of the sample were stored at -80ºC.

2.8 Complex III Enzyme Activity

The Mitochondrial Complex III Activity Assay Kit purchased from BioVision Incorporated (Milpitas, CA) was utilized to observe changes in the enzyme activity of complex III in HT-29 cells treated with Mancozeb. Complex III is responsible for the transfer of electrons from reduced coenzyme Q to cytochrome *c*, resulting in the reduction of cytochrome *c*. This reduced cytochrome *c* is a substrate for complex IV of the electron transport chain (ETC). This assay is based on the reduction of cytochrome *c* through the activity of complex III. The absorbance of reduced cytochrome *c* is measured at 550 nm.

The assay was performed as per the kit protocol. All materials and prepared reagents were allowed to equilibrate to room temperature before use. The mitochondrial samples were thawed on ice. After the samples were thawed, protein content was determined using the Bradford Protein Assay. A reduced cytochrome *c* standard curve was done. For the standard curve, a 750 mM DTT solution was prepared by mixing 1M DTT solution and Assay buffer in a 3:1 ratio. A series of wells of 0, 4, 8, 12, 16, and 20 nmol/well of cytochrome *c* was generated by adding 0, 2, 4, 6, 8, and 10 µL of 2.0 mM cytochrome *c* respectively. The volume of each well was then adjusted to a final volume of 23 µL/well with Complex III Assay Buffer. Then 2 µL of the 750 mM DTT solution was added to each well to completely reduce cytochrome *c*. The contents of the wells were mixed and incubated at room temperature for 5 minutes. The absorbance was measured at 550 nm in the Bio-Rad iMark™ Microplate Reader.

Three types of reaction mixes were prepared: background control, sample mix, and sample mix with complex III inhibitor (antimycin A). Background control wells

contained per well 17 µL of Assay Buffer and 2µL of DMSO (anhydrous). Sample mix wells contained per well 15 µL of Assay Buffer and 2µL of DMSO (anhydrous). Sample mix with inhibitor wells contained per well 15 µL of Assay Buffer and 2µL of inhibitor. To each sample mix and sample mix with inhibitor wells 1 to 2 µL of mitochondrial samples (1.5 to 10 µg protein) was added. Bovine heart mitochondria were used as a positive control and only 1 µL of sample was used. For isolated mitochondria from HT-29 cells 2 µL of sample was used. Contents of wells were mixed well and 6 µL of cytochrome *c* was added. Bubbles were popped with a fine needle as rapidly as possible before the absorbance of each well was read in the Bio-Rad iMark™ Microplate Reader in kinetic mode. The plate was read at 550 nm at room temperature for 10 minutes with absorbance measurements taken every 30 seconds. Results are expressed as rate of activity divided by protein content.

2.9 Complex IV Enzyme Activity

The Complex IV Human Enzyme Activity Microplate Assay Kit (Abcam) was utilized to observe changes in the enzyme activity of complex IV in HT-29 cells treated with Mancozeb. The target, complex IV enzyme, is immunocaptured in the wells by an anti-complex IV monoclonal antibody. After the target has been immobilized in the well and substrate is added, the enzyme activity is determined colorimetrically by following the oxidation of reduced cytochrome *c*. The reaction results in a decrease in absorbance at 550 nm.

The assay was performed as per the kit protocol. All materials and prepared reagents were allowed to equilibrate to room temperature before use. The samples were prepared in the following manner. The mitochondrial samples were thawed on ice. After

the samples were thawed, 10X Detergent solution was added to lyse the mitochondria and release mitochondrial proteins including complex IV enzyme. The Detergent solution was added to the samples to give a final dilution of 1/100. The detergent/samples mixture was mixed well and incubated on ice for 30 minutes to allow solubilization. The samples were then centrifuged at 12,000 x g at 4ºC for 20 minutes. The supernatant was collected and transferred to a clean tube kept on ice. The protein concentration of each sample was determined prior to the assay using the Bradford protein assay.

All samples and bovine heart mitochondria were diluted to 0.08 µg/µL using Solution 1. To the plate 200 µL of prepared sample, 200 µL of Solution 1 as background control, and 200 µL of prepared bovine heart mitochondria as a positive control. The samples were run in triplicate. The plate was incubated at room temperature for 3 hours. After the incubation period was completed, the wells were emptied by turning the plate over and shaking out any remaining liquid and blotted face down on a paper towel. Then 300 µL of Solution 1 was added to each well. The wells were then emptied again and rinsed with 300 µL of Solution 1. Another 300 µL of Solution 1 was added to the wells. The Assay Solution was then prepared according to kit instructions. After the Assay Solution was prepared the wells were emptied of Solution 1. To each well, 200 µL of Assay Solution was added and bubbles were popped with a fine needle as rapidly as possible before the absorbance of each well was read in the Bio-Rad iMark™ Microplate Reader in kinetic mode. The plate was read at 550 nm at room temperature for 120 minutes with absorbance measurements taken every 5 minutes.

2.10 Mitochondrial Membrane Potential

The Mitochondria Membrane Potential Kit (Sigma-Aldrich) was utilized to observe changes in the mitochondrial membrane potential (MMP) in HT-29 cells treated with Mancozeb. The activity of enzymes of the electron transport chain causes the generation of a potential across the mitochondrial membrane. Collapse of the MMP during apoptosis, coincides with the opening of the mitochondrial permeability transition pores. The kit detects the loss of MMP in cells using a cationic, hydrophobic dye. The mitochondrial potential dye accumulates in normal mitochondria resulting in an increase in fluorescence (λ_{ex}=540/ λ_{em}=590 nm). In apoptotic cells, a decrease in fluorescence is observed due to the collapse of MMP.

Cells were seeded at a density of 20,000 cells/well/100 µL into black-walled, clear bottom, 96-well plates. They were grown in standard incubation settings for 1 day until they reached 90% confluency. Growth media were removed and cells were treated with 100 µL of Mancozeb solution (60 µM, 100 µM, and 140 µM) for 24 hours.

The assay was performed as per the kit protocol. All materials and prepared reagents were allowed to equilibrate to room temperature before use. The plate and reagents were protected from direct light during the assay. The Dye Loading Solution was prepared by adding 50 µL of the 200x Mitochondrial Potential Dye to 10 mL of Assay Buffer A. The treatment media were removed and 100 µL of the Loading Dye Solution were added to each well. The plate was incubated for 30 minutes in a 5% CO_2, 37°C incubator. After the incubation period, 50 µL of Assay Buffer B were added to each well and the plate was incubated for 20 minutes in the incubator. The plate was read at λ_{ex}=540/ λ_{em}=590 nm in the Infinite M Plex, Tecan (Männedorf, Switzerland).

2.11 CellROX® Assay

The CellROX® Orange Reagent (ThermoFisher Scientific) was used to measure reactive oxygen species in HT-29 cells treated with Mancozeb. This cell-permeable reagent is localized in the cytoplasm. In the reduce state it is non-fluorescent or very weakly fluorescent and upon oxidation it exhibits a strong fluorescent signal. The fluorescent signal generated by the reagent can be read at λ_{ex}=540/ λ_{em}=570 nm.

Cells were seeded at a density of 20,000 cells/well/100 µL into black-walled, clear bottom, 96-well plates. They were grown in standard incubation settings for 1 day until they reached 90% confluency. Growth media were removed and cells were treated with 100 µL of Mancozeb solution (60 µM, 100 µM, and 140 µM) for 24 hours.

The assay was performed as per the kit protocol. All materials and prepared reagents were allowed to equilibrate to room temperature before use. The plate and reagents were protected from direct light during the assay. The CellROX® Orange Reagent was diluted from the stock concentration of 2.5 mM to a working solution of 10 µM. At the end of treatment period, 100 µL of the 10 µM working solution was added to 100 µL of treatment in each well, making the final concentration 5 µM. The plate was incubated for 30 minutes in a 5% CO_2, 37°C incubator. After the incubation period, the plate was decanted to remove the reagent and the cells were washed with 200 µL of PBS in each well. After washing, 200 µL of PBS were added to each well and the plate was read in a Tecan Infinite M Plex at λ_{ex}=540/ λ_{em}=570 nm.

2.12 Mitochondrial Superoxide

The Mitochondrial Superoxide Detection Kit (Abcam) was used to detect intracellular superoxide radical in HT-29 cells treated with Mancozeb. Mitochondria are

one of the major producers of intracellular superoxide. Low to moderate levels of superoxide are essential for the regulation of many cellular processes including gene expression and signal transduction. However, cellular oxidative stress and damage occurs when mitochondrial superoxide production is uncontrolled. Mitochondrial superoxide present in the cell reacts with the MitoROS 580 dye generating a red fluorescent signal that can be read at λ_{ex}=540/ λ_{em}=590 nm. Detection of mitochondrial superoxide is important to understanding cellular redox regulation and the impact of dysregulation on various pathologies.

Cells were seeded at a density of 20,000 cells/well/100 µL into black-walled, clear bottom, 96-well plates. They were grown in standard incubation settings for 1 day until they reached 90% confluency. Growth media were removed and cells were treated with 100 µL of Mancozeb solution (60 µM, 100 µM, and 140 µM) for 24 hours.
The assay was performed as per the kit protocol. All materials and prepared reagents were allowed to equilibrate to room temperature before use. The plate and reagents were protected from direct light during the assay. The MitoROS 580 Stain Working Solution was prepared by adding 25 µL of the 500x MitoROS 580 Stain Stock Solution to 10 mL of Assay Buffer. At the end of treatment period, 100 µL of the MitoROS 580 Stain Working Solution were added to each well. The plate was incubated for 60 minutes in a 5% CO_2, 37°C incubator. After the incubation period, the plate was read in a Tecan Infinite M Plex at λ_{ex}=540/ λ_{em}=590 nm.

2.13 Superoxide Dismutase 2

The Human SOD2 SimpleStep ELISA® Kit (Superoxide Dismutase 2) (Abcam) was used to measure the levels of SOD2 protein in cell lysates of HT-29 cells treated with

Mancozeb. The SOD family is comprised of cellular antioxidant enzymes that dismutate superoxide into hydrogen peroxide, which can be detoxified further by other cellular defenses such as glutathione and catalase. In mammals three forms of SOD exist including CuZnSOD (SOD1), MnSOD (SOD2), and extracellular SOD (SOD3). SOD1 is localized mainly to the cytosol while SOD2 is present in the mitochondrial matrix.

The SimpleStep ELISA® is able to immunocapture the sample analyte by using both capture and detector antibodies. The capture antibody is labeled with a tag that allows the capture antibody/analyte/detector antibody complex to be immobilized by the affinity to the anti-tag antibody that coats the well. To perform the assay, standards and samples are added to the wells followed by the antibody mix. After an incubation period, unbound material is removed by washing. TMB Development Solution is added and during the incubation is catalyzed by HRP, generating a blue color. Stop Solution is added to stop the reaction changing the color from blue to yellow. The solution can be read at 450 nm the signal generated is proportional to the amount of bound analyte.

Cells were seeded into T75 flasks at a density of 800,000 cells per flask and grown for a minimum of 5 days until they reached 90% confluency. Media were removed and cells were treated with 15 mL of 60 µM, 100 µM, and 140 µM Mancozeb solution. After the 24-hour treatment period, cells from the control and treatment groups were collected in 15 mL conical tubes by scraping and centrifuged at 500 x g for 5 minutes at 4ºC in an Eppendorf 5804R 15-amp refrigerated centrifuge. Flasks and pellets were kept on ice during this process to prevent protein degradation. Supernatant was removed and the pellets were washed twice in 10 mL of ice cold PBS and centrifuged at 500 x g for 5 minutes at 4ºC. The supernatant was discarded, and the pellet was solubilized at $2x10^7$

cell/mL in chilled 1X Cell Extraction Buffer PTR (Control 1 mL, 60µM MZ 750µL, 100µM MZ 500 µL, 140µM MZ 250 µL). Pellets were incubated on ice for 20 minutes and then centrifuged at 18,000 x g for 20 minutes at 4ºC. The supernatants were transferred to clean microcentrifuge tubes and the pellets discarded. Aliquots of the supernatant were stored at -80ºC.

The assay was performed as per the kit protocol. All materials and prepared reagents were allowed to equilibrate to room temperature before use. The cell lysate samples were thawed on ice. After the samples were thawed, protein content was determined using the Bradford Protein Assay. Samples were diluted to a concentration of 3 µg/mL using 1X Cell Extraction Buffer PTR. SOD2 standard were prepared to generate a SOD2 standard curve. A stock standard solution of 100 ng/mL was prepared by reconstituting SOD2 Human Lyophilized Recombinant Protein in 200 µL of 1X Cell Extraction Buffer PTR. A serial dilution was performed using the 1X Cell Extraction Buffer PTR as diluent to produce standards with the following concentrations: 50, 25, 12.5, 6.25, 3.12, 1.56, and 0.78 ng/mL SOD2. The 1X Cell Extraction Buffer PTR served as the blank. To each well, 50 µL of standard or sample were added. Then, 50 µL of Antibody Cocktail were added to each well. The plate was then sealed and incubated on an orbital shaker set at 120 rpm at room temperature for 1 hour. The wells were then washed three times with 350 µL 1X Wash Buffer PT. After the last wash, 100 µL of TMB Development Solution were added to each well and the plate was incubated in the dark on an orbital shaker set at 120 rpm at room temperature for 10 minutes. After incubation with the TMB Development Solution, 100 µL of Stop Solution were added to each well and the plate was incubated on an orbital shaker set at 120 rpm at room

temperature for 1 minute. The plate was read at 450 nm in the Bio-Rad iMark™ Microplate Reader. Results are expressed as SOD2 protein (ng/mL).

2.14 Total Antioxidant Capacity

The Antioxidant Assay Kit (Cayman Chemical Company) was used to measure the total antioxidant capacity of cell lysates of HT-29 cells treated with Mancozeb. Organisms have developed complex antioxidant systems to counteract and reduce the effects of ROS which include damaging lipids, proteins, and DNA. Antioxidant systems include enzymes such as superoxide dismutase, catalase, and glutathione peroxidase; macromolecules including albumin, ceruloplasmin, and ferritin; and small molecules such as uric acid, bilirubin, reduced glutathione, ascorbic acid, α-tocopherol, and β-carotene. Total antioxidant capacity can be represented by the combination of both endogenous and food-derived antioxidants and may provide more relevant biological information as it considers the cumulative effect of all antioxidants present.

The protocol does not separate aqueous and lipid soluble antioxidants. The assay relies on the ability of antioxidants present in the samples to inhibit the oxidation of ABTS® (2,2'-Azino-di-[3-ethylbenzthiazoline sulphonate]) to $ABTS^{®•+}$ by metmyoglobin. Reading the sample at 750 nm can monitor the amount of $ABTS^{®•+}$ produced as the antioxidants in the sample cause suppression of the absorbance at 750 nm which is proportional to their concentration. Trolox, a water-soluble tocopherol analogue, is used to compare the capacity of antioxidants in the sample that prevent ABTS® oxidation which is quantified as millimolar Trolox equivalents.

Cells were seeded into T75 flasks at a density of 800,000 cells per flask and grown for a minimum of 5 days until they reached 90% confluency. Media were then

removed and cells were treated with 15 mL of 60 µM, 100 µM, and 140 µM Mancozeb solution. After the 24-hour treatment period, cells from the control and treatment groups were collected in 15 mL conical tubes by scraping and centrifuged at 5,000 rpm for 5 minutes at 4ºC in a refrigerated centrifuge (Eppendorf 5804R 15-amp). Flasks and pellets were kept on ice during this process to prevent protein degradation. Supernatant was removed and the pellets were washed in 10 mL of ice cold PBS and centrifuged at 5,000 rpm for 5 minutes at 4ºC. The pellets were then resuspended in 1 mL of PBS and centrifuged at 2,000 x g for 5 min at 4ºC. Supernatant was discarded and the pellet was homogenized in 0.5 mL of Antioxidant Assay Buffer (1X) supplemented with protease inhibitors. Samples were then centrifuged at 10,000 x g for 15 min at 4ºC. Aliquots of the supernatant were stored at -80ºC.

The assay was performed as per the kit protocol. All materials and prepared reagents were allowed to equilibrate to room temperature before use. The cell lysate samples were thawed on ice. After the samples were thawed, protein content was determined using the Bradford Protein Assay. Trolox standards were prepared to generate a Trolox standard curve. For the standard curve a series of microtubes containing 0, 0.068, 0.135, 0.203, 0.270, 0.338, and 0.495 mM Trolox were prepared by adding 0, 30, 60, 90, 120, 150, and 220 µL of 2.25 mM Trolox standard. The volume of each tube was then adjusted to a final volume of 1,000 µL with Antioxidant Assay Buffer (1X). Trolox standard wells contained per well 10 µL of Trolox standard, 10 µL of metmyoglobin, and 150 µL of chromogen. Sample wells contained per well 10 µL of sample, 10 µL of metmyoglobin, and 150 µL of chromogen. To all wells 40 µL of hydrogen peroxide working solution (441µM) was added. The plate was incubated at room temperature on

an orbital shaker set at 80 rpm for 5 minutes. The plate was read at 750 nm in the Bio-Rad iMark™ Microplate Reader. Results are expressed as Trolox equivalents (mM) divided by protein content.

2.15 Cellular Antioxidant Study

The cells were seeded at a density of 20,000 cells per well in 24-well plates. They were grown in an incubator at 37ºC in 5% CO_2 for a minimum of five days until they reached 90% confluency. Once the cells were confluent the old media were removed and the cells were treated. Cells were either co-treated with BHT and Mancozeb or pre-treated with BHT followed by Mancozeb treatment. BHT stock solution of 200 µM was prepared immediately before use in DMSO and then diluted to appropriate concentrations in media devoid of serum or antibiotic. Co-treatment with BHT and Mancozeb included concentrations of: 25 µM BHT and 100 µM MZ, 50 µM BHT and 100 µM MZ, 75 µM BHT and 100 µM MZ and of 100 µM BHT and 100 µM MZ. Co-treatments were incubated for 24 hours, before the cell viability was analyzed using the MTT assay. Pre-treatment with BHT was conducted for 12 hours using BHT concentrations of 25 µM, 50 µM, 75 µM, and 100 µM BHT. Following BHT exposure, the treatments were removed and replaced with 100 µM MZ treatment. Mancozeb treatment, following BHT exposure, was allowed to incubate for 24 hours before the MTT assay was used to measure cell viability.

2.16 Mitochondrial Antioxidant Study

The cells were seeded at a density of 20,000 cells per well in 24-well plates. They were grown in an incubator at 37ºC in 5% CO_2 for a minimum of five days until they reached 90% confluency. Once the cells were confluent the old media were removed and

the cells were treated. Cells were either co-treated with MitoQ and Mancozeb or pre-treated with MitoQ followed by Mancozeb treatment. MitoQ stock solution of 200 μM was prepared immediately before use in DMSO and then diluted to appropriate concentrations in media devoid of serum or antibiotic. Co-treatment with MitoQ and Mancozeb included concentrations of: 0.5 μM MitoQ and 100 μM MZ, 0.75 μM MitoQ and 100 μM MZ. Co-treatments were incubated for 24 hours, before the cell viability was analyzed using the MTT assay. Pre-treatment with MitoQ was conducted for 12 hours using MitoQ concentrations of 0.75 μM, and 1 μM MitoQ. Following MitoQ exposure, the treatments were removed and replaced with 100 μM MZ treatment. Mancozeb treatment, following MitoQ exposure, was allowed to incubate for 24 hours before the MTT assay was used to measure cell viability.

2.17 Statistical Analysis

Statistical analysis was performed using GraphPad Prism ® version 5 (GraphPad Software, Inc; La Jolla, CA). Results are expressed as the mean ± standard error of the mean (SEM) and compared by one-way analysis of variance (ANOVA) followed by Tukey's Multiple Comparison post-hoc test. Results of treated groups were considered statistically significant from controls when $p < 0.05$.

3. RESULTS

3.1 Confirmatory viability of Mancozeb determined by the MTT Assay

The MTT assay was used to confirm previously established HT-29 cell viability by exposing cells to various purities of Mancozeb. Mancozeb with purities of 94.1%, 97.5% and 99.6% were tested at concentrations of 40 µM, 60 µM, 80 µM, 100 µM, 120 µM, 140 µM, 160 µM, 180 µM, and 200 µM for 24 hours. Mancozeb with a purity of 97.5% was used in previous experiments. A concentration-dependent decrease in cell viability was observed as cells were 94.20%, 83.36%, 69.20%, 54.76%, 39.34%, 24.98%, 6.58%, 2.96%, and 2.51% viable at concentrations of 40 µM, 60 µM, 80 µM, 100 µM, 120 µM, 140 µM, 160 µM, 180 µM, and 200 µM respectively, compared to untreated cells. Significant reductions in cell viability were observed at all treatment groups after 24 hours of treatment when compared to untreated cells (Table 1). From the MTT assay data, the calculated LC_{50} for Mancozeb, with a purity of 97.5%, in HT-29 cells was 104.21 µM. Due to the inability to continue to obtain Mancozeb with a purity of 97.5% from the vendor, Mancozeb with purities of 94.1% and 99.6% were tested to determine if cytotoxic effects were similar to the established results of Mancozeb with a purity of 97.5%. For Mancozeb with a purity of 94.1%, a concentration-dependent decrease in cell viability was observed as cells were 90.67%, 83.62%, 75.44%, 63.78%, 56.95%, 55.34%, 49.63%, 40.89%, and 36.22% viable at concentrations of 40 µM, 60 µM, 80 µM, 100 µM, 120 µM, 140 µM, 160 µM, 180 µM, and 200 µM respectively, compared to untreated cells. Significant reductions in cell viability were observed at all treatment groups after 24 hours of treatment when compared to untreated cells (Table 1). From the MTT assay data, the calculated LC_{50} for Mancozeb, with a purity of 94.1%, in HT-29 cells was 153.90 µM. For Mancozeb with a purity of 99.6%, a concentration-dependent

decrease in cell viability was observed as cells were 88.39%, 83.34%, 72.88%, 55.47%, 41.63%, 28.34%, 12.51%, 2.84%, and 2.29% viable at concentrations of 40 µM, 60 µM, 80 µM, 100 µM, 120 µM, 140 µM, 160 µM, 180 µM, and 200 µM respectively, compared to untreated cells. Significant reductions in cell viability were observed at all treatment groups after 24 hours of treatment when compared to untreated cells (Table 1). From the MTT assay data, the calculated LC_{50} for Mancozeb, with a purity of 99.6%, in HT-29 cells was 105.82 µM. The results confirmed that Mancozeb with a purity of 99.6% yielded a similar calculated LC_{50} to that of Mancozeb with a purity of 97.5%. Therefore, for all further experiments Mancozeb with a purity of 99.6% was used.

3.2 Activity of mitochondrial complex enzymes in HT-29 cells treated with Mancozeb

The activity of mitochondrial complex enzymes, complex III and complex IV, were investigated using kinetic assays. The assays were used to evaluate and compare the effect of Mancozeb treatment on the mitochondrial activity of these two complexes in HT-29 cells. Complex III activity was tested on mitochondria isolated from untreated HT-29 cells and cells treated with 60 µM and 100 µM of Mancozeb for 24 hours. A concentration-dependent decrease in complex III enzyme activity was observed. Significant decrease in activity was observed in the mitochondria isolated from both treatment groups. [**0 µM MZ:** 0.0357±0.00360 units/µg protein; **60 µM MZ:** 0.0212±0.00327 units/µg protein; **100 µM MZ:** 0.0199±0.00192 units/µg protein] (Figure 5). The activity of complex IV was tested on mitochondria isolated from untreated HT-29 cells and cells treated with 60 µM, 100 µM, and 140 µM of Mancozeb for 24 hours. A significant and concentration-dependent decrease in complex IV enzyme

activity was observed for all treatment groups. [**0 µM MZ:** 0.983±0.0190 mOD/min; **60 µM MZ:** 0.490±0.0155 mOD/min; **100 µM MZ:** 0.210±0.0212 mOD/min; **140 µM MZ:** 0.229±0.0280 mOD/min] (Figure 6).

3.3 Scanning electron microscopy of Mancozeb treated HT-29 cells

Scanning electron microscopy was utilized to observe changes in cellular topography in Mancozeb exposed cells (0-160 µM MZ). Figure 7 and Figure 8 are representative micrographs of untreated HT-29 cells. Small cellular projections present on the surface of the cell are microvilli. Cells treated with 60 µM MZ appear similar in morphology to untreated cells (Figure 9 and Figure 10). Loss of cellular projections cause the cells to appear primarily smooth with some apparent surface blebbing after treatment with 80 and 100 µM MZ (Figures 11-14). Cells treated with 120 µM MZ appear completely smooth as there is complete loss of cellular projections and cellular blebbing is present (Figure 15 and Figure 16). Treatment with 140 and 160 µM MZ caused cells to appear completely smooth. Blebbing and deterioration of the plasma membrane were also present (Figures 17-20). Cell blebbing was quantified in micrographs (0, 60, 100, and 140 µM MZ) by determining the mean percentage of blebbed cells per field of view. The percentage of blebbed cells was significantly higher in 100 µM MZ cells as compared to untreated cells (Table 2). There was no significant difference in the percentage of blebbed cells in either the 60 µM or 140 µM MZ treatment groups as compared to untreated cells (Table 2).

3.4 Transmission electron microscopy of Mancozeb treated HT-29 cells

Transmission electron microscopy was utilized to investigate ultrastructural mitochondrial alterations after exposure of HT-29 cells to 100 µM MZ. Figures 21-24 are

representative micrographs of untreated HT-29 cells that have normal mitochondria with characteristic shape and intact and well-defined cristae. After treatment with 100 μM MZ, drastic alteration to cellular morphology was observed. Mitochondria were grossly swollen with loss of cristae after treatment with Mancozeb (Figures 25-29).

3.5 Mitochondrial Membrane Potential

To further investigate mitochondrial dysfunction resulting in apoptosis, mitochondrial membrane potential was measured in HT-29 cells exposed to Mancozeb concentrations of 60 μM, 100 μM, and 140 μM for 24 hours. Treatment resulted in a significant and concentration-dependent decrease in mitochondrial membrane potential for all treatment groups. [**0 μM MZ:** 192.08±3.20 RFU; **60 μM MZ:** 150.17±7.11 RFU; **100 μM MZ:** 14.42±0.85 RFU; **140 μM MZ**: 11.33±0.10 RFU] (Figure 30).

3.6 Cellular Reactive Oxygen Species

The production of cellular reactive oxygen species was measured in HT-29 cells exposed to concentrations of 60 μM, 100 μM, and 140 μM of Mancozeb for 24 hours. A significant increase in cellular reactive oxygen species was observed in cells treated with 100 μM and 140 μM of Mancozeb. [**0 μM MZ:** 20.17±0.58 RFU; **60 μM MZ:** 17.83±0.49 RFU; **100 μM MZ:** 46.17±2.97 RFU; **140 μM MZ:** 46.33±2.98 RFU] (Figure 31).

3.7 Mitochondrial Superoxide

To determine if Mancozeb exposure resulted in alterations in mitochondrial reactive oxygen species, HT-29 cells were exposed to concentrations of 60 μM, 100 μM, and 140 μM of Mancozeb for 24 hours and mitochondrial superoxide levels were measured. A significant increase in mitochondrial superoxide levels was observed for

cells treated with 100 µM and 140 µM of Mancozeb. [**0 µM MZ:** 26.05±0.69 RFU; **60 µM MZ:** 34.43±2.87 RFU; **100 µM MZ:** 93.48±4.02 RFU; **140 µM MZ:** 82.14±3.60 RFU] (Figure 32).

3.8 Superoxide Dismutase 2

Superoxide dismutase 2 protein levels were measured in HT-29 cells exposed to concentrations of 60 µM, 100 µM, and 140 µM of Mancozeb for 24 hours. Superoxide dismutase 2 protein levels were significantly increased in cells treated with 100 µM and 140 µM of Mancozeb. [**0 µM MZ:** 2748.04±12.02 ng/mL; **60 µM MZ:** 2372.39±26.05 ng/mL; **100 µM MZ:** 3549.56±215.40 ng/mL; **140 µM MZ:** 3999.33±242.70 ng/mL] (Figure 33).

3.9 Total Antioxidant Capacity

To evaluate if Mancozeb exposure resulted in altered total antioxidant capacity, HT-29 cells were exposed to concentrations of 60 µM, 100 µM, and 140 µM of Mancozeb for 24 hours. A concentration-dependent decrease in total antioxidant capacity was observed. Cells treated with concentrations of 100 and 140 µM Mancozeb had a significant decrease in total antioxidant capacity. [**0 µM MZ:** 0.288±0.0379 antioxidant mM/µg protein; **60 µM MZ:** 0.194±0.0220 antioxidant mM/µg protein; **100 µM MZ:** 0.172±0.0272 antioxidant mM/µg protein; **140 µM MZ:** 0.142±0.00555 antioxidant mM/µg protein] (Figure 34).

3.10 Mitoquinol Antioxidant Study

The effects of Mitoquinol (MitoQ) as a mitochondrial antioxidant were evaluated by conducting both a co-treatment (MitoQ and Mancozeb) and pre-treatment (MitoQ followed by Mancozeb). Cell viability following co-treatment and pre-treatment were

evaluated using the MTT assay. The cytotoxic effect of MitoQ on HT-29 cells was determined using the MTT assay and exposing cells to concentrations of 0.5 µM, 0.75 µM, 1.0 µM, 1.5 µM, and 2.0 µM MitoQ for 24 hours. Cell viability was observed as cells were 97.56±0.62%, 98.21±0.86%, 96.70±0.96%, 92.61±1.22%, 87.68±2.41% viable at concentrations of 0.5 µM, 0.75 µM, 1.0 µM, 1.5 µM, and 2.0 µM respectively, compared to untreated cells. Significant reductions in cell viability were observed at concentrations of 1.5 µM and 2.0 µM MitoQ after 24 hours of treatment when compared to untreated cells (Figure 35). Therefore, for co-treatment and pre-treatment experiments concentrations of 1.5 µM and 2.0 µM MitoQ were excluded. Co-treatment with MitoQ and Mancozeb for 24 hours caused a significant decrease in cell viability for all co-treatment groups as compared to untreated cells. [**0 µM:**100±0.00%; **0.75 µM MitoQ:**100±1.49%; **1 µM MitoQ:** 99.45±2.21%; **100 µM MZ:** 52.53±1.41%; **0.75 µM MitoQ+100 µM MZ:** 55.14±0.97%; **1 µM MitoQ+100 µM MZ:** 52.51±1.10%] (Figure 36). Pre-treatment with MitoQ for 12 hours followed by Mancozeb exposure for 24 hours resulted in a significant decrease in cell viability for all pre-treatment groups as compared to untreated cells. [**0 µM:**100±0.00%; **0.5 µM MitoQ:** 94.69±1.10%; **0.75 µM MitoQ:** 94.21±1.48%; **100 µM MZ:** 55.21±2.44%; **0.5 µM MitoQ+100 µM MZ:** 55.91±2.16%; **0.75µM MitoQ+100 µM MZ:** 59.16±2.99%] (Figure 37).

3.11 BHT Antioxidant Study

The effects of butylated hydroxytoluene (BHT) as a cellular antioxidant were evaluated by conducting both a co-treatment (BHT and Mancozeb) and pre-treatment (BHT followed by Mancozeb). Cell viability following co-treatment and pre-treatment were evaluated using the MTT assay. The cytotoxic effect of BHT on HT-29 cells was

determined using the MTT assay and exposing cells to concentrations of 25 µM, 50 µM, 75 µM, and 100 µM BHT for 24 hours. Cell viability was observed as cells were 98.567±1.18%, 97.74±1.08%, 98.93±1.097%, 99.56±1.45% viable at concentrations of 25 µM, 50 µM, 75 µM, and 100 µM respectively, compared to untreated cells. No significant reductions in cell viability were observed after 24 hours of BHT treatment when compared to untreated cells (Figure 38). Co-treatment with BHT and Mancozeb for 24 hours caused a significant decrease in cell viability for all co-treatment groups as compared to untreated cells. [**0 µM:**100±0.00%; **100 µM MZ:**53.75±0.89%; **25 µM BHT+100 µM MZ:** 54.01±0.84%; **50 µM BHT+100 µM MZ:** 55.00±0.74%; **75 µM BHT+100 µM MZ:** 56.18±1.19%; **100 µM BHT+100 µM MZ:** 55.88±1.20%] (Figure 39). Pre-treatment with BHT for 12 hours followed by Mancozeb exposure for 24 hours resulted in a significant decrease in cell viability for all pre-treatment groups as compared to untreated cells. [**0 µM:**100±0.00%; **100 µM MZ:**52.10±0.86%; **25 µM BHT+100 µM MZ:** 40.56±1.09%; **50 µM BHT+100 µM MZ:** 41.06±1.03%; **75 µM BHT+100 µM MZ:** 40.69±1.20%; **100 µM BHT+100 µM MZ:** 40.10±1.24%] (Figure 40).

MZ Concentration (μM)	Percent Viability (%)		
	94.1% Purity	97.5% Purity	99.6% Purity
0	100±0.00	100±0.00	100±0.00
40	90.67±1.69 ***	94.20±1.64***	88.39±1.31***
60	83.62±1.34***	83.36±1.53***	83.34±1.41***
80	75.44±1.64***	69.20±1.38***	72.88±1.03***
100	63.78±2.28***	54.76±1.34***	55.47±1.05***
120	56.95±1.92***	39.34±0.65***	41.63±1.09***
140	55.34±1.26***	24.98±1.24***	28.34±0.80***
160	49.63±1.31***	6.58±0.87***	12.51±0.70***
180	40.89±1.28***	2.96±0.39***	2.84±0.24***
200	36.22±1.53***	2.51±0.45***	2.29±0.77***
Calculated LC_{50} (μM)	153.90	104.21	105.82

Table 1: Cytotoxicity of MZ on HT-29 cells as determined by the MTT Assay.

HT-29 cells were treated for 24 hours with various concentrations ranging from 40-200 μM MZ. Significant decreases in cell viability were observed from 40-200 μM MZ treatment groups as compared to untreated cells for various purities of MZ. Data represent mean as a percentage of control ± SEM of three independent experiments (n=4). Data were analyzed using a one-way ANOVA followed by Tukey's Multiple Comparison post-hoc test. ***$p<0.001$.

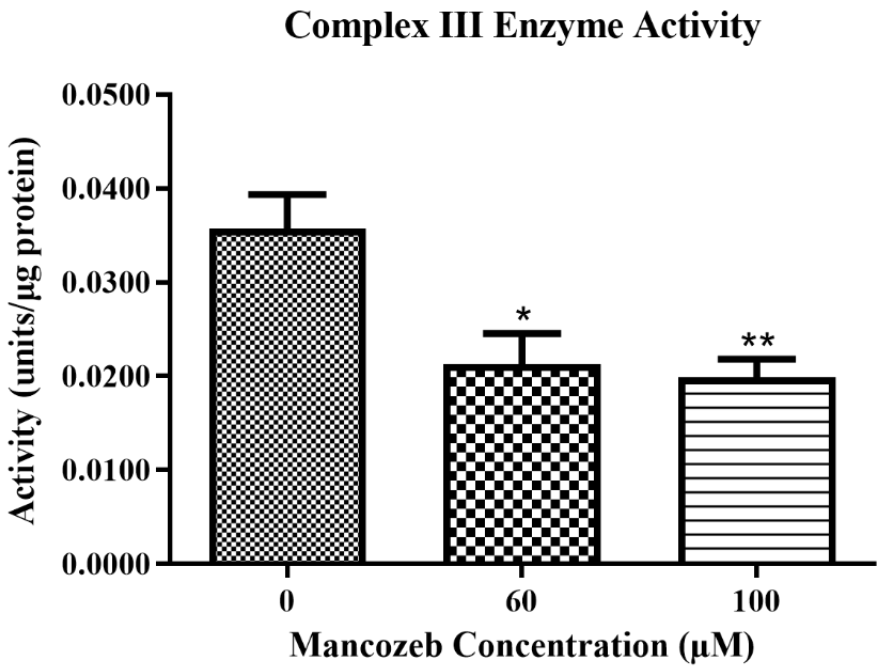

Figure 5: Complex III Enzyme Activity of Mitochondria Isolated from HT-29 cells treated with Mancozeb.

HT-29 cells were treated with 60 µM and 100 µM of Mancozeb for 24 hours before mitochondrial isolation. Significant decreases in complex III enzyme activity were observed for both treatment groups as compared to control. Results are expressed as the rate of activity divided by protein content. The experiment was performed in duplicate. Control (n=8), 60 µM and 100 µM (n=4). Data was analyzed using a one-way ANOVA followed by Tukey's Multiple Comparison post-hoc test. *Significantly different from control, $p<0.05$.**Significantly different from control, $p<0.01$.

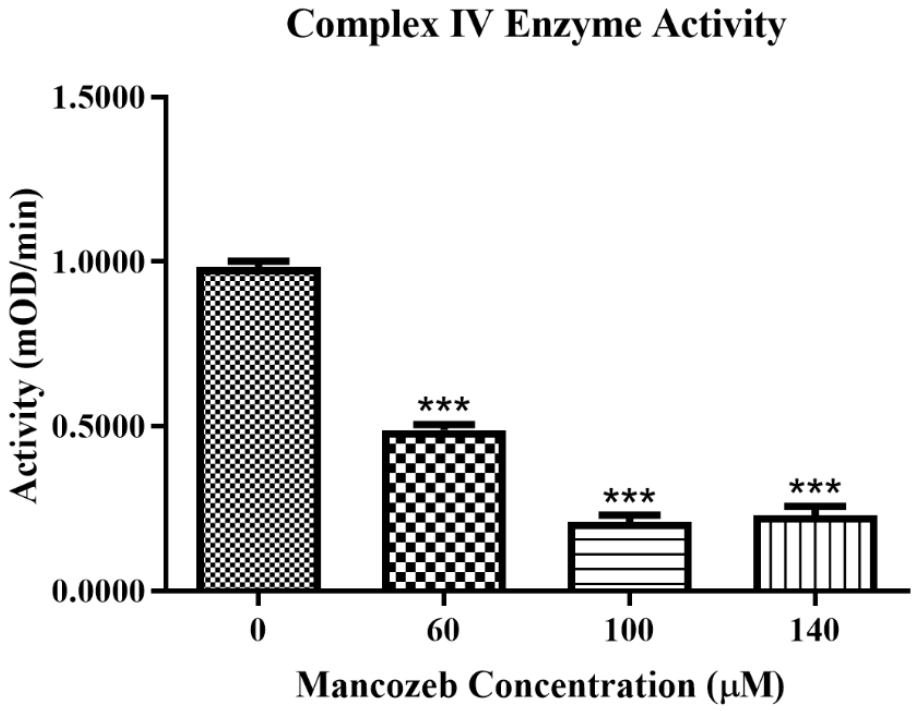

Figure 6: Complex IV Enzyme Activity of Mitochondria Isolated from HT-29 cells treated with Mancozeb.

HT-29 cells were treated with 60 μM, 100 μM, and 140 μM of Mancozeb for 24 hours before mitochondrial isolation. Significant decreases in complex IV enzyme activity were observed for all treatment groups as compared to control. Results are expressed as the rate of activity. The experiment was performed in triplicate. Control and 100 μM (n=4), 60 μM (n=5), and 140 μM treatment groups (n=3). Data was analyzed using a one-way ANOVA followed by Tukey's Multiple Comparison post-hoc test. ***Significantly different from control, $p<0.001$.

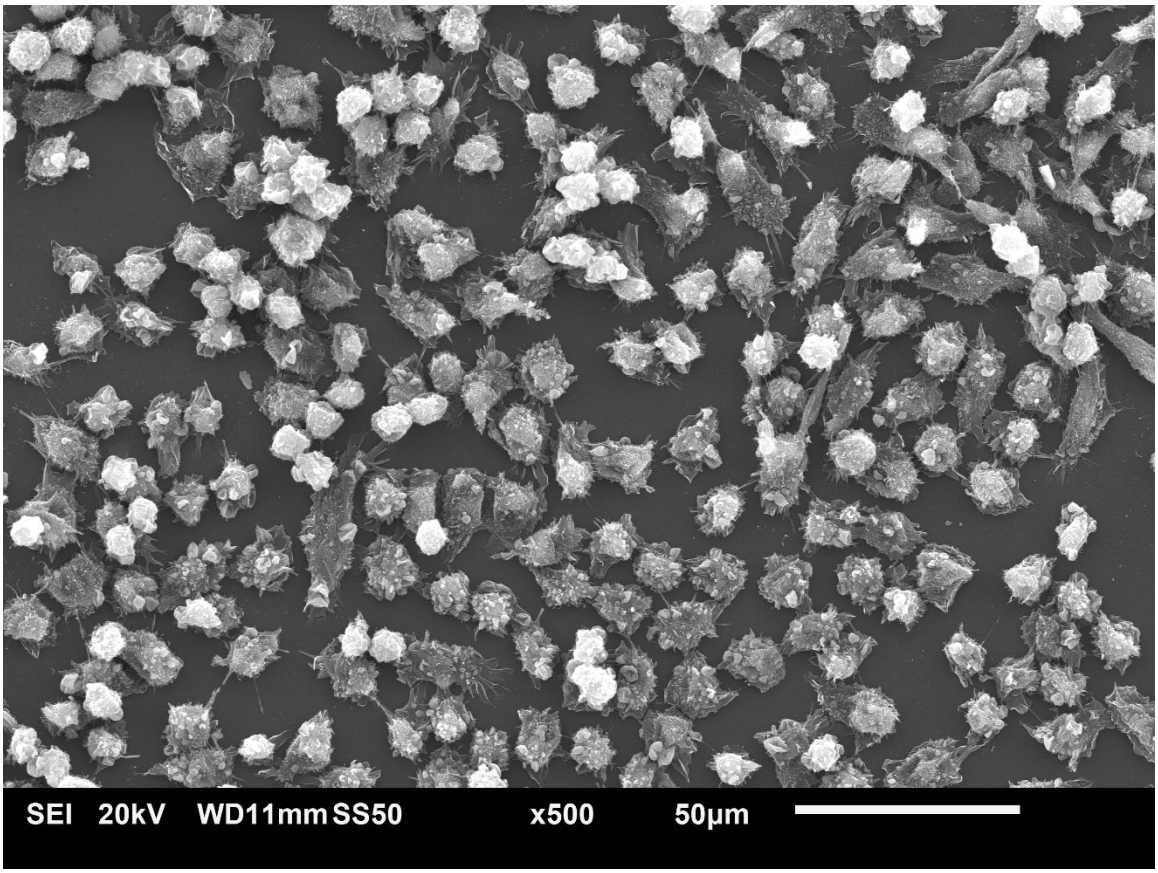

Figure 7: Low power scanning electron micrograph of HT-29 cells.

Representative micrograph of untreated cells. The small cellular projections on the surface of the cells are microvilli, which are characteristic of the cell line. Total magnification, x500.

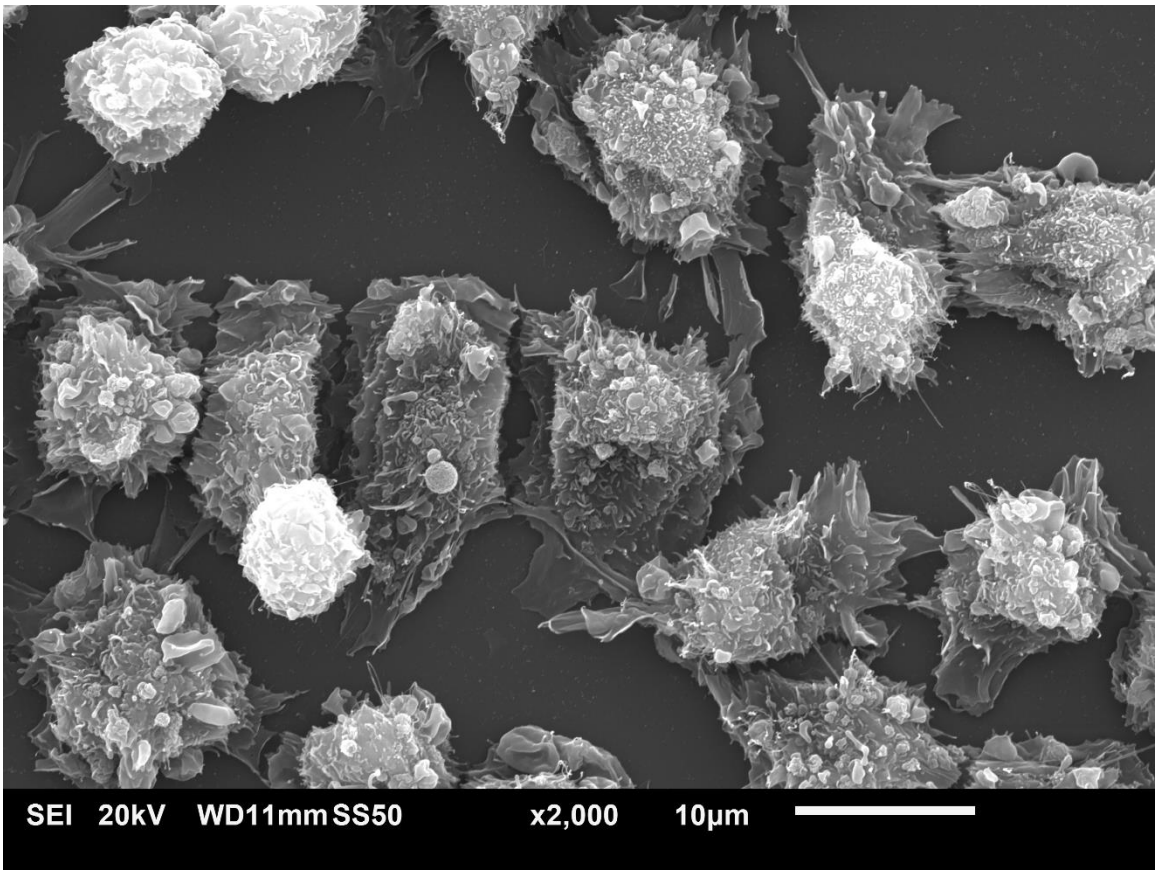

Figure 8: High power scanning electron micrographs of HT-29 cells.

Representative micrograph of untreated cells. The small cellular projections on the surface of the cells are microvilli, which are characteristic of this cell line. Total magnification, x2,000.

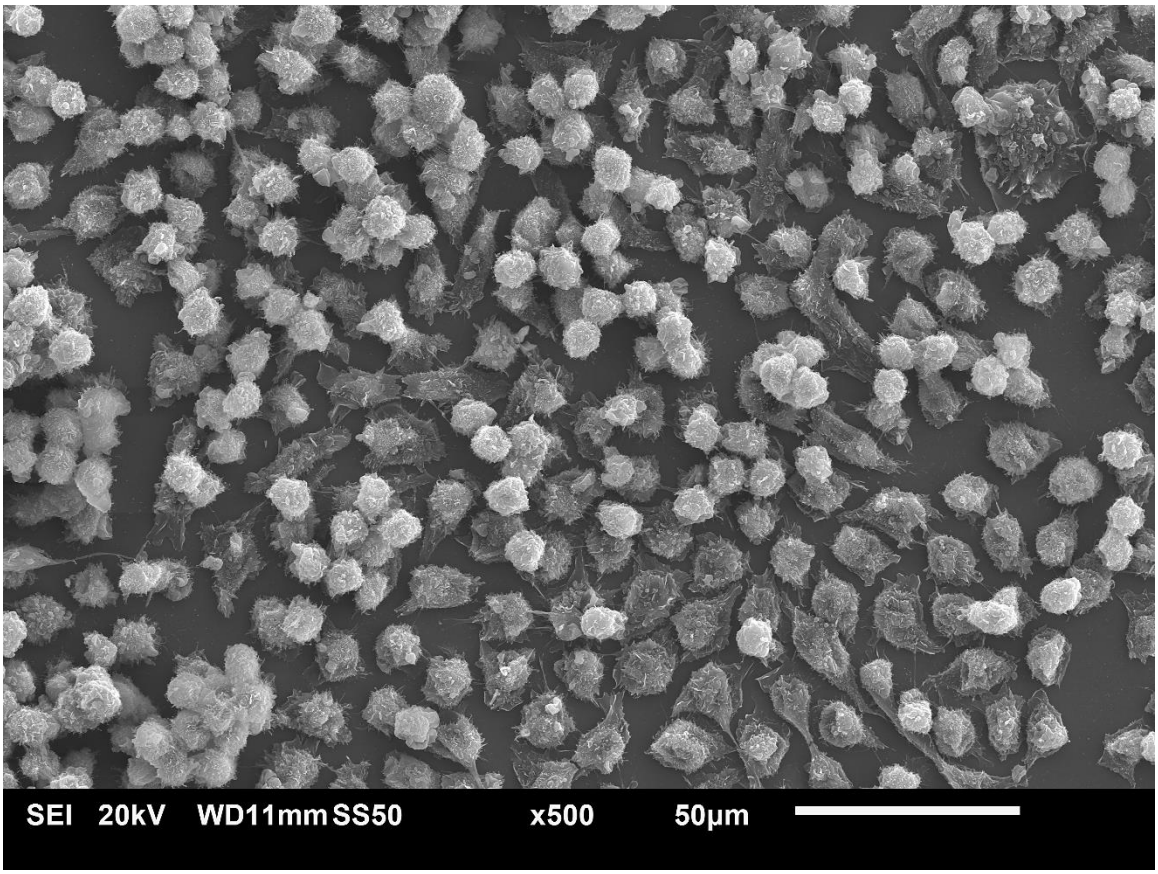

Figure 9: Low power scanning electron micrograph of HT-29 cells treated with 60 µM Mancozeb.

Micrograph is representative of cells treated with 60 µM Mancozeb for 24 hours. Cells appear similar in morphology to untreated cells. Total magnification, x500.

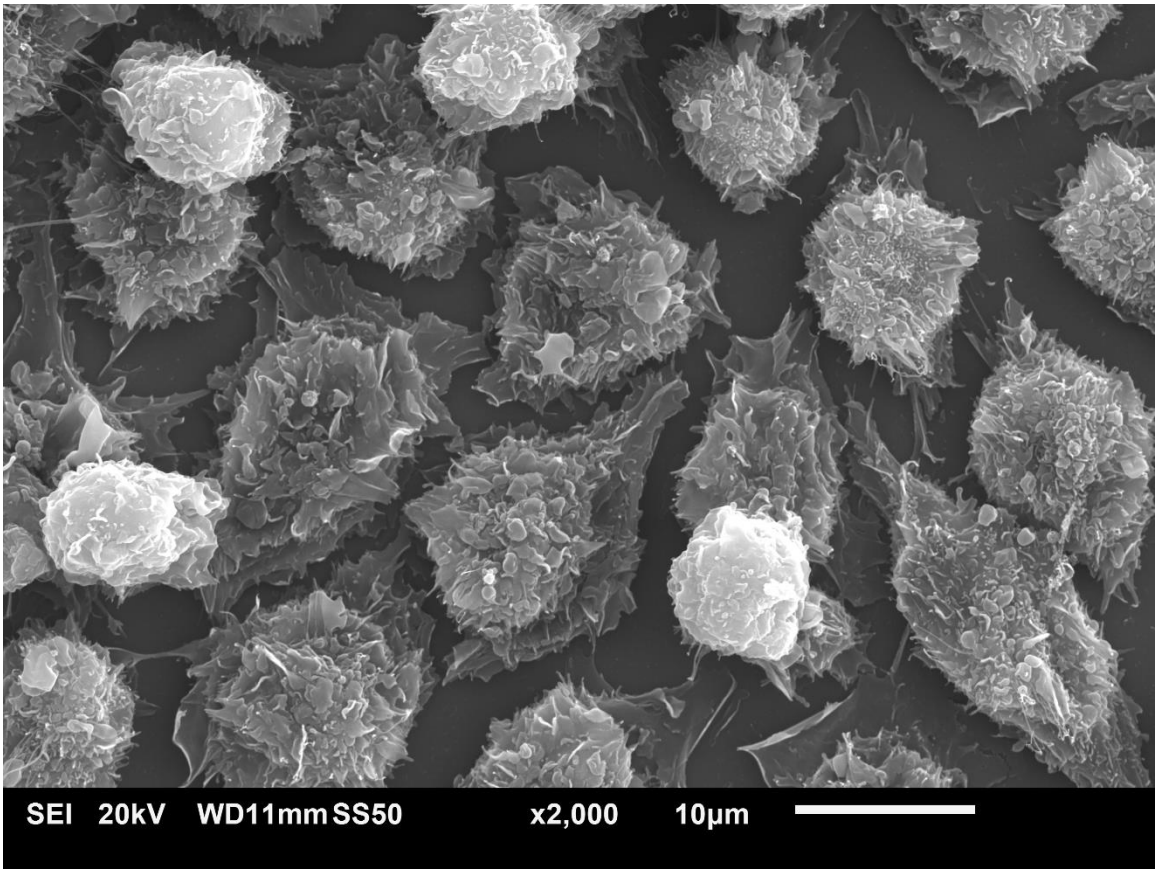

Figure 10: High power scanning electron micrograph of HT-29 cells treated with 60 µM Mancozeb.

Micrograph is representative of cells treated with 60 µM Mancozeb for 24 hours. Cells appear similar in morphology to untreated cells. Total magnification, x2,000.

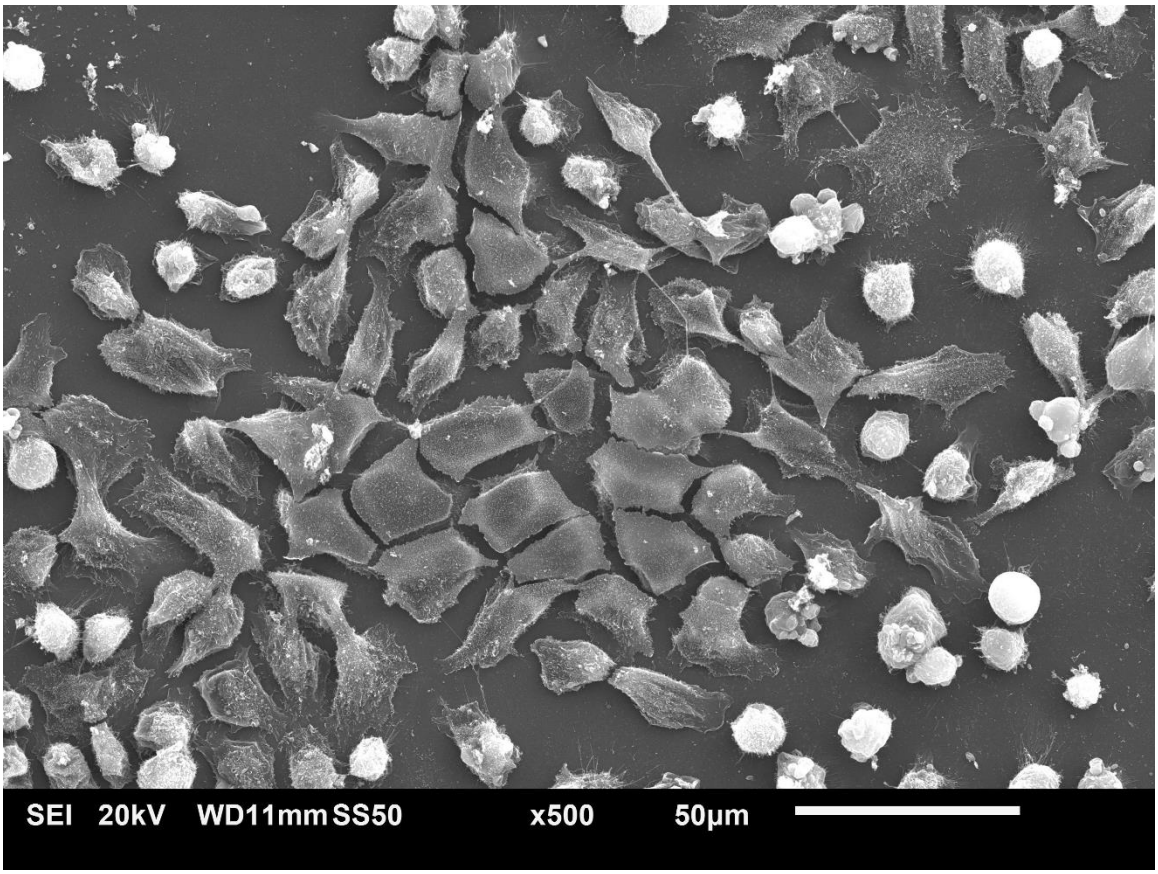

Figure 11: Low power scanning electron micrograph of HT-29 cells treated with 80 µM Mancozeb.

Micrograph is representative of cells treated with 80 µM Mancozeb for 24 hours. Cells appear primarily smooth with loss of cellular projections. Some blebbing is observed. Total magnification, x500.

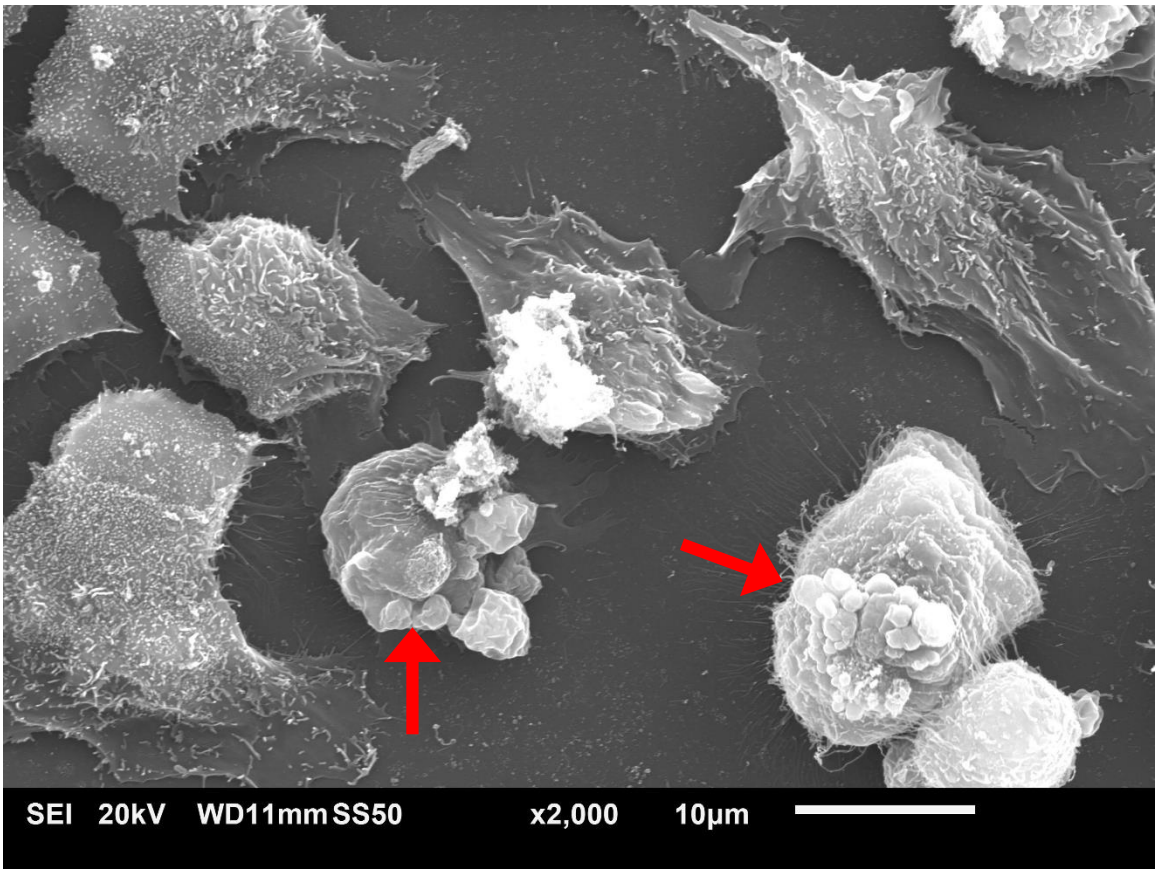

Figure 12: High power scanning electron micrograph of HT-29 cells treated with 80 µM Mancozeb.

Micrograph is representative of cells treated with 80 µM Mancozeb for 24 hours. Cells appear smooth as there is loss of cellular projections and blebbing (arrows) is present. Total magnification, x2,000.

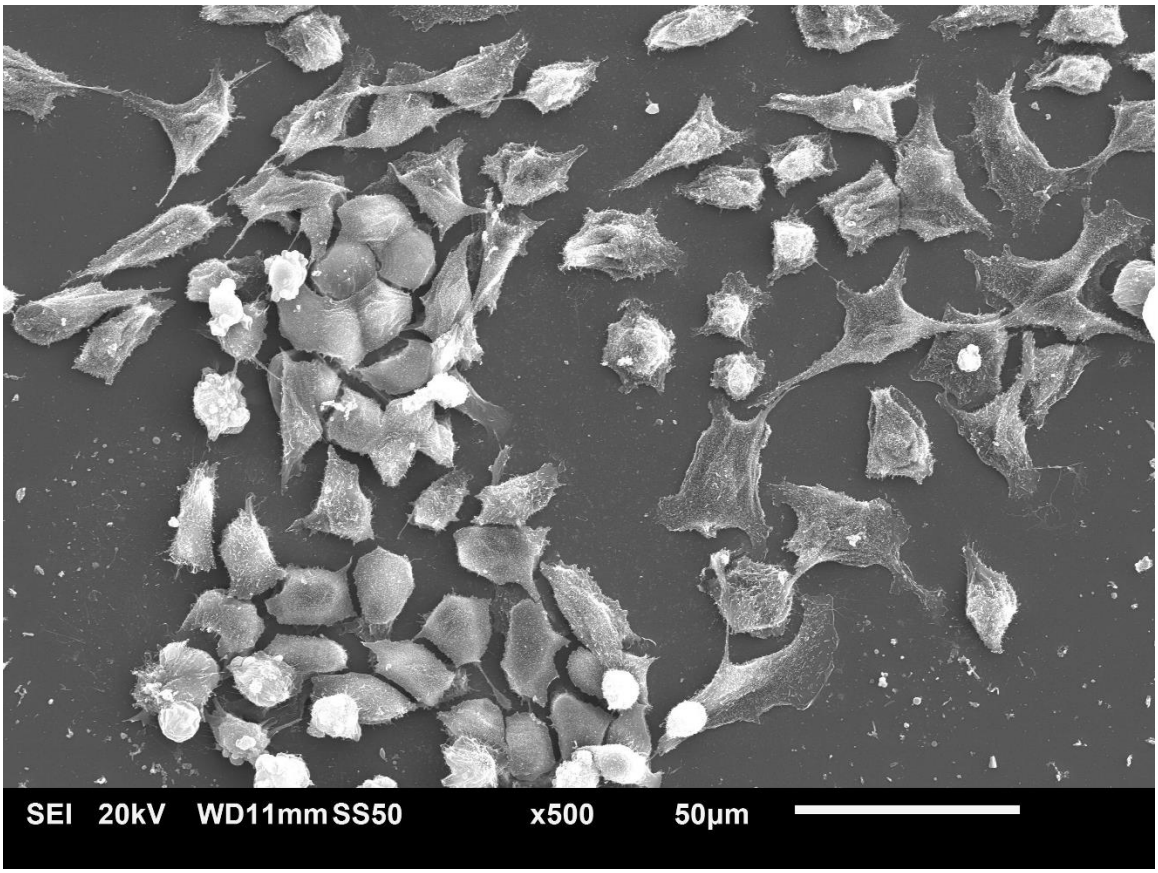

Figure 13: Low power scanning electron micrograph of HT-29 cells treated with 100 µM Mancozeb.

Micrograph is representative of cells treated with 100 µM Mancozeb for 24 hours. Cells appear smooth as there is loss of cellular projections and blebbing is present. Total magnification, x500.

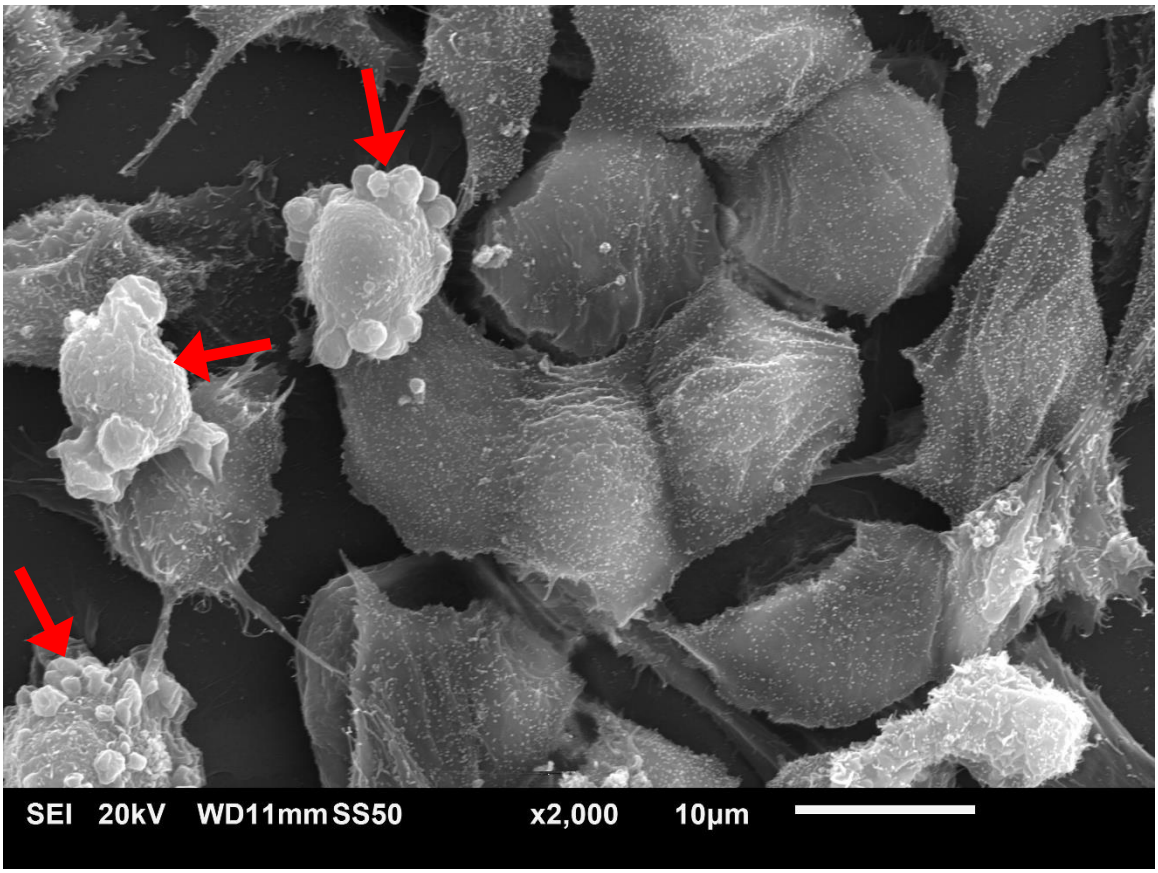

Figure 14: High power scanning electron micrograph of HT-29 cells treated with 100 µM Mancozeb.

Micrograph is representative of cells treated with 100 µM Mancozeb for 24 hours. Cells appear primarily smooth and demonstrate greatly reduced microvilli. Cell surface blebbing (arrows) is present. Total magnification, x2,000.

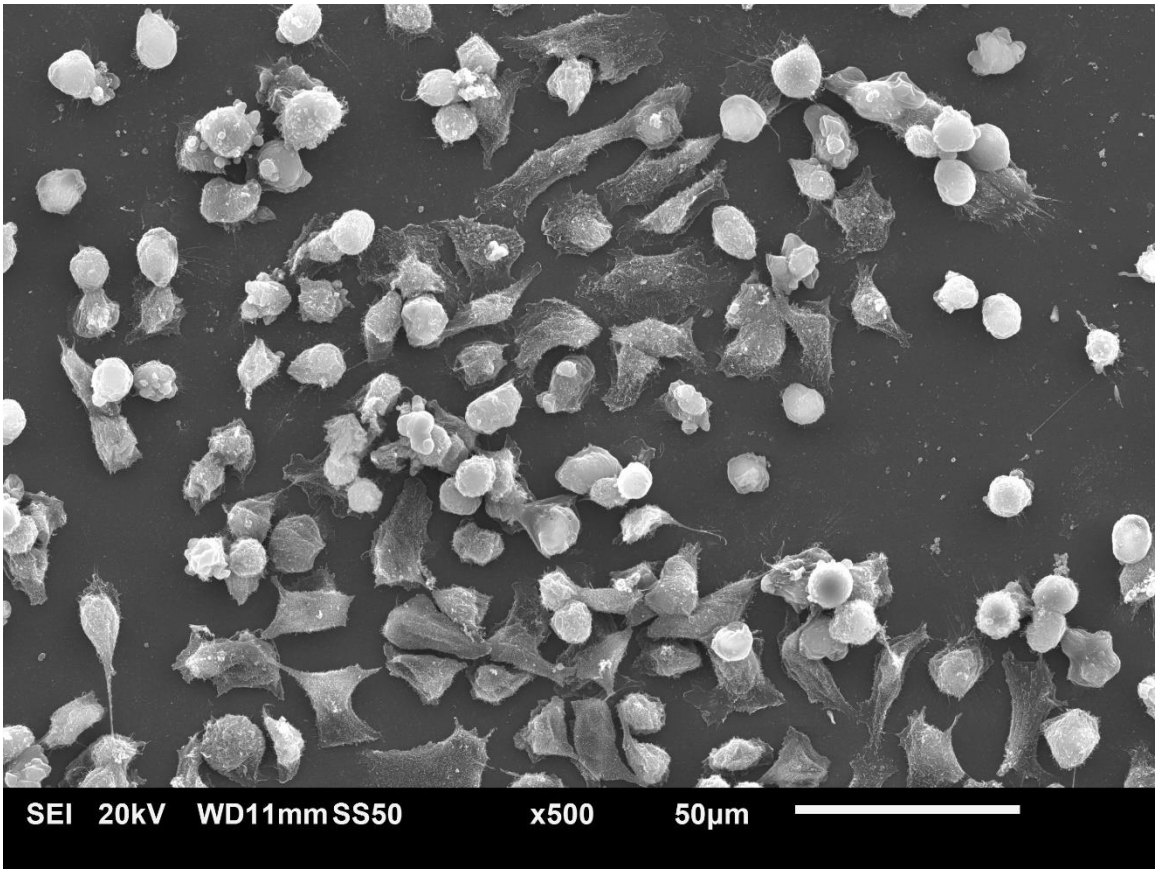

Figure 15: Low power scanning electron micrograph of HT-29 cells treated with 120 µM Mancozeb.

Micrograph is representative of cells treated with 120 µM Mancozeb for 24 hours. Numerous rounded cells and cells devoid of cellular projections are noted. Cell surface blebbing is noted. Total magnification, x500.

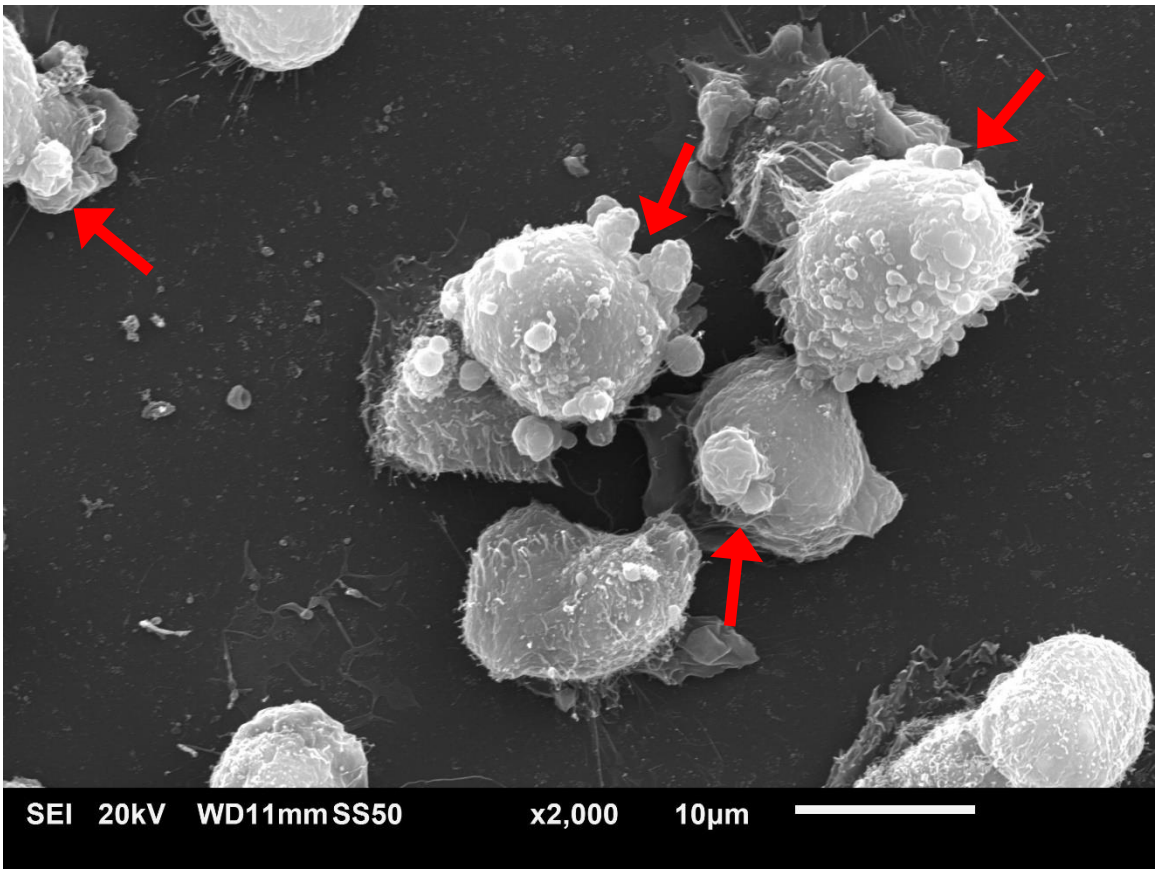

Figure 16: High power scanning electron micrograph of HT-29 cells treated with 120 µM Mancozeb.

Micrograph is representative of cells treated with 120 µM Mancozeb for 24 hours. Cells appear completely smooth as there is loss of cellular projections and blebbing (arrows) is present. Total magnification, x2,000.

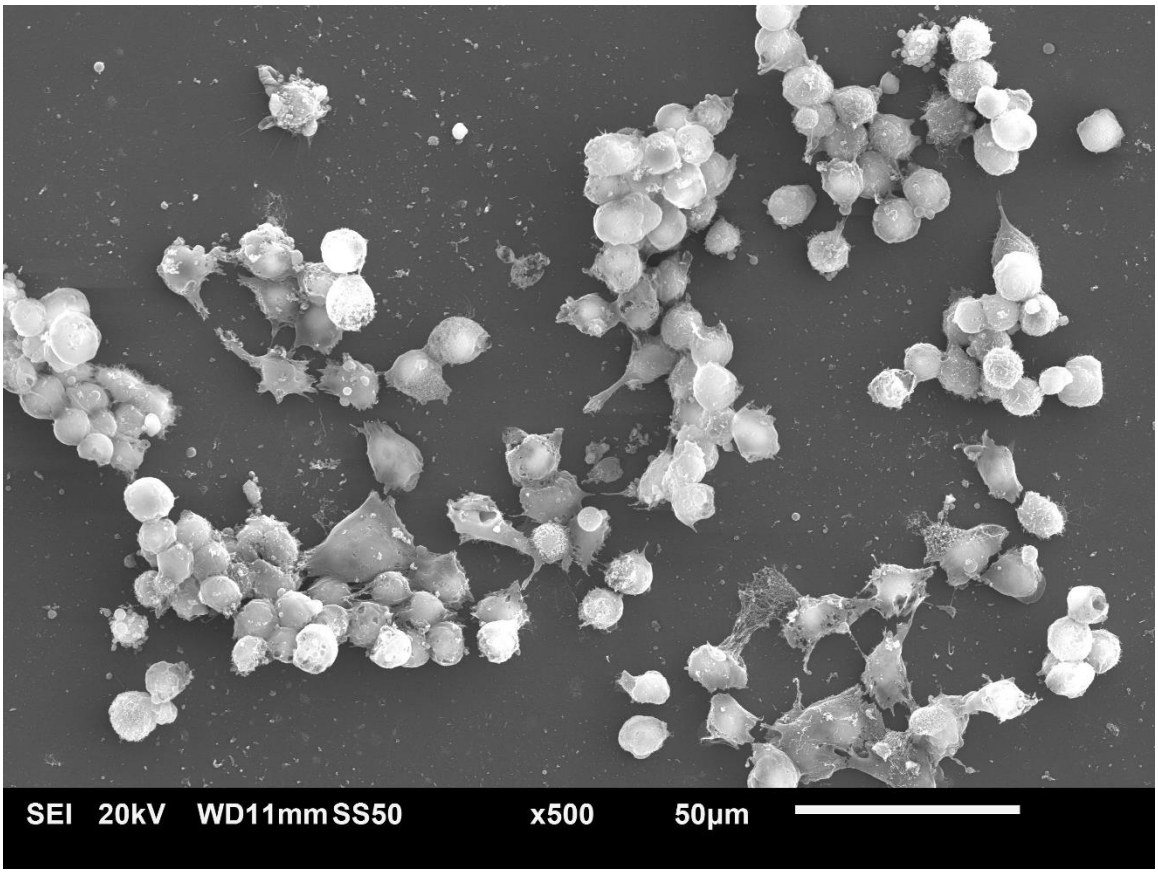

Figure 17: Low power scanning electron micrograph of HT-29 cells treated with 140 µM Mancozeb.

Micrograph is representative of cells treated with 140 µM Mancozeb for 24 hours. Cells are primarily rounded with complete loss of cellular projections. Blebbing and cell surface changes are present. Total magnification, x500.

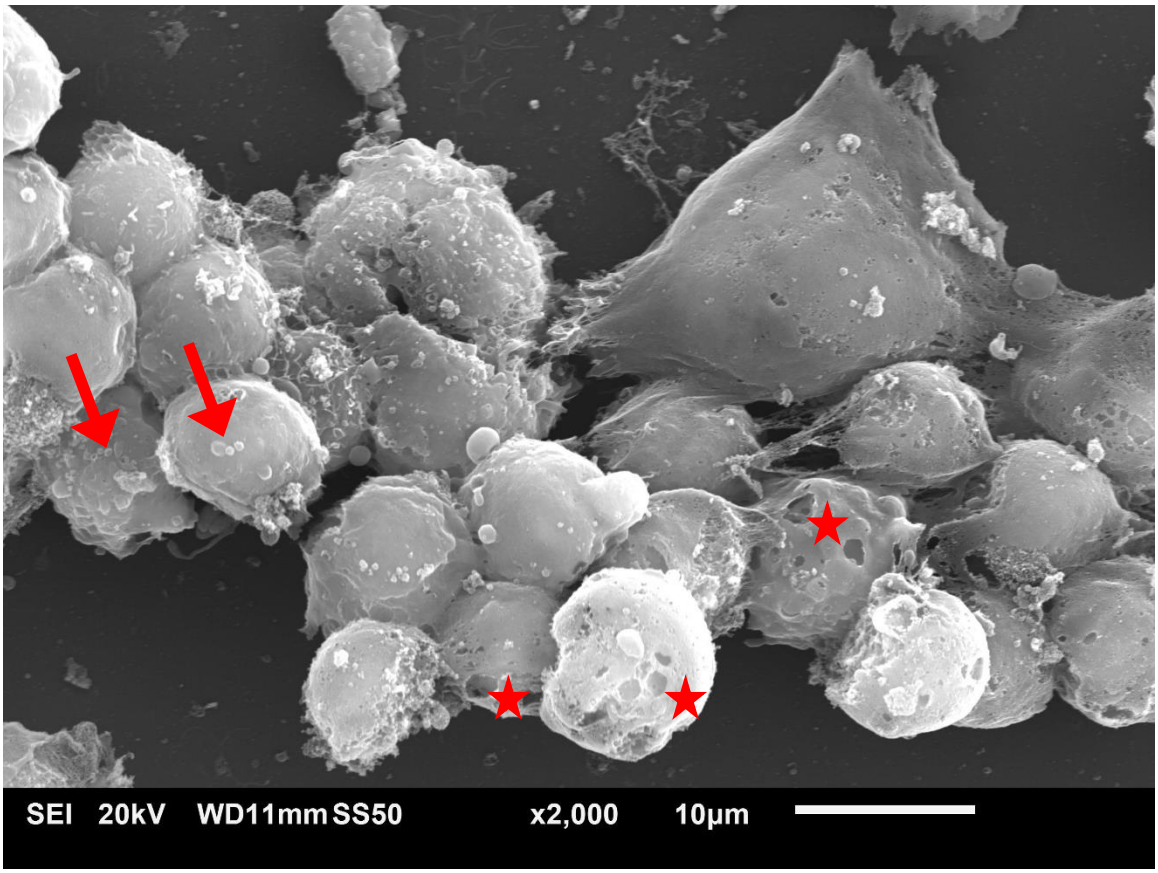

Figure 18: High power scanning electron micrograph of HT-29 cells treated with 140 µM Mancozeb.

Micrograph is representative of cells treated with 140 µM Mancozeb for 24 hours. Cells appear completely smooth as there is a complete loss of cellular projections. Blebbing (arrows) and visual deterioration in plasmalemma (stars) are apparent. Total magnification, x2,000.

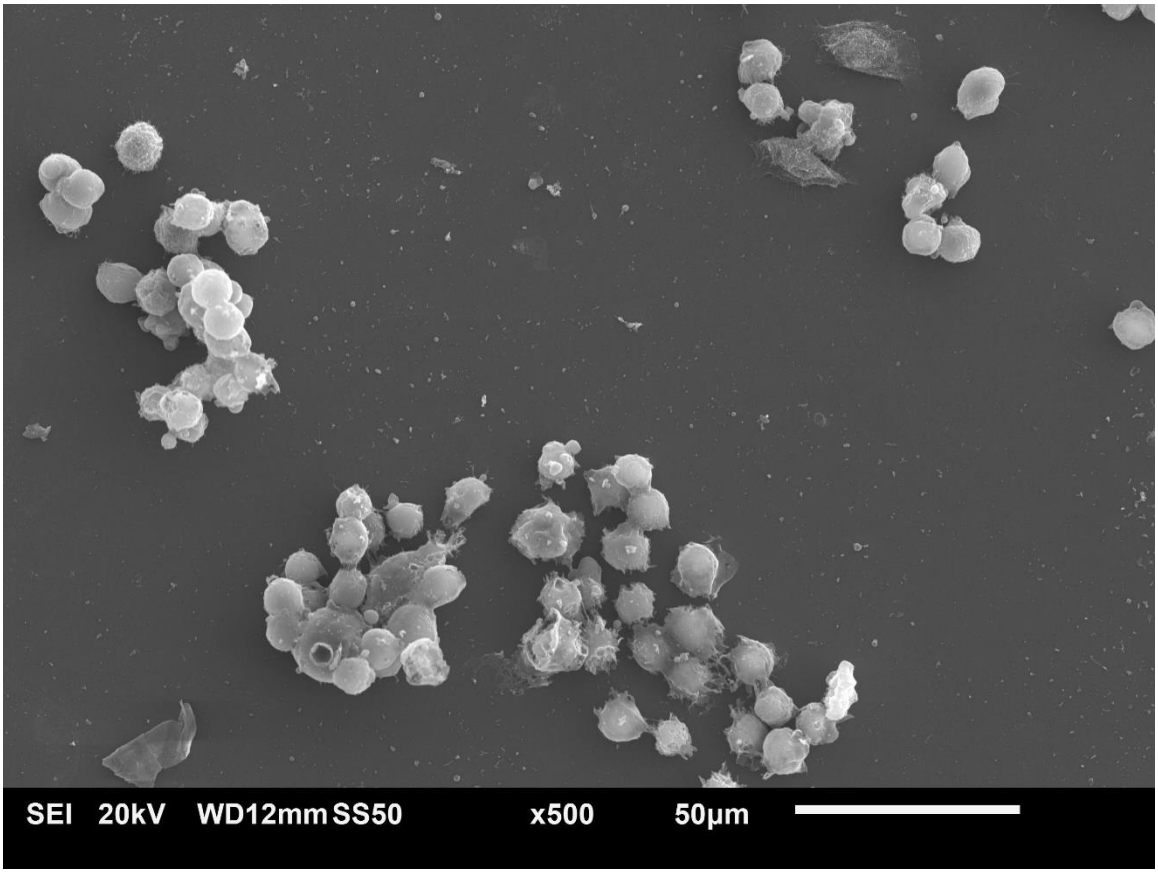

Figure 19: Low power scanning electron micrograph of HT-29 cells treated with 160 µM Mancozeb.

Micrograph is representative of cells treated with 160 µM Mancozeb for 24 hours. There is a visible loss of cells. Cells are rounded and completely smooth as there is complete loss of microvilli. Visual deterioration in plasmalemma is present. Total magnification, x500.

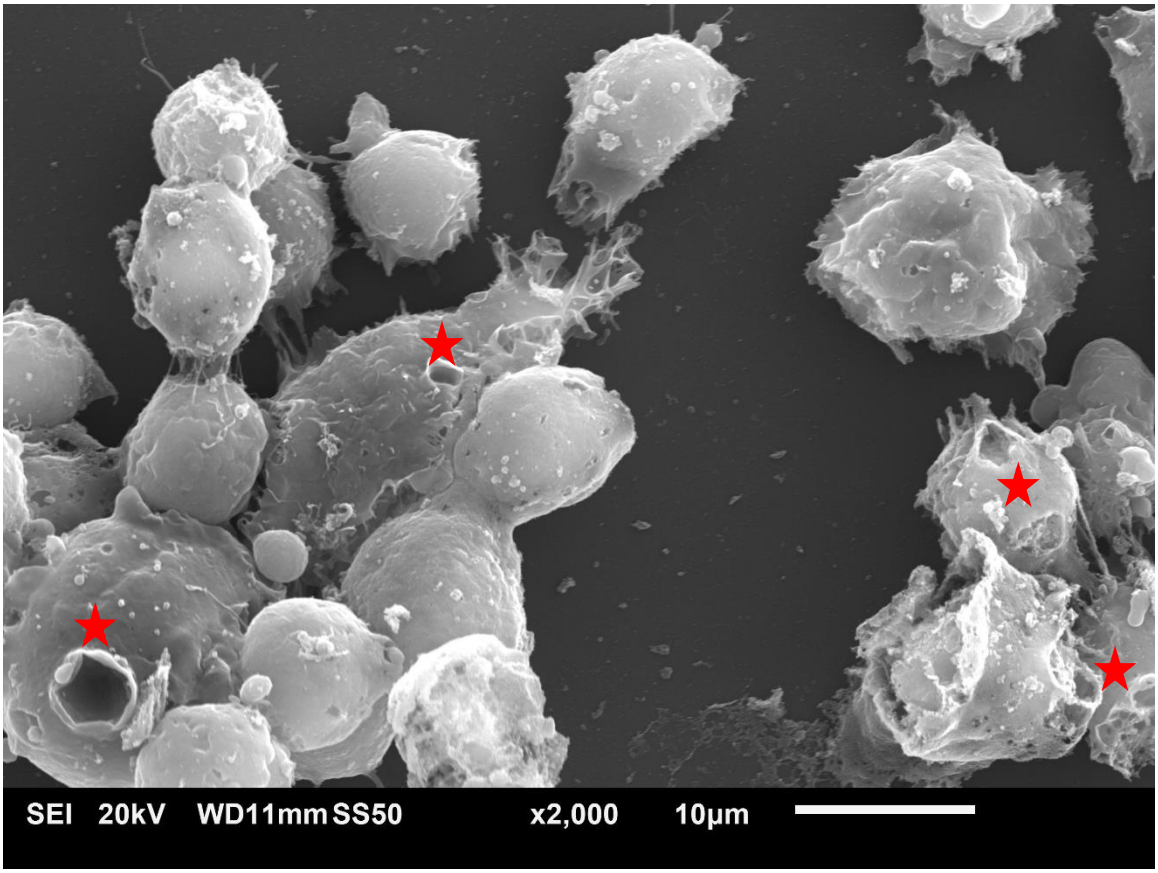

Figure 20: High power scanning electron micrograph of HT-29 cells treated with 160 µM Mancozeb.

Micrograph is representative of cells treated with 160 µM Mancozeb for 24 hours. Cells appear completely smooth as there is loss of cellular projections and visual deterioration in plasmalemma (stars) are present. Total magnification, x2,000.

Cell Blebbing Quantitation			
Concentration (μM)	Fields of View (N)	Mean Percentage of Blebbed Cells	Mean Rank
0	20	3.382±1.105	33.20
60	20	1.982±1.052	24.95
100	20	27.12±5.046	64.08***
140	20	7.572±1.867	39.78

Table 2: Quantification of cell blebbing of HT-29 cells treated with MZ.

HT-29 cells were treated for 24 hours with MZ (60 μM, 100 μM, and 140 μM). Cell blebbing was quantitated in SEM micrographs by determining the mean percentage of blebbed cells per field of view. A significant increase in the percentage of blebbed cells was observed at 100 μM MZ as compared to control. Data represent mean ± SEM of twenty fields of view (n=20). Ranking was done using a Kruskal-Wallis Test and followed by Dunn's Multiple Comparison post-hoc test. ***$p<0.001$.

Figure 21: Transmission electron micrograph of HT-29 cells.

Micrograph is representative of a monolayer of untreated cells. The cytoplasm of cells contains numerous dense polyribosomes. Microvilli (stars) are present on the border of cells. Cell to cell interface denoted by arrowhead. The nuclei (N) have well defined borders and there is no evidence of nuclear disruption. Total magnification, x6,000.

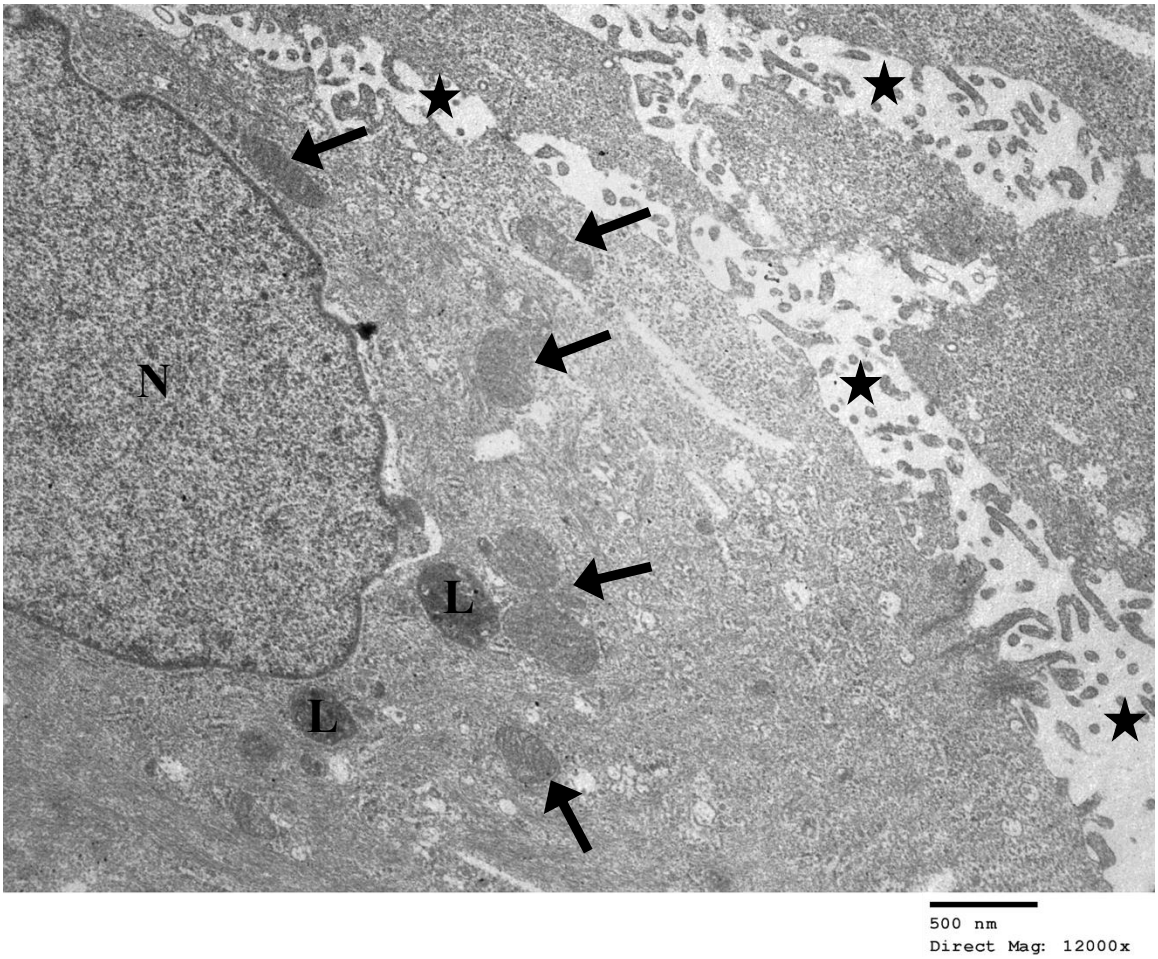

Figure 22: Transmission electron micrograph of HT-29 cells.

This micrograph is representative of untreated cells with mitochondria that are oval and have intact membranes and well-defined cristae (arrows). Nucleus (N) has a defined border and there is no evidence of nuclear disruption. Lysosomes (L) are present. Microvilli (stars) are also present on the border of the cell. Total magnification, x12,000.

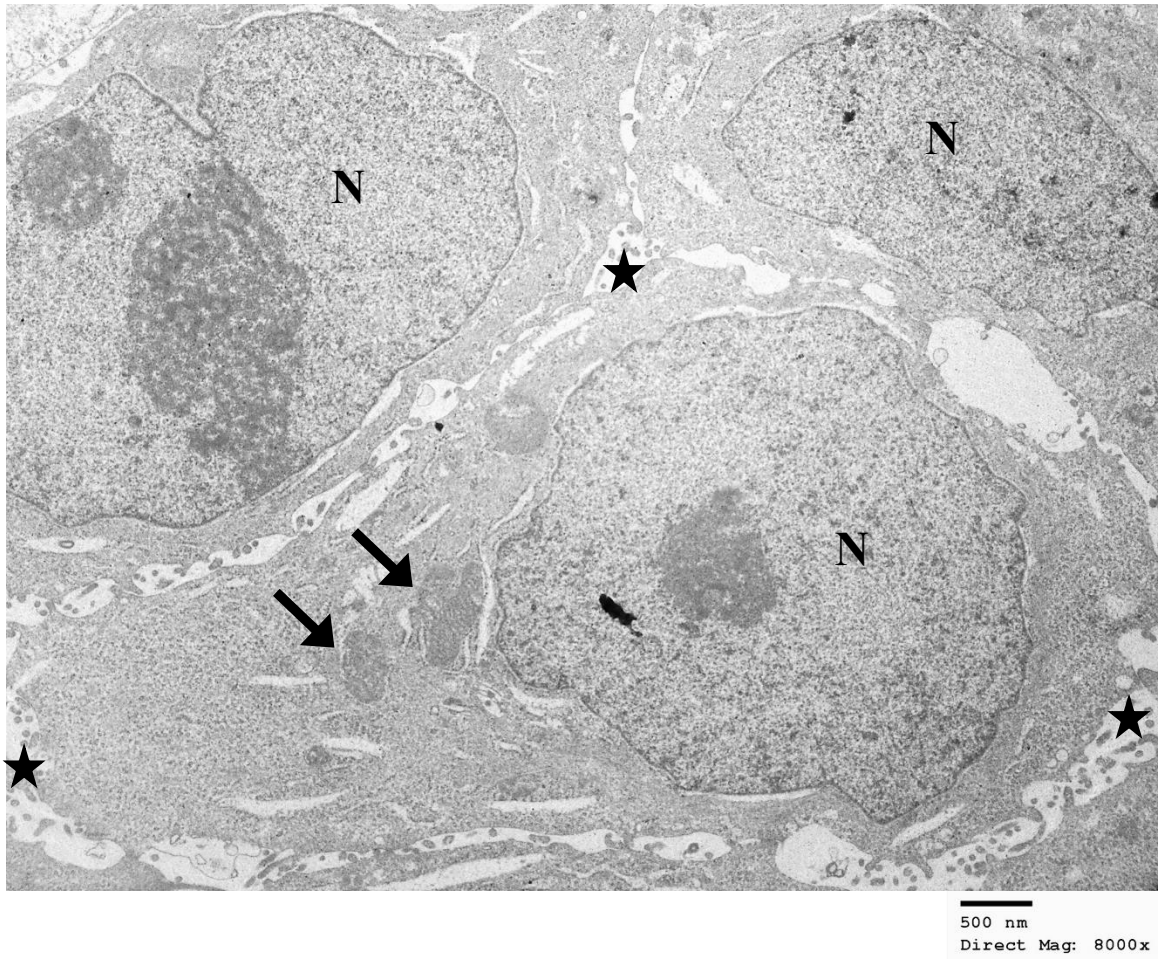

Figure 23: Transmission electron micrograph of HT-29 cells.

This micrograph is representative of untreated cells with nuclei (N) that have well-defined borders with no evidence of nuclear disruption. Mitochondria are oval in shape and have intact membranes and well-defined cristae (arrows). Microvilli (stars) are also present on the border of the cell. Total magnification, x8,000.

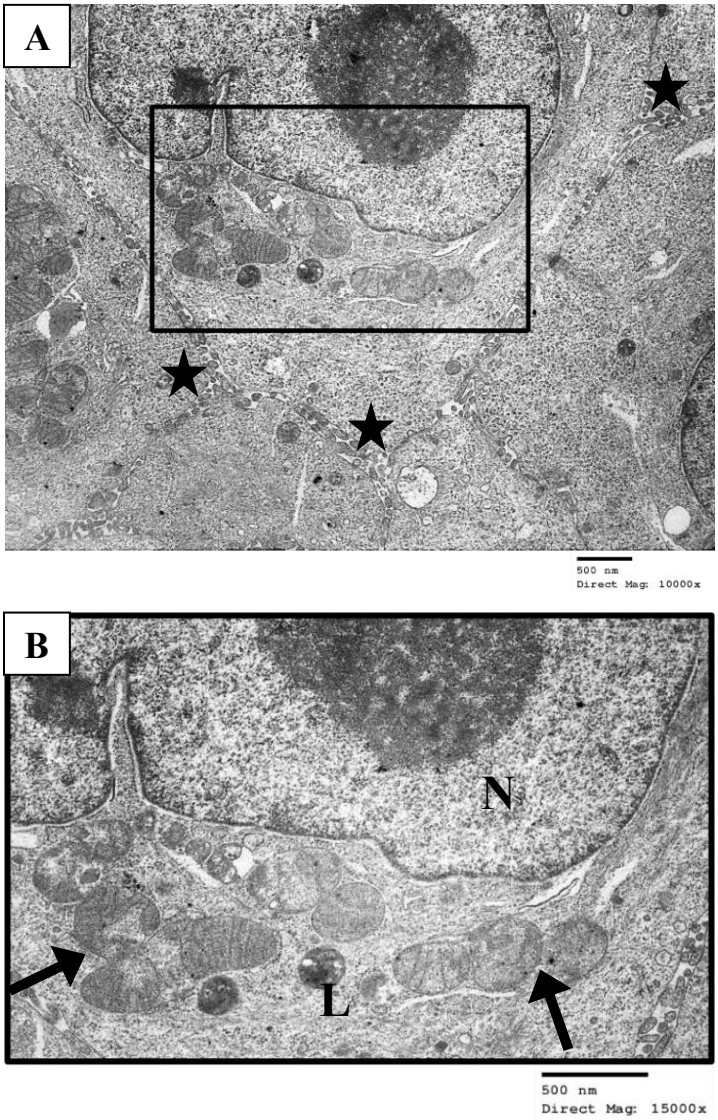

Figure 24: Transmission electron micrograph of HT-29 cells.

A. Micrograph is representative of untreated cells with characteristic mitochondria. Microvilli (stars) are present between border of cells. Total magnification, x10,000. **B.** Mitochondria have intact membranes and well-defined cristae (arrows). Nucleus (N) and lysosome (L) are also present. Total magnification, x15,000.

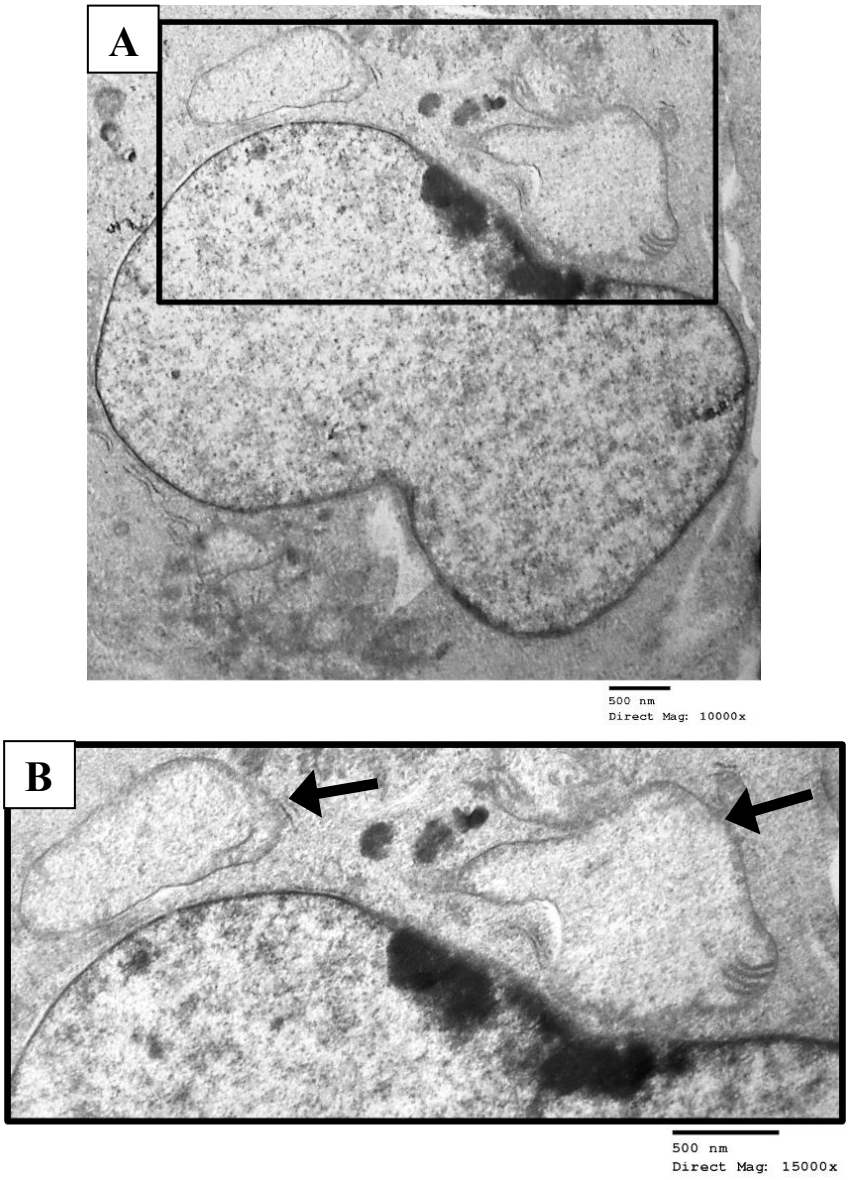

Figure 25: Transmission electron micrograph of HT-29 cells treated with 100 µM MZ.

A. Micrograph is representative of cells treated with 100 µM Mancozeb for 24 hours. Total magnification, x10,000. **B** Mitochondria are grossly swollen with loss of cristae (arrows). Total magnification, x15,000.

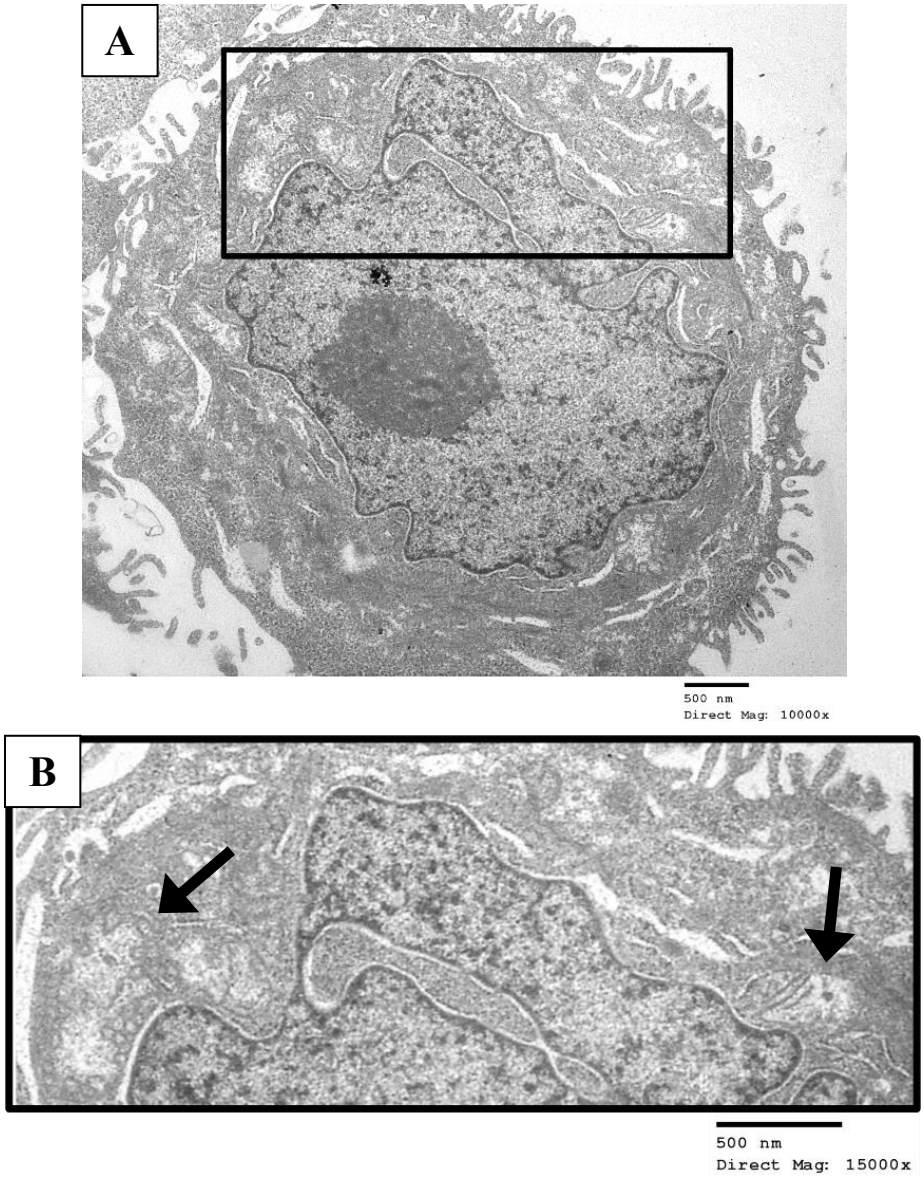

Figure 26: Transmission electron micrograph of HT-29 cells treated with 100 µM MZ.

A. Micrograph is representative of cells treated with 100 µM Mancozeb for 24 hours. Total magnification, x10,000. **B** Mitochondria are grossly swollen with loss of cristae (arrows). Total magnification, x15,000.

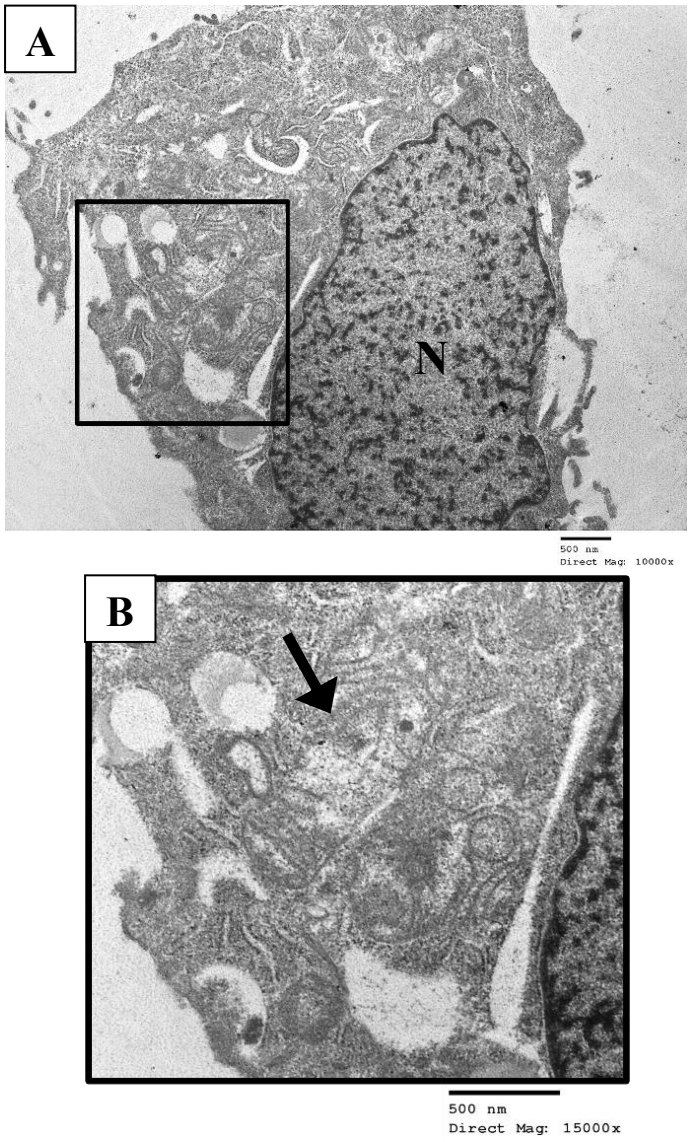

Figure 27: Transmission electron micrograph of HT-29 cells treated with 100 µM MZ.

A. Micrograph is representative of cells treated with 100 µM Mancozeb for 24 hours. Chromatin has begun to condense within the nucleus (N). Cytoplasmic disturbances are present. Total magnification, x10,000. **B** Mitochondria are grossly swollen with loss of cristae (arrow). Total magnification, x15,000.

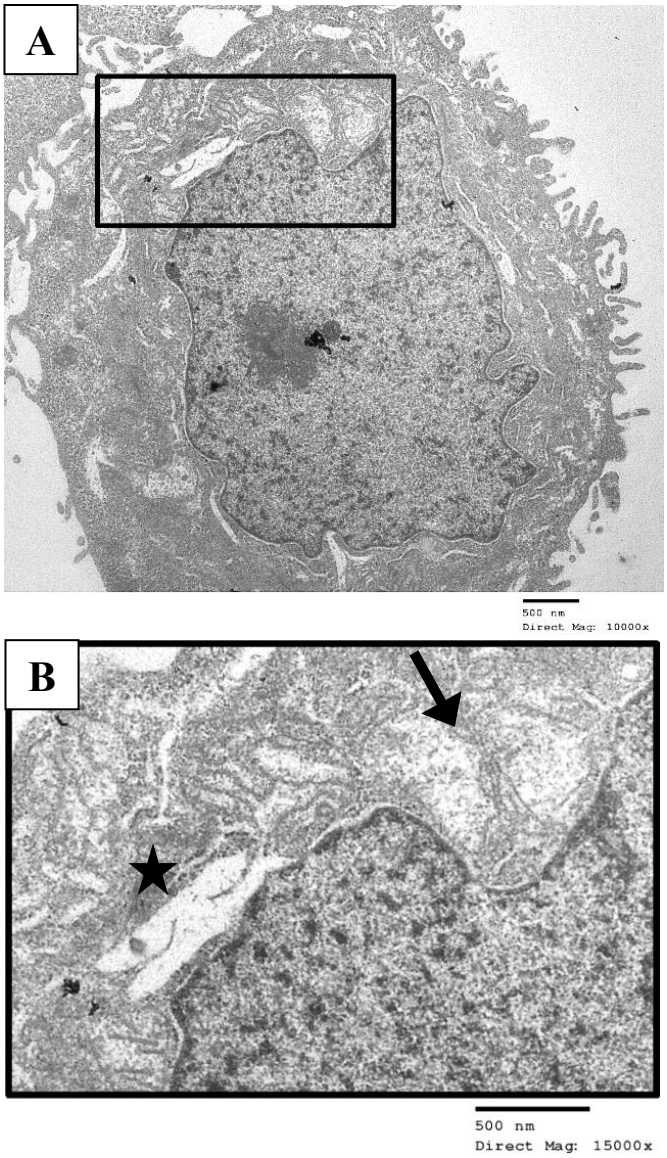

Figure 28: Transmission electron micrograph of HT-29 cells treated with 100 µM MZ.

A. Micrograph is representative of cells treated with 100 µM Mancozeb for 24 hours. Total magnification, x10,000. **B** Mitochondria are grossly swollen with loss of cristae (arrow). Endoplasmic reticulum appear dilated (star). Total magnification, x15,000.

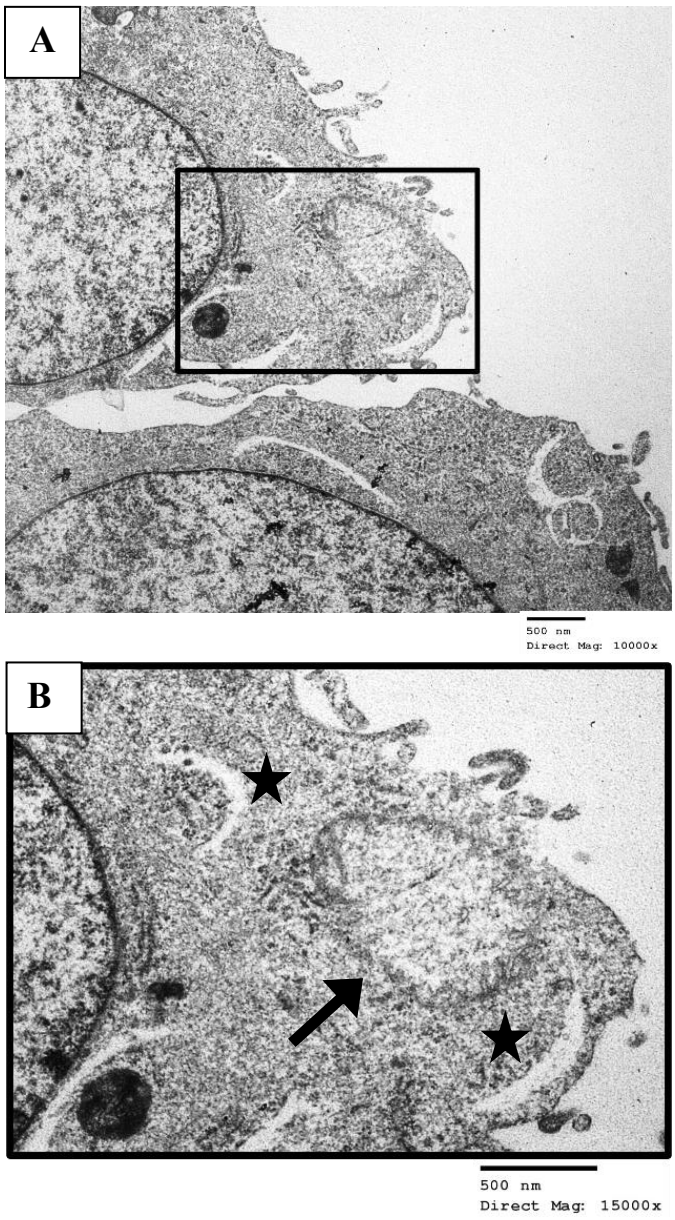

Figure 29: Transmission electron micrograph of HT-29 cells treated with 100 µM MZ.

A. Micrograph is representative of cells treated with 100 µM Mancozeb for 24 hours. Total magnification, x10,000. **B** Mitochondria are grossly swollen with loss of cristae (arrow). Endoplasmic reticulum appear slightly dilated (stars). Total magnification, x15,000.

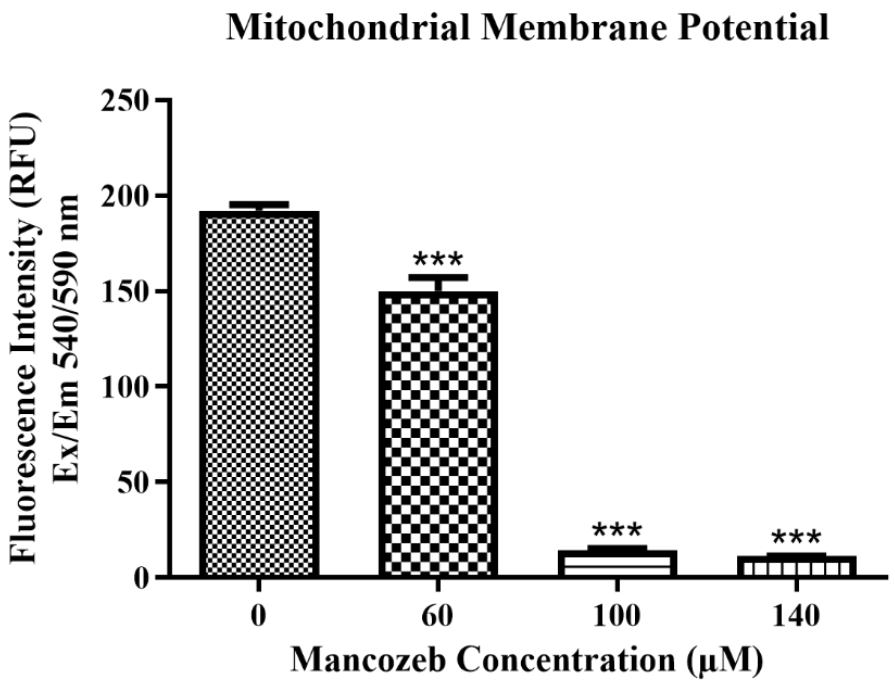

Figure 30: Mitochondrial Membrane Potential of HT-29 cells treated with Mancozeb.

HT-29 cells were treated with 60 µM, 100 µM, and 140 µM of Mancozeb for 24 hours. Significant decreases in mitochondrial membrane potential were observed for all treatment groups as compared to control. The experiment was performed in a replicate of six. Control and treatment groups (n=3). Data was analyzed using a one-way ANOVA followed by Tukey's Multiple Comparison post-hoc test. ***Significantly different from control, $p<0.001$.

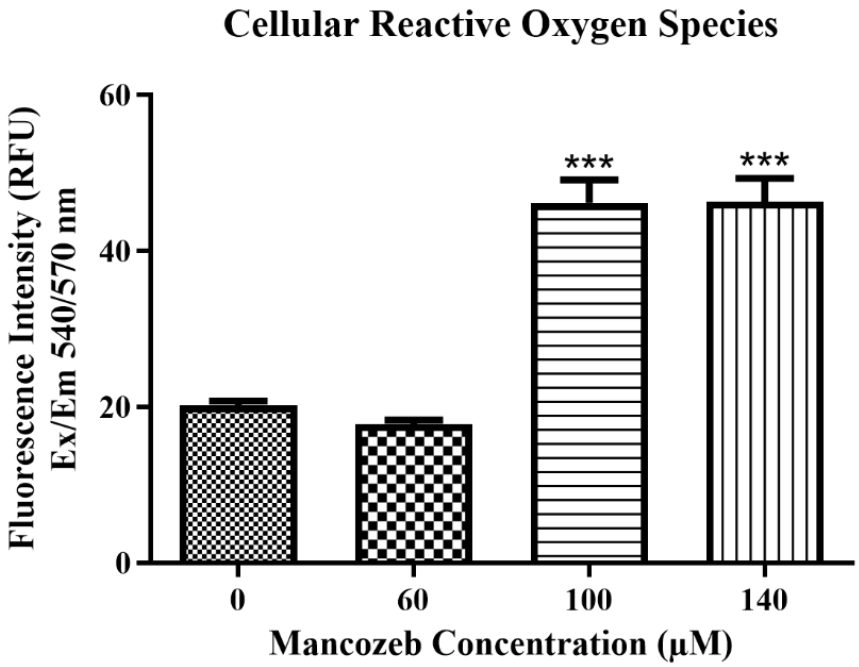

Figure 31: Cellular Reactive Oxygen Species Production of HT-29 cells treated with Mancozeb.

HT-29 cells were treated with 60 µM, 100 µM, and 140 µM of Mancozeb for 24 hours. Significant increases of cellular reactive oxygen species production were observed for cells treated with 100 µM and 140 µM MZ as compared to control. The experiment was performed in a replicate of six. Control and treatment groups (n=3). Data was analyzed using a one-way ANOVA followed by Tukey's Multiple Comparison post-hoc test. ***Significantly different from control, $p<0.001$.

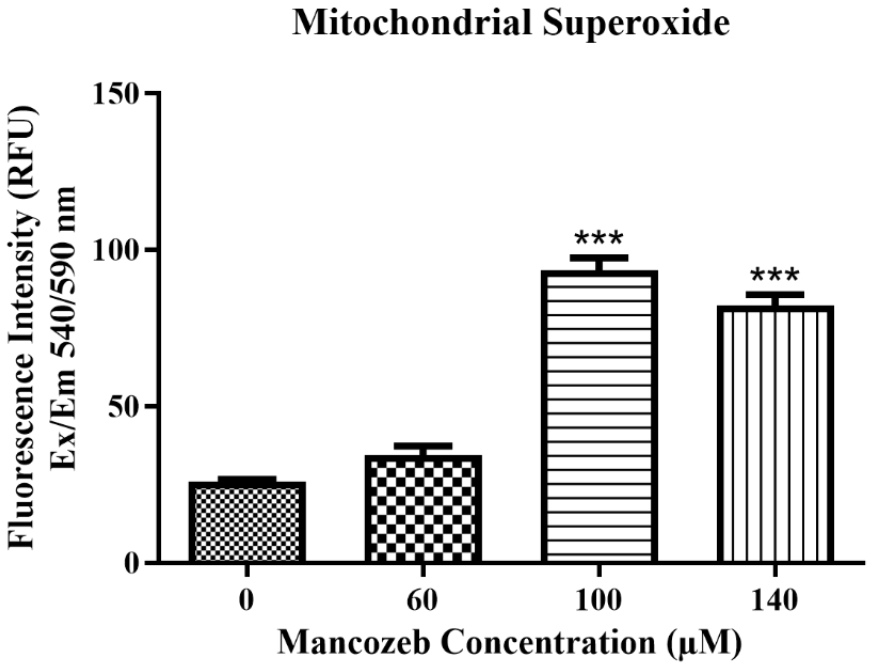

Figure 32: Mitochondrial Superoxide Production of HT-29 cells treated with Mancozeb.

HT-29 cells were treated with 60 µM, 100 µM, and 140 µM of Mancozeb for 24 hours. Significant increases in mitochondrial superoxide production were observed for cells treated with 100 µM and 140 µM MZ as compared to control. The experiment was performed in a replicate of six. Control and treatment groups (n=3). Data was analyzed using a one-way ANOVA followed by Tukey's Multiple Comparison post-hoc test. ***Significantly different from control, $p<0.001$.

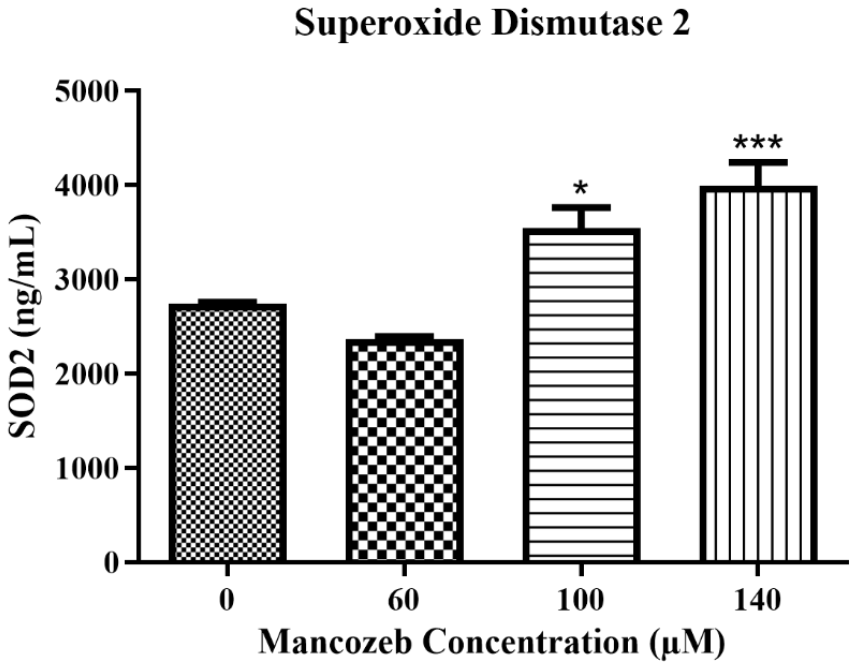

Figure 33: Superoxide Dismutase 2 Protein Levels of HT-29 cells treated with Mancozeb.

HT-29 cells were treated with 60 µM, 100 µM, and 140 µM of Mancozeb for 24 hours. Significant increases in superoxide dismutase 2 protein levels were observed for cells treated with 100 µM and 140 µM MZ as compared to control. The experiment was performed in duplicate. Control and treatment groups (n=4). Data was analyzed using a one-way ANOVA followed by Tukey's Multiple Comparison post-hoc test. *Significantly different from control, $p<0.05$.**Significantly different from control, $p<0.01$.

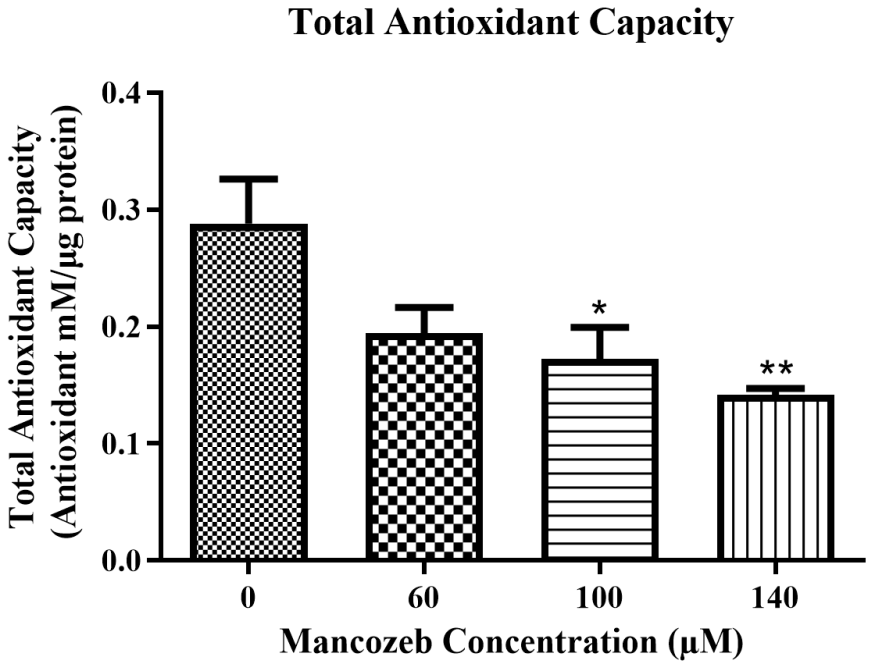

Figure 34: Total Antioxidant Capacity of HT-29 cells treated with Mancozeb.

HT-29 cells were treated with 60 µM, 100 µM, and 140 µM of Mancozeb for 24 hours. Significant decreases in total antioxidant capacity were observed for cells treated with 100 µM and 140 µM MZ as compared to control. The experiment was performed in triplicate. Control and treatment groups (n=4). Data was analyzed using a one-way ANOVA followed by Tukey's Multiple Comparison post-hoc test. *Significantly different from control, $p<0.05$.**Significantly different from control, $p<0.01$.

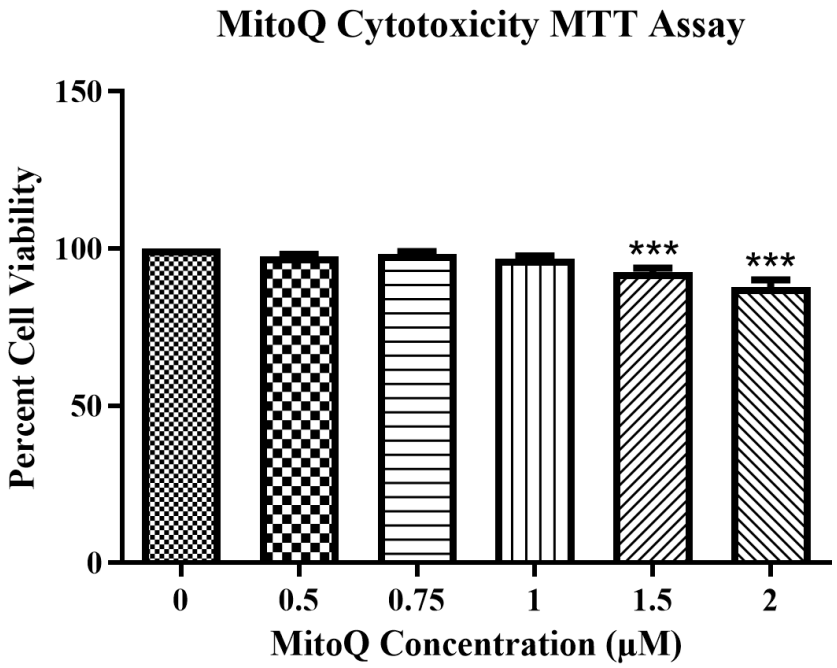

Figure 35: Cytotoxicity of MitoQ on HT-29 cells as determined by the MTT Assay.

HT-29 cells were treated for 24 hours with various concentrations ranging from 0.5-2 µM MitoQ. Significant decreases in cell viability were observed at concentrations of 1.5 µM and 2 µM MitoQ as compared to control. Data represent mean as a percentage of control ± SEM of three independent experiments (n=4). Data were analyzed using a one-way ANOVA followed by Tukey's Multiple Comparison post-hoc test. ***$p<0.001$.

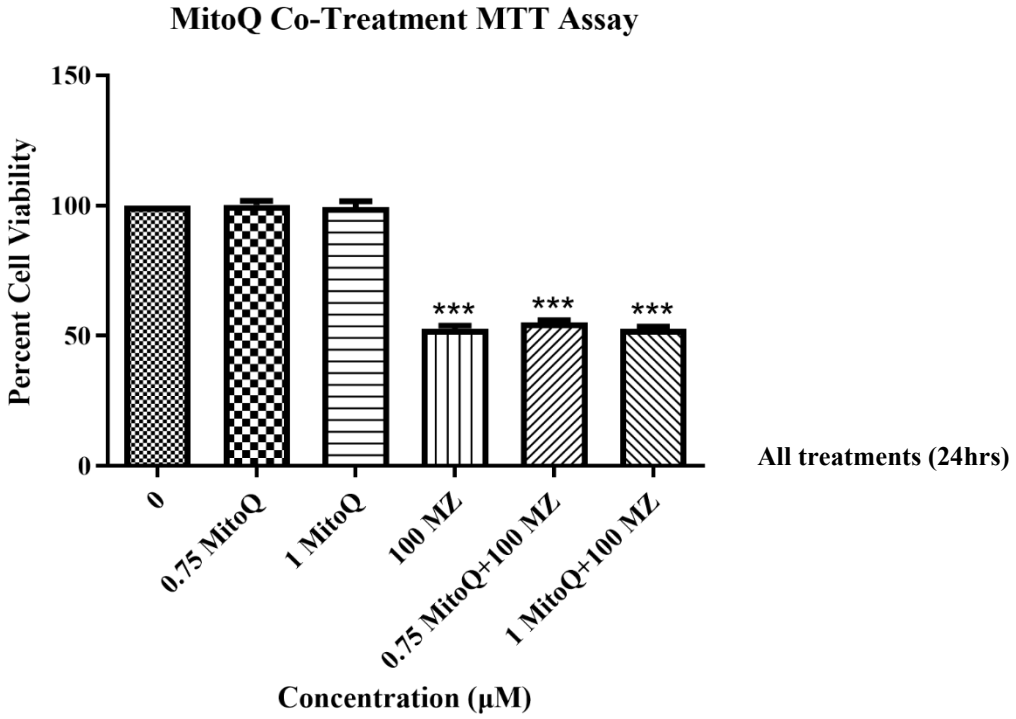

Figure 36: Co-treatment of MitoQ and Mancozeb on HT-29 cells as determined by the MTT Assay.

HT-29 cells were treated for 24 hours with co-treatment of MitoQ and Mancozeb. Co-treatment concentrations were 0.75 µM MitoQ+100 µM MZ and 1 µM MitoQ+100 µM MZ. Significant decreases in cell viability were observed at concentrations of 100 µM MZ, 0.75 µM MitoQ+100 µM MZ and 1µM MitoQ+100 µM MZ as compared to control. Data represent mean as a percentage of control ± SEM of three independent experiments (n=4). Data were analyzed using a one-way ANOVA followed by Tukey's Multiple Comparison post-hoc test. ***$p<0.001$.

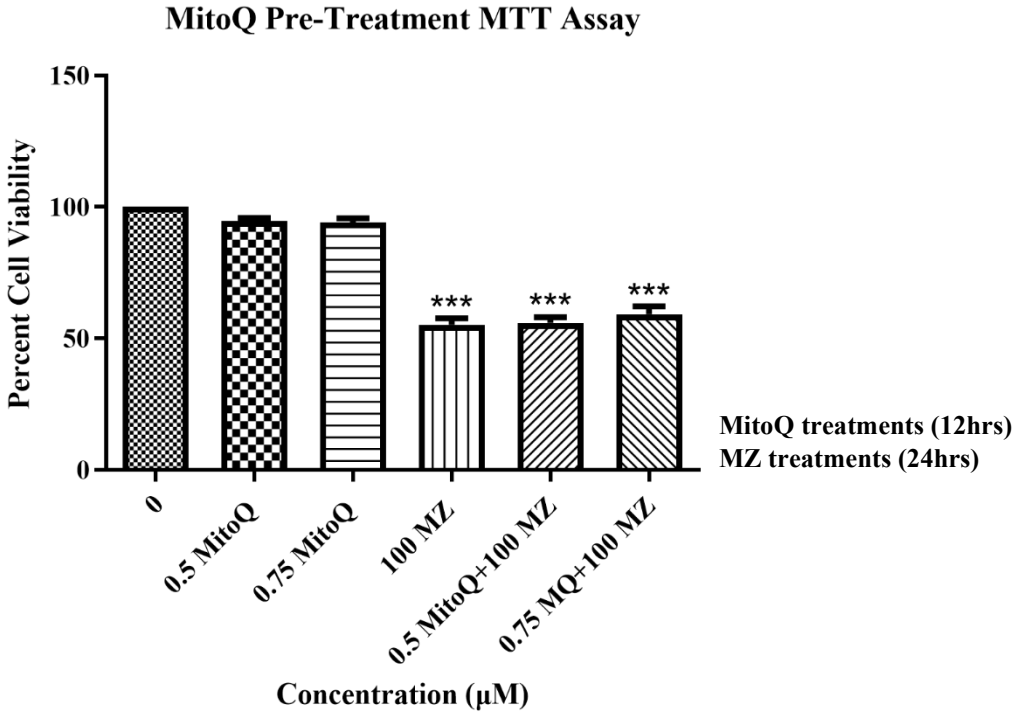

Figure 37: Pre-treatment of MitoQ and Mancozeb on HT-29 cells as determined by the MTT Assay.

HT-29 cells were treated for 12 hours with MitoQ followed by treatment with 100 µM Mancozeb for 24 hours. Cells were pre-treated with either 0.5 µM or 0.75 µM MitoQ. Significant decreases in cell viability were observed at concentrations of 100 µM MZ and cell pre-treated with either 0.5 µM or 0.75 µM MitoQ followed by Mancozeb exposure as compared to control. Data represent mean as a percentage of control ± SEM of three independent experiments (n=4). Data were analyzed using a one-way ANOVA followed by Tukey's Multiple Comparison post-hoc test. ***$p<0.001$.

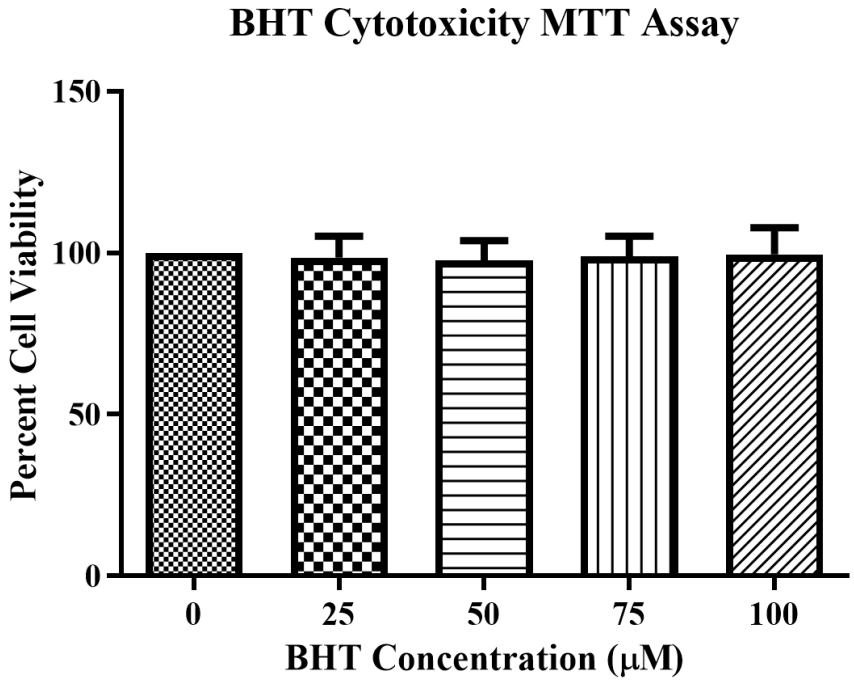

Figure 38: Cytotoxicity of BHT on HT-29 cells as determined by the MTT Assay.

HT-29 cells were treated for 24 hours with various concentrations ranging from 25-100 μM BHT. No significant decreases in cell viability were observed as compared to control. Data represent mean as a percentage of control ± SEM of three independent experiments (n=4). Data were analyzed using a one-way ANOVA followed by Tukey's Multiple Comparison post-hoc test.

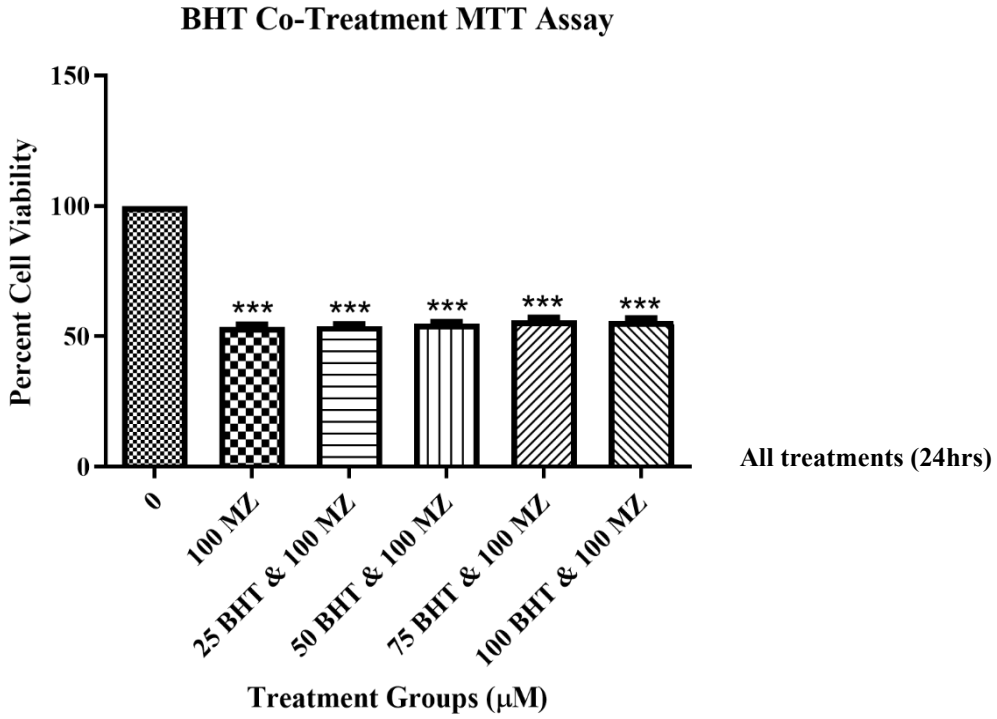

Figure 39: Co-treatment of BHT and Mancozeb on HT-29 cells as determined by the MTT Assay.

HT-29 cells were treated for 24 hours with co-treatment of BHT and Mancozeb. Co-treatment concentrations were 25 μM BHT+100 μM MZ, 50 μM BHT+100 μM MZ, 75 μM BHT+100 μM MZ, and 100 μM BHT+100 μM MZ. Significant decreases in cell viability were observed at concentrations of 100 μM MZ, 25 μM BHT+100 μM MZ, 50 μM BHT+100 μM MZ, 75 μM BHT+100 μM MZ, and 100 μM BHT+100 μM MZ as compared to control. Data represent mean as a percentage of control ± SEM of three independent experiments (n=4). Data were analyzed using a one-way ANOVA followed by Tukey's Multiple Comparison post-hoc test. ***$p<0.001$.

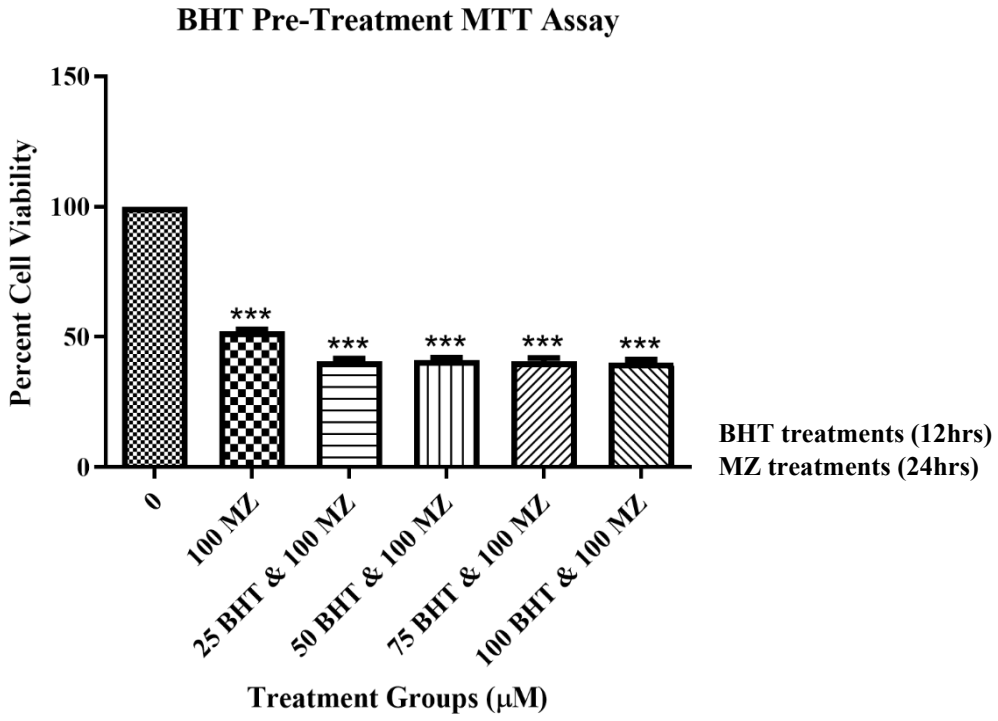

Figure 40: Pre-treatment of BHT and Mancozeb on HT-29 cells as determined by the MTT Assay.

HT-29 cells were treated for 12 hours with BHT followed by treatment with 100 μM Mancozeb for 24 hours. Cells were pre-treated with 25 μM, 50 μM, 75 μM, or 100 μM BHT. Significant decreases in cell viability were observed at concentrations of 100 μM MZ and cell pre-treated with either 25 μM, 50 μM, 75 μM, or 100 μM BHT followed by Mancozeb exposure as compared to control. Data represent mean as a percentage of control ± SEM of three independent experiments (n=4). Data were analyzed using a one-way ANOVA followed by Tukey's Multiple Comparison post-hoc test. ***$p<0.001$.

4. DISCUSSION

Ethylene bisdithiocarbamate pesticides, including Mancozeb, have been purported to have low acute human toxicity and short environmental persistence in addition to providing good foliar protection in its use as a fungicide (Calviello et al., 2006; Costa and Aschner, 2014). Occupational workers have the highest risk of pesticide exposure and adverse effects to agents such has Mancozeb, but the general population that consumes food treated with pesticides is also at risk (López-Fernández et al., 2012; Maroni et al., 2000). Detectable levels of ethylene bisdithiocarbamate pesticide residues have been found on a variety of produce (Caldas et al., 2006; Kayne et al., 2015; López-Fernández et al., 2012). Studies have implicated Mancozeb exposure to toxicity in various organ systems including the thyroid, liver, kidney, reproductive organs, nervous system, and gastrointestinal tract (Domico et al., 2006, 2007; Hoffman and Hardej, 2012; Hoffman et al., 2016; Ksheerasagar and Kaliwal, 2003; Pandy and Mohanty, 2015; Pirozzi et al., 2016). The work of Hoffman and Hardej (2012) demonstrated that Mancozeb results in oxidative stress and apoptotic cell death in HT-29, Caco-2, and CCD-18Co cell lines. Mitochondrial inhibition contributes to these cytotoxic effects. Previous work in the laboratory has proven that Mancozeb exposure to HT-29 cells results in inhibition of mitochondrial complex I, II, and V leading to apoptosis. Furthermore, previous studies have established Mancozeb as a mitochondrial toxicant causing oxidative stress and leading to mitochondrial dysfunction (Bailey et al. 2016; Domico et al. 2006, 2007; Iorio et al. 2015; Kumar et al. 2019; Todt et al. 2016).

The present study further investigated the effect of Mancozeb exposure on mitochondrial activity on HT-29 cells, specifically complex III and IV. The work of Dhaneshwar and Hardej, (2021) documented Mancozeb's effects on complex I-V. The

present work continued exploring the role of oxidative stress in mitochondrial dysfunction. In addition, this study is the first to investigate the effect of Mancozeb exposure on mitochondrial activity and role of oxidative stress leading to mitochondrial dysfunction in the HT-29 cell line.

Previous work of Dhaneshwar and Hardej (2021) described cell viability using a concentration of Mancozeb at 97.5% purity. However, Mancozeb could no longer be obtained of that purity. The current investigation used Mancozeb with purities of 94.1% and 99.6%, tests showed that the cytotoxic effects were similar to the established results of Mancozeb with a purity of 97.5%. The MTT assay measures viability by assessing the capability of mitochondrial dehydrogenase enzymes to reduce a yellow tetrazolium salt to a purple formazan crystal (Mosmann, 1983). Data from the MTT assay demonstrated that Mancozeb caused a concentration-dependent decrease in cell viability with significant decreases ranging from 40-200 μM Mancozeb for all purities. The calculated LC_{50} of the various purities of 94.1%, 97.5%, and 99.6% were 153.90 μM, 104.21 μM, and 105.82 μM respectively. The results confirmed that Mancozeb with a purity of 99.6% yielded a similar calculated LC_{50} to that of Mancozeb with a purity of 97.5%. The MTT data are consistent with previous results in our laboratory showing significant decreases in HT-29 cell viability between 120-260 μM Mancozeb (Hoffman and Hardej, 2012).

The cytotoxic effects of Mancozeb on HT-29 cells were confirmed by scanning electron microscopy. Micrographs demonstrated cellular blebbing at concentrations of 80-140 μM Mancozeb, a significant hallmark of apoptosis (Poon et al., 2010). Quantification of cell blebbing from SEM micrographs at doses of 0 μM, 60 μM, 100 μM, and 140 μM Mancozeb revealed that there was an increase in the mean percentage

of blebbed cells at concentrations of 100 μM (27.12%) and 140 μM (7.57%), but only a significant increase at 100 μM when compared to untreated cells. This is consistent with results of the previous work in our laboratory that report apoptosis in the HT-29 cell line after Mancozeb exposure. The previous work of Dhaneshwar and Hardej (2021), confirmed that Mancozeb exposure results in apoptosis at doses of 60 μM, 100 μM, 140 μM Mancozeb in fluorescent micrographs with positive FITC-Annexin V staining. In addition, the 140 μM dose showed that cells in late apoptosis exhibited both positive FITC-Annexin V and Ethidium Homodimer-III staining. Late apoptosis occurs when apoptotic cells persist and are not yet cleared by phagocytes. The cell membrane also becomes more permeable in this state (Poon et al., 2010). In addition, during this stage, the cells have already begun the apoptotic process and are ready to be cleared by phagocytes, so blebbing is less apparent. As previously noted, during late apoptosis the cell membrane also becomes more permeable, which is seen by the deterioration of the plasmalemma in the SEM micrograph of cells treated with 140 μM Mancozeb. Previous *in vitro* studies have also documented the activation of apoptosis following Mancozeb exposure (Calviello et al., 2006; Hoffman and Hardej, 2012; Srivastava et al., 2016). Rat fibroblasts and peripheral blood mononucleated cells resulted in a pro-oxidant effect that altered the expression of apoptotic proteins such as Bcl-2 and c-MYC following Mancozeb exposure (Calviello et al., 2006). Evidence of apoptosis in cultured human lymphocytes exposed to Mancozeb included increased Bax expression, decreased Bcl-2 expression, up-regulation of cytochrome *c*, and decreased mitochondrial membrane potential (Srivastava et al., 2016). In addition, the work of Hoffman and Hardej (2012)

reported that Mancozeb exposure activates caspase 3/7, 8 and 9 indicating that both the intrinsic and extrinsic apoptotic pathways were activated in HT-29 cells.

The intrinsic apoptotic pathway is the result of mitochondrial dysfunction that can result from calcium accumulation, dissipation of mitochondrial membrane potential, or overproduction of ROS/RNS. Furthermore, the previously listed events contribute to an increase in mitochondrial inner membrane permeability, which is known as mitochondrial permeability transition (MPT). This permeability is believed to be caused by the opening of a proteinaceous pore termed the mitochondrial permeability transition pore (MPTP). MPTP spans both mitochondrial membranes and is permeable to solutes of 1,500 daltons. Opening of the MPTP allows free influx of protons into the matrix space causing a complete dissipation of the membrane potential, cessation of ATP synthesis, and mitochondrial swelling due to the osmotic influx of water. Furthermore, calcium accumulated in the matrix space effluxes through the pore flooding the cytoplasm. Disruption of the mitochondrial membrane potential causes the translocation of Bax and release of cytochrome *c* from the intermembrane space to the cytosol. Cytochrome *c* can then bind to and activate apoptotic protease activation factor 1 (Apaf-1) and pro-caspase 9 to form an apoptosome. The apoptosome causes the cleavage of pro-caspase 9 to caspase 9, which then cleaves and activates downstream effector caspase 3, resulting in apoptosis (Circu and Aw, 2010; Elmore, 2007; Strubbe-Rivera et al., 2021). Mancozeb has been demonstrated to generate ROS, playing a role in mitochondrial dysfunction, and ultimately leading to apoptotic cell death (Calviello et al., 2006; Kumar et al., 2019; Srivastava et al., 2016).

The present study evaluated the activity of complexes III and IV to determine if Mancozeb exposure results in mitochondrial dysfunction in the HT-29 cell line. It has been previously documented that exposure to Mancozeb inhibits activity of complex I, II, and V in HT-29 cells. Data from the current study exhibited that Mancozeb exposure to HT-29 cells inhibits complex III and IV activity as well. Taken together, this is the first study that has determined that all mitochondrial complexes are affected by Mancozeb in a single *in vitro* model. Decrease in mitochondrial complex activity by other manganese containing EBDC compounds have been demonstrated in other studies. In isolated brain mitochondria of rats, manganese EBDC, a major active element of Maneb, has been shown to inhibit complex I, II, and III (Zhang et al., 2003). Furthermore, *Caenorhabditis elegans* exposed to Manzate, fungicide with Mancozeb as active ingredient, reduced mitochondrial respiration, which can be attributed to complex I inhibition and decreased ATP levels (Bailey et al., 2016; Todt et al., 2016).

The current investigation demonstrated in transmission electron micrographs that a dose of 100 µM Mancozeb showed severe mitochondrial distortions including gross mitochondrial swelling and loss of cristae. Other studies have described edematous mitochondria in mouse hippocampus and cortex following exposure to Mancozeb (Morales-Ovalles et al., 2018; Peña-Contreras et al., 2016). Additionally, the mitochondria of skeletal and cardiac muscle of rats treated with Mancozeb exhibited swollen mitochondria with distorted cristae (Stephenson and Trombetta, 2020). These ultrastructural changes documented that Mancozeb exposure alters mitochondrial architecture resulting in mitochondrial dysfunction. Mitochondrial dysfunction occurs when there is an insufficient number of mitochondria present within the cell, an inability

to provide substrates to the mitochondria, or disruption in their transport of electrons and synthesis of ATP. Dysfunction of mitochondria can manifest in a number of disease states including neurodegenerative diseases, neurobehavioral and psychiatric disease, cardiovascular disease, autoimmune diseases, musculoskeletal disease, chronic infection, and cancer (Nicolson, 2014; Pieczenik and Neustadt, 2007). Cellular changes that can result from mitochondrial dysfunction include, alterations of ETC (electron transport chain) function, reduction in ATP synthesis, reduction in the transport of critical metabolites to the mitochondria, and loss of both the electrical and chemical transmembrane potential of the inner mitochondrial membrane (Nicolson, 2014).

The current work has demonstrated that Mancozeb exposure leads to inhibition of mitochondrial complex enzyme activity. Additionally, significant loss of mitochondria membrane potential occurs at doses of 60 μM, 100 μM, and 140 μM Mancozeb has been shown. The mitochondrial membrane potential is a classic indicator of the energetic state of the mitochondria. A significant loss of mitochondrial membrane potential promotes the production of reactive oxygen species and depletes the cell of energy (Meyer et al., 2013). The generation of the proton gradient by complex I, III, and IV is largely responsible for mitochondrial membrane potential (Navarro and Boveris, 2007). Inhibition of the previously mentioned complexes may contribute to the loss of mitochondrial membrane potential documented in HT-29 cells following Mancozeb exposure. Loss of mitochondrial membrane potential allows for initiation of apoptosis by the translocation of Bax and the release of cytochrome *c* into the cytosol (Elmore, 2007). These results also corroborate the induction of apoptosis seen at these doses in positive FITC-Annexin V staining (Dhaneshwar and Hardej, 2021). Other studies have shown

similar effects of Mancozeb in a number of *in vitro* models. Depolarized membrane potential, decreased ATP levels, and increased oxidative stress have been reported in mouse granulosa cells exposed to a low dose of Mancozeb (0.01 μg/mL) (Iorio et al., 2015). Mancozeb exposure to mesencephalic neuronal cultures caused uncoupling of the ETC at low doses (15 μM) and inhibits mitochondrial respiration at higher doses (30 μM) (Domico et al., 2006). In human gastric adenocarcinoma cells, production of reactive oxygen species and loss of mitochondrial membrane potential resulted from Mancozeb exposure (5-10 μM) (Kumar et al., 2019). Although the effects mentioned in the previous *in vitro* studies occur at much lower doses than that reported in the current study, it has been noted that the presence of goblet cells in the HT-29 cell line contributes to its resistance to cellular injury (Wikman-Larhed and Artursson, 1995). Furthermore, the ADI of Mancozeb is comparable to micromolar concentrations of 0-100 μM, according to Medjdoub et al. (2011), making the doses used in the present study (60-140 μM) physiologically relevant.

The generation of reactive oxygen species by EBDC pesticides, including Mancozeb, via Fenton-like reactions has been shown to be a major component of toxicity, which can result in mitochondrial dysfunction and apoptosis (Erikson and Aschner, 2003; Fitsanakis et al., 2002; Nzengue et al., 2011; Prabhakaran et al., 2009). Oxidative damage can result from changes in the antioxidant defense system, including both endogenous (glutathione peroxidase, catalase, and superoxide dismutase) and dietary (ascorbic acid, α-tocopherol, and β-carotene) (Halliwell, 1966; Nicolson, 2014; Turrens, 2003). Oxidative damage to the cardiolipin and other phospholipid membranes of the inner mitochondrial membrane results in loss of ETC function due to loss of the

electrochemical gradient (Nicolson, 2014). Previous studies have shown the ability of metals, such as copper and zinc, to reduce glutathione levels and contribute to oxidative stress (Nzengue et al., 2011). Widespread mitochondrial dysfunction leading to cell damage is associated with glutathione deficiency (Navarro and Boveris, 2007). Mancozeb exposure in HT-29 cells has shown significantly decreased reduced glutathione (GSH) to oxidized glutathione (GSSG) ratio at concentrations ranging from 100-200 μM Mancozeb (Hoffman et al., 2016). The current study supports the previous finding through the documentation of significant decreases of the total antioxidant capacity in HT-29 cells at doses of 100 μM and 140 μM of Mancozeb. Decreased total antioxidant capacity leaves the cells lacking in the ability to detoxify reactive oxygen species and thus results in increased susceptibility to oxidative stress. The current study also documented a significant increase in cellular reactive oxygen species which correlates perfectly with the doses (100 μM and 140 μM) demonstrated to have reduced antioxidant capacity. Furthermore, Hoffman and Hardej (2012) demonstrated that following Mancozeb exposure in this cell line there were significant increases in TBARS (thiobarbituric acid reactive substances) levels (160 μM and 200 μM), indicating lipid peroxidation. Higher doses of Mancozeb used in the present work (140 μM and 160 μM), resulted in obvious deterioration of the plasmalemma, consistent with lipid peroxidation effects observed in Hoffman and Hardej (2012).

Although oxidative phosphorylation is a vital part of cellular metabolism, it also produces deleterious products such as reactive oxygen species. Electrons can escape from the electron transport chain primarily at two sites, complex I and complex III, to form superoxide anion radical (Pieczenik and Neustadt, 2007). In addition, an overflow of free

electrons from the respiratory chain leading to the production of superoxide anion radical can result from inhibition of complex IV by nitric oxide, carbon monoxide, or cyanide (Meyer et al., 2013). The majority of mitochondrial superoxide anion is released into the mitochondrial matrix (70-80%) where it encounters SOD2, while a smaller amount (20-30%) is released into the intermembrane space and reacts with SOD1 (Navarro and Boveris, 2007). Increases in mitochondrial superoxide were documented in this study at doses of 100 μM and 140 μM in HT-29 cells exposed to Mancozeb. When transition metals are present in high intra-cellular concentrations, they catalyze the formation of reactive oxygen species through the Fenton reaction. The findings of Hoffman and Hardej (2012) revealed that Mancozeb exposure to HT-29 cells resulted in elevated levels of manganese and zinc concentrations. Elevated copper levels were reported as a result of metal trans-chelation of the EBDC backbone of Mancozeb in the work of Hoffman et al. (2016). These data suggest that Mancozeb's ability to induce increases in oxidative stress is due either to the inhibition of mitochondrial complex enzymes or alteration in cellular metal homeostasis, or a combination of both.

The reported increase in mitochondrial superoxide in HT-29 cells following Mancozeb exposure prompted the investigation of SOD2 levels. This enzyme is located in the mitochondria and uses manganese as a cofactor to transform the superoxide anion radical into hydrogen peroxide, thus protecting against oxidative stress (Circu and Aw, 2010; Halliwell, 1966). The present investigation revealed that Mancozeb exposure to the HT-29 cells resulted in significantly increased SOD2 levels (100 μM and 140 μM). These results correlate to the doses at which significant increases of mitochondrial superoxide levels were documented following Mancozeb exposure. Increase in SOD2 levels may be

correlated to increased SOD2 activity in response to excess reactive oxygen species that are generated following Mancozeb exposure. Previous *in vivo* studies have demonstrated that Mancozeb exposure decreased overall SOD levels in liver and ovary samples, which may be a result of the chronic exposure to Mancozeb and timepoint of analysis (Bao et al., 2022; Saber et al., 2019; Sakr, 2007). *In vitro* studies provide an analysis of more acute exposure to toxic agents, such as Mancozeb. Furthermore, increased levels of both SOD1 and SOD2 following Mancozeb exposure have been documented in yeast (Santos et al., 2009).

Since Mancozeb has been shown to be capable of increasing oxidants in HT-29 cells, the effects of the antioxidants butylated hydroxy toluene (BHT) and MitoQ were evaluated in this study. In the current study, we decided to keep the exposure period of Mancozeb 24 hours in conducting our antioxidant experiments, since this is the timepoint at which altered oxidative stress parameters were documented. BHT was tested as an overall cellular antioxidant and MitoQ was tested as a mitochondrial antioxidant since the results of the current study show that both cellular and mitochondrial reactive oxygen species are increased following Mancozeb exposure. BHT is a synthetic phenolic antioxidant that is used as a food preservative. It behaves as an alpha-tocopherol analog and has been shown to terminate lipid peroxidation chain reactions and act as a free radical scavenger (Lambert et al., 1996). Unpublished data from our lab has reported a significant increase in cell viability in HT-29 cells pre-treated with BHT for 24 hours followed by Mancozeb exposure for 12 hours. In addition, rat hippocampal astrocytes post-treated with BHT for 24 hours after an hour of Mancozeb exposure had both increased cellular viability and total antioxidant capacity when compared to Mancozeb

treated cells (Tsang and Trombetta, 2007). The current study evaluated the ability of BHT pre-treatment and co-treatment to increase cellular viability of Mancozeb exposed HT-29 cells. Neither pre-treatment or co-treatment with BHT was able to increase cell viability in Mancozeb exposed HT-29 cells. The study also evaluated the ability of MitoQ pre-treatment and co-treatment to increase cellular viability of Mancozeb exposed HT-29 cells. MitoQ, a mitochondria-targeted antioxidant, is described in the literature as either mitoquinol, mitoquinone, or a mixture of these redox forms (O'Malley et al., 2006). For the current study mitoquinol (MitoQ) was used for solubility purposes. Furthermore, MitoQ consists of an analog of ubiquinone, (coenzyme Q), which is an electron carrier of the ETC. The ubiquinone analog of MitoQ is bound to the cation triphenylphosphine (TPP^{+}), which makes the antioxidant's ability to penetrate the mitochondria dependent on mitochondrial membrane potential. Although the exact mechanism of action is not well defined, it is believed that MitoQ decreases lipid peroxidation by the quinol moiety acting as a chain-breaking antioxidant (O'Malley et al., 2006). Neither pre-treatment or co-treatment with MitoQ was able to increase cell viability in Mancozeb exposed HT-29 cells. Furthermore, MitoQ has been reported to cause mitochondrial swelling and depolarization at a dose of 500 nmol/L in kidney proximal tubule cells. These toxic effects are believed to be a result of increased inner mitochondrial membrane permeability due to the alkyl chain backbone rather than the quinone component of the molecule (Gottwald et al., 2018). Failure of either BHT or MitoQ to increase cellular viability is presumed to be related to the exposure time to Mancozeb (24 hours), which may indicate that the cellular antioxidant system may have been too overwhelmed at this timepoint to be rescued or has not started as of yet.

In conclusion, the current work has demonstrated in the HT-29 cell line that Mancozeb exposure results in mitochondrial disruption of complex III and IV enzymes which contributes to mitochondrial dysfunction as a result of oxidative stress. The inhibition of mitochondrial complex enzymes is a result of either Mancozeb interacting directly on thiol groups of mitochondrial complex enzymes or Mancozeb induced reactive oxygen species. In either case, the loss of mitochondrial membrane potential and gross mitochondrial morphological changes suggest Mancozeb's ability to elicit mitochondrial toxicity. However, it is the alteration of oxidative stress parameters such as cellular reactive oxygen species, mitochondrial superoxide, superoxide dismutase 2, and total antioxidant capacity that demonstrate that the underlying mechanism of Mancozeb toxicity that contributes to mitochondrial dysfunction is oxidative stress.

REFERENCES

Akthar, I., Wang, Z., Wijayagunawardane, M. P. B., Ratnayake, C. J., Siriweera, E. H., Lee, K. F., & Kodithuwakku, S. P. (2020). In vitro and in vivo impairment of embryo implantation by commonly used fungicide Mancozeb. *Biochemical and Biophysical Research Communications*, *527*(1), 42–48. https://doi.org/10.1016/j.bbrc.2020.04.051.

Aschner, J. L., & Aschner, M. (2005). Nutritional aspects of manganese homeostasis. *Molecular Aspects of Medicine*, *26*(4-5 SPEC. ISS.), 353–362. https://doi.org/10.1016/j.mam.2005.07.003.

Atwood, D., & Paisley-Jones, C. (2017). *US EPA - Pesticides Industry Sales and Usage 2008 - 2012*.

Axelstad, M., Boberg, J., Nellemann, C., Kiersgaard, M., Rosenskjold Jacobsen, P., Christiansen, S., Sørig Hougaard, K., & Hass, U. (2014). Exposure to the widely used fungicide Mancozeb causes thyroid hormone disruption in rat dams but no behavioral effects in the offspring Downloaded from. In *Laurentian University on December* (Vol. 5). http://toxsci.oxfordjournals.org/.

Bailey, D. C., Todt, C. E., Orfield, S. E., Denney, R. D., Snapp, I. B., Negga, R., Montgomery, K. M., Bailey, A. C., Pressley, A. S., Traynor, W. L., & Fitsanakis, V. A. (2016). Caenorhabditis elegans chronically exposed to a Mn/Zn ethylene-bis-dithiocarbamate fungicide show mitochondrial Complex I inhibition and increased reactive oxygen species. *NeuroToxicology*, *56*, 170–179. https://doi.org/10.1016/j.neuro.2016.07.011.

Baligar, P. N., & Kaliwal, B. B. (2001). Induction of Gonadal Toxicity to Female Rats after Chronic Exposure to Mancozeb. In *Industrial Health* (Vol. 39).

Bao, J., Zhang, Y., Wen, R., Zhang, L., & Wang, X. (2022). Low level of mancozeb exposure affects ovary in mice. *Ecotoxicology and Environmental Safety*, *239*, 113670. https://doi.org/10.1016/j.ecoenv.2022.113670.

Baysal, M., & Atlı-Eklioğlu, Ö. (2021). Comparison of the toxicity of pure compounds and commercial formulations of imidacloprid and acetamiprid on HT-29 cells: Single and mixture exposure. *Food and Chemical Toxicology*, *155*. https://doi.org/10.1016/j.fct.2021.112430.

Bindali, B. B., & Kaliwal, B. B. (2002). Anti-implantation Effect of a Carbamate Fungicide Mancozeb in Albino Mice. In *Industrial Health* (Vol. 40).

Caldas, E. D., Miranda, M. C. C., Conceição, M. H., & de Souza, L. C. K. R. (2004). Dithiocarbamates residues in Brazilian food and the potential risk for consumers. *Food and Chemical Toxicology*, *42*(11), 1877–1883. https://doi.org/10.1016/j.fct.2004.07.006.

Calviello, G., Piccioni, E., Boninsegna, A., Tedesco, B., Maggiano, N., Serini, S., Wolf, F. I., & Palozza, P. (2006). DNA damage and apoptosis induction by the pesticide Mancozeb in rat cells: Involvement of the oxidative mechanism. *Toxicology and Applied Pharmacology*, *211*(2), 87–96. https://doi.org/10.1016/j.taap.2005.06.001.

Canossa, E., Angiuli, G., Garasto, G., Buzzoni, A., & de Rosa, E. (1993). INDICATORI DI DOSE IN AGRICOLTORI ESPOSTI A MANCOZEB. *Medicina Del Lavoro*, *84*(1), 42–50.

Circu, M. L., & Aw, T. Y. (2010). Reactive oxygen species, cellular redox systems, and apoptosis. *Free Radical Biology and Medicine*, *48*(6), 749–762. https://doi.org/10.1016/j.freeradbiomed.2009.12.022.

Colosio, C., Maroni, M., Alcini, D., Cavallo, D., Foà, V., Barcellini, W., Galli, A., Rizzardi, G. P., Bersani, M., Meroni, P., Pastorelli, R., & Soleo, L. (1996). Immunomodulatory effects of occupational exposure to mancozeb. *Archives of Environmental Health*, *51*(6), 445–451. https://doi.org/10.1080/00039896.1996.9936044.

Corsini, E., Birindelli, S., Fustinoni, S., de Paschale, G., Mammone, T., Visentin, S., Galli, C. L., Marinovich, M., & Colosio, C. (2005). Immunomodulatory effects of the fungicide Mancozeb in agricultural workers. *Toxicology and Applied Pharmacology*, *208*(2), 178–185. https://doi.org/10.1016/j.taap.2005.02.011.

Costa, L. G., & Aschner, M. (2014). Toxicology of Pesticides. In *Reference Module in Biomedical Research* (Third Edit). Elsevier. https://doi.org/10.1016/B978-0-12-801238-3.00208-7.

Dallagnol, J. C., Pezzini Ferri M., Uribe Suarez N., & Joveleviths, D. (2021). *Systemic effects of the pesticide mancozeb – A literature review*.

Damalas, C. A., & Eleftherohorinos, I. G. (2011). Pesticide exposure, safety issues, and risk assessment indicators. In *International Journal of Environmental Research and Public Health* (Vol. 8, Issue 5, pp. 1402–1419). MDPI. https://doi.org/10.3390/ijerph8051402.

Dhaneshwar, A., & Hardej, D. (2021). Disruption of mitochondrial complexes, cytotoxicity, and apoptosis results from Mancozeb exposure in transformed human colon cells. *Environmental Toxicology and Pharmacology*, *84*. https://doi.org/10.1016/j.etap.2021.103614.

Domico, L. M., Cooper, K. R., Bernard, L. P., & Zeevalk, G. D. (2007). Reactive oxygen species generation by the ethylene-bis-dithiocarbamate (EBDC) fungicide mancozeb and its contribution to neuronal toxicity in mesencephalic cells. *NeuroToxicology*, *28*(6), 1079–1091. https://doi.org/10.1016/j.neuro.2007.04.008.

Domico, L. M., Zeevalk, G. D., Bernard, L. P., & Cooper, K. R. (2006). Acute neurotoxic effects of mancozeb and maneb in mesencephalic neuronal cultures are

associated with mitochondrial dysfunction. *NeuroToxicology*, *27*(5), 816–825. https://doi.org/10.1016/j.neuro.2006.07.009.

Elmore, S. (2007). *Apoptosis: A Review of Programmed Cell Death*.

Environmental Protection Agency (2005). Mancozeb facts. (accessed: 1/26/23). https://www.epa.gov.

Erikson, K. M., & Aschner, M. (2003). Manganese neurotoxicity and glutamate-GABA interaction. *Neurochemistry International*, *43*(4–5), 475–480. https://doi.org/10.1016/S0197-0186(03)00037-8.

Fitsanakis, V. A., Amarnath, V., Moore, J. T., Montine, K. S., Zhang, J., & Montine, T. J. (2002). Catalysis of catechol oxidation by metal-dithiocarbamate complexes in pesticides. *Free Radical Biology and Medicine*, *33*(12), 1714–1723. https://doi.org/10.1016/S0891-5849(02)01169-3.

Fogh, J., Wright, W. C., & Loveless, J. D. (1977). Absence of HeLa cell contamination in 169 cell lines derived from human tumors. *Journal of the National Cancer Institute*, *58*(2), 209–214. https://doi.org/10.1093/jnci/58.2.209.

Gagnon, M., Zihler Berner, A., Chervet, N., Chassard, C., & Lacroix, C. (2013). Comparison of the Caco-2, HT-29 and the mucus-secreting HT29-MTX intestinal cell models to investigate Salmonella adhesion and invasion. *Journal of Microbiological Methods*, *94*(3), 274–279. https://doi.org/10.1016/j.mimet.2013.06.027.

Goel, A., Boland, C. R., & Chauhan, D. P. (2001). Specific inhibition of cyclooxygenase-2 (COX-2) expression by dietary curcumin in HT-29 human colon cancer cells. *Cancer Letters*, *172*(2), 111–118. https://doi.org/10.1016/S0304-3835(01)00655-3.

Goldner, W. S., Sandler, D. P., Yu, F., Hoppin, J. A., Kamel, F., & Levan, T. D. (2010). Pesticide use and thyroid disease among women in the agricultural health study. *American Journal of Epidemiology*, *171*(4), 455–464. https://doi.org/10.1093/aje/kwp404.

Gottwald, E. M., Duss, M., Bugarski, M., Haenni, D., Schuh, C. D., Landau, E. M., & Hall, A. M. (2018). The targeted anti-oxidant MitoQ causes mitochondrial swelling and depolarization in kidney tissue. *Physiological Reports*, *6*(7). https://doi.org/10.14814/phy2.13667.

Gowers DS, Gordon CF (1980). Some public health aspects of the manufacture and use of zinc and manganese ethylenebisdithiocarbamate fungicides. *Instytut Ochrony Roślin - Państwowy Instytut Badawczy.* 491–522.

Guo, Y., Zhang, T., Jiang, B., Miao, M., & Mu, W. (2014). The effects of an antioxidative pentapeptide derived from chickpea protein hydrolysates on oxidative stress in Caco-2 and HT-29 cell lines. *Journal of Functional Foods*, *7*(1), 719–726. https://doi.org/10.1016/j.jff.2013.12.013.

Halliwell, B. (1966). Antioxidants in Human Health and Disease. *Annual Review of Nutrition*, 33–50.

Hoffman, L., & Hardej, D. (2012). Ethylene bisdithiocarbamate pesticides cause cytotoxicity in transformed and normal human colon cells. *Environmental Toxicology and Pharmacology*, *34*(2), 556–573. https://doi.org/10.1016/j.etap.2012.06.015.

Hoffman, L., Trombetta, L., & Hardej, D. (2016). Ethylene bisdithiocarbamate pesticides Maneb and Mancozeb cause metal overload in human colon cells. *Environmental Toxicology and Pharmacology*, *41*, 78–88. https://doi.org/10.1016/j.etap.2015.11.002.

Huet, G., Kim, I., de Bolos, C., Lo-Guidice, J. M., Moreau, O., Hemon, B., Richet, C., Delannoy, P., Real, F. X., & Degand, P. (1995). Characterization of mucins and proteoglycans synthesized by a mucin-secreting HT-29 cell subpopulation. *Journal of Cell Science*, *108*, 1275–1285.

Iorio, R., Castellucci, A., Rossi, G., Cinque, B., Cifone, M. G., Macchiarelli, G., & Cecconi, S. (2015). Mancozeb affects mitochondrial activity, redox status and ATP production in mouse granulosa cells. *Toxicology in Vitro*, *30*(1), 438–445. https://doi.org/10.1016/j.tiv.2015.09.018.

Janz, D. M. (2014). Dithiocarbamates. In *Encyclopedia of Toxicology: Third Edition* (pp. 212–214). Elsevier. https://doi.org/10.1016/B978-0-12-386454-3.00139-1.

Kalaiselvi, P., Rajashree, K., Bharathi Priya, L., & Padma, V. V. (2013). Cytoprotective effect of epigallocatechin-3-gallate against deoxynivalenol-induced toxicity through anti-oxidative and anti-inflammatory mechanisms in HT-29 cells. *Food and Chemical Toxicology*, *56*, 110–118. https://doi.org/10.1016/j.fct.2013.01.042.

Kaye, E., Nyombi, A., Mutambuze, I. L., & Muwesa, R. (2015). Mancozeb Residue on Tomatoes in Central Uganda. *Journal of Health and Pollution*, *5*(8), 1–6. https://doi.org/10.5696/i2156-9614-5-8.1.

Kim, W. K., Bang, M. H., Kim, E. S., Kang, N. E., Jung, K. C., Cho, H. J., & Park, J. H. Y. (2005). Quercetin decreases the expression of ErbB2 and ErbB3 proteins in HT-29 human colon cancer cells. *Journal of Nutritional Biochemistry*, *16*(3), 155–162. https://doi.org/10.1016/j.jnutbio.2004.10.010.

Kistinger, B. R., & Hardej, D. (2022). The ethylene bisdithiocarbamate fungicides mancozeb and nabam alter essential metal levels in liver and kidney and glutathione enzyme activity in liver of Sprague-Dawley rats. *Environmental Toxicology and Pharmacology*, *92*. https://doi.org/10.1016/j.etap.2022.103849.

Ksheerasagar, R. L., & Kaliwal, B. B. (2003). Temporal effects of mancozeb on testes, accessory reproductive organs and biochemical constituents in albino mice.

Environmental Toxicology and Pharmacology, *15*(1), 9–17. https://doi.org/10.1016/j.etap.2003.08.006.

Kühlbrandt, W. (2015). Structure and function of mitochondrial membrane protein complexes. In *BMC Biology* (Vol. 13, Issue 1). BioMed Central Ltd. https://doi.org/10.1186/s12915-015-0201-x.

Kumar, K., Sabarwal, A., & Singh, R. P. (2019). Mancozeb selectively induces mitochondrial-mediated apoptosis in human gastric carcinoma cells through ROS generation. *Mitochondrion*, *48*(2017), 1–10. https://doi.org/10.1016/j.mito.2018.06.003.

Kurttio, P., & Savolainen, K. (1990). Ethylenethiourea in air and in urine as an indicator of exposure to ethylenebisdithiocarbamate fungicides. *Scandinavian Journal of Work, Environment and Health*, *16*(3), 203–207. https://doi.org/10.5271/sjweh.1793.

Lambert, C. R., Black, H. S., & George Truscott, T. (1996). BUTYLATED HYDROXYTOLUENE. In *Radical Biology & Medicine* (Vol. 21, Issue 3).

Li, F., Jiao, X., Zhao, J., Liao, X., Wei, Y., & Li, Q. (2022). Antitumor mechanisms of an exopolysaccharide from Lactobacillus fermentum on HT-29 cells and HT-29 tumor-bearing mice. *International Journal of Biological Macromolecules*, *209*, 552–562. https://doi.org/10.1016/j.ijbiomac.2022.04.023.

López-Fernández, O., Rial-Otero, R., González-Barreiro, C., & Simal-Gándara, J. (2012). Surveillance of fungicidal dithiocarbamate residues in fruits and vegetables. *Food Chemistry*, *134*(1), 366–374. https://doi.org/10.1016/j.foodchem.2012.02.178.

Mahmoud, I. F., Kanthimathi, M. S., & Abdul Aziz, A. (2020). ROS/RNS-mediated apoptosis in HT-29 colorectal cancer cells by methanolic extract of Tamarindus indica seeds. *European Journal of Integrative Medicine*, *40*. https://doi.org/10.1016/j.eujim.2020.101244.

Maranghi, F., de Angelis, S., Tassinari, R., Chiarotti, F., Lorenzetti, S., Moracci, G., Marcoccia, D., Gilardi, E., di Virgilio, A., Eusepi, A., Mantovani, A., & Olivieri, A. (2013). Reproductive toxicity and thyroid effects in Sprague Dawley rats exposed to low doses of ethylenethiourea. *Food and Chemical Toxicology*, *59*, 261–271. https://doi.org/10.1016/j.fct.2013.05.048.

Maroni, M., Colosio, C., Ferioli, A., & Fait, A. (2000). Biological Monitoring of Pesticide Exposure: a review. Introduction. In *Toxicology* (Vol. 143, Issue 1). https://doi.org/10.1016/S0300-483X(99)00163-8.

Medjdoub, A., Merzouk, S. A., Merzouk, H., Chiali, F. Z., & Narce, M. (2011). Effects of Mancozeb and Metribuzin on in vitro proliferative responses and oxidative stress of human and rat spleen lymphocytes stimulated by mitogens. *Pesticide*

Biochemistry and Physiology, *101*(1), 27–33. https://doi.org/10.1016/j.pestbp.2011.06.002.

Meyer, J. N., Leung, M. C. K., Rooney, J. P., Sendoel, A., Hengartner, M. O., Kisby, G. E., & Bess, A. S. (2013). Mitochondria as a target of environmental toxicants. In *Toxicological Sciences* (Vol. 134, Issue 1, pp. 1–17). Oxford University Press. https://doi.org/10.1093/toxsci/kft102.

Morales-Ovalles, Y., Miranda-Contreras, L., Peña-Contreras, Z., Dávila-Vera, D., Balza-Quintero, A., Sánchez-Gil, B., & Mendoza-Briceño, R. V. (2018). Developmental exposure to mancozeb induced neurochemical and morphological alterations in adult male mouse hypothalamus. *Environmental Toxicology and Pharmacology*, *64*, 139–146. https://doi.org/10.1016/j.etap.2018.10.004.

Mosmann, T. (1983). Rapid colorimetric assay for cellular growth and survival: Application to proliferation and cytotoxicity assays. *Journal of Immunological Methods*, *65*(1–2), 55–63. https://doi.org/10.1016/0022-1759(83)90303-4.

Naman, M., Masoodi, F. A., Wani, S. M., & Ahad, T. (2022). CHANGES IN CONCENTRATION OF PESTICIDE RESIDUES IN FRUITS AND VEGETABLES DURING HOUSEHOLD PROCESSING. *Toxicology Reports*. https://doi.org/10.1016/j.toxrep.2022.06.013.

Navarro, A., & Boveris, A. (2007). The mitochondrial energy transduction system and the aging process. *American Journal of Physiology - Cell Physiology*, *292*(2), 670–686. https://doi.org/10.1152/ajpcell.00213.2006.

Nicolson, G. L. (2014). Mitochondrial dysfunction and chronic disease: Treatment with natural supplements. *Integrative Medicine (Boulder)*, *13*(4), 35–43.

Nordby, K.-C., Andersen, A., & Kristensen, P. (2005). Indicators of mancozeb exposure in relation to thyroid cancer and neural tube defects in farmers' families. In *Scandinavian Journal of Work* (Vol. 31, Issue 2).

Nzengue, Y., Candéias, S. M., Sauvaigo, S., Douki, T., Favier, A., Rachidi, W., & Guiraud, P. (2011). The toxicity redox mechanisms of cadmium alone or together with copper and zinc homeostasis alteration: Its redox biomarkers. *Journal of Trace Elements in Medicine and Biology*, *25*(3), 171–180. https://doi.org/10.1016/j.jtemb.2011.06.002.

O'Malley, Y., Fink, B. D., Ross, N. C., Prisinzano, T. E., & Sivitz, W. I. (2006). Reactive oxygen and targeted antioxidant administration in endothelial cell mitochondria. *Journal of Biological Chemistry*, *281*(52), 39766–39775. https://doi.org/10.1074/jbc.M608268200.

Pandey, S. P., & Mohanty, B. (2015). The neonicotinoid pesticide imidacloprid and the dithiocarbamate fungicide mancozeb disrupt the pituitary-thyroid axis of a wildlife

bird. *Chemosphere*, *122*, 227–234. https://doi.org/10.1016/j.chemosphere.2014.11.061.

Pelaseyed, T., Bergström, J. H., Gustafsson, J. K., Ermund, A., Birchenough, G. M. H., Schütte, A., van der Post, S., Svensson, F., Rodríguez-Piñeiro, A. M., Nyström, E. E. L., Wising, C., Johansson, M. E. V., & Hansson, G. C. (2014). The mucus and mucins of the goblet cells and enterocytes provide the first defense line of the gastrointestinal tract and interact with the immune system. In *Immunological Reviews* (Vol. 260, Issue 1, pp. 8–20). Blackwell Publishing Ltd. https://doi.org/10.1111/imr.12182.

Peña-Contreras, Z., Miranda-Contreras, L., Morales-Ovalles, Y., Colmenares-Sulbarán, M., Dávila-Vera, D., Balza-Quintero, A., Salmen, S., & Mendoza-Briceño, R. V. (2016). Atrazine and mancozeb induce excitotoxicity and cytotoxicity in primary cultures of mouse cerebellar cortex. *Toxicological and Environmental Chemistry*, *98*(8), 959–976. https://doi.org/10.1080/02772248.2016.1151020.

Perkins, G. A., & Frey, T. G. (2000). Recent structural insight into mitochondria gained by microscopy. *Micron*, *31*(1), 97–111. https://doi.org/10.1016/S0968-4328(99)00065-7.

Pieczenik, S. R., & Neustadt, J. (2007). Mitochondrial dysfunction and molecular pathways of disease. *Experimental and Molecular Pathology*, *83*(1), 84–92. https://doi.org/10.1016/j.yexmp.2006.09.008.

Pirozzi, A. V. A., Stellavato, A., la Gatta, A., Lamberti, M., & Schiraldi, C. (2016). Mancozeb, a fungicide routinely used in agriculture, worsens nonalcoholic fatty liver disease in the human HepG2 cell model. *Toxicology Letters*, *249*, 1–4. https://doi.org/10.1016/j.toxlet.2016.03.004.

Poon, I. K. H., Hulett, M. D., & Parish, C. R. (2010). Molecular mechanisms of late apoptotic/necrotic cell clearance. *Cell Death and Differentiation*, *17*(3), 381–397. https://doi.org/10.1038/cdd.2009.195.

Prabhakaran, K., Chapman, G. D., & Gunasekar, P. G. (2009). BNIP3 up-regulation and mitochondrial dysfunction in manganese-induced neurotoxicity. *NeuroToxicology*, *30*(3), 414–422. https://doi.org/10.1016/j.neuro.2009.02.012.

Roede, J., & Miller, G. (2014). Mancozeb. In *Encyclopedia of Toxicology* (Vol. 3). https://doi.org/10.1016/B978-0-12-386454-3.00157-3.

Saber, T. M., Abo-Elmaaty, A. M. A., & Abdel-Ghany, H. M. (2019). Curcumin mitigates mancozeb-induced hepatotoxicity and genotoxicity in rats. *Ecotoxicology and Environmental Safety*, *183*. https://doi.org/10.1016/j.ecoenv.2019.109467.

Saha, S., Chakrabarty, P. K., & Banerjee, K. (2022). Producing Crops without Mancozeb? Perspectives on Recent Regulatory Dilemmas and Ways Out. In *ACS*

Agricultural Science and Technology (Vol. 2, Issue 2, pp. 272–275). American Chemical Society. https://doi.org/10.1021/acsagscitech.2c00047.

Sakr, S. A. (2007). Ameliorative Effect of Ginger (Zingiber officinale) on Mancozeb Fungicide Induced Liver Injury in Albino Rats. *Australian Journal of Basic and Applied Sciences*, *1*(4), 650–656.

Santos, P. M., Simões, T., & Sá-Correia, I. (2009). Insights into yeast adaptive response to the agricultural fungicide mancozeb: A toxicoproteomics approach. *Proteomics*, *9*(3), 657–670. https://doi.org/10.1002/pmic.200800452.

Shoubridge, E. A. (2001). Nuclear genetic defects of oxidative phosphorylation. *Human Molecular Genetics*, *10*(20), 2277–2284. https://doi.org/10.1093/hmg/10.20.2277.

Srivastava, A. K., Ali, W., Singh, R., Bhui, K., Tyagi, S., Al-Khedhairy, A. A., Srivastava, P. K., Musarrat, J., & Shukla, Y. (2012). Mancozeb-induced genotoxicity and apoptosis in cultured human lymphocytes. *Life Sciences*, *90*(21–22), 815–824. https://doi.org/10.1016/j.lfs.2011.12.013.

Stephenson, O. J., & Trombetta, L. D. (2020). Comparative effects of Mancozeb and Disulfiram-induced striated muscle myopathies in Long-Evans rats. *Environmental Toxicology and Pharmacology*, *74*(November 2019), 103300. https://doi.org/10.1016/j.etap.2019.103300.

Strubbe-Rivera, J. O., Schrad, J. R., Pavlov, E. v., Conway, J. F., Parent, K. N., & Bazil, J. N. (2021). The mitochondrial permeability transition phenomenon elucidated by cryo-EM reveals the genuine impact of calcium overload on mitochondrial structure and function. *Scientific Reports*, *11*(1). https://doi.org/10.1038/s41598-020-80398-8.

Supruniuk, K., Czarnomysy, R., Muszyńska, A., & Radziejewska, I. (2022). Anti-cancer effects of pyrazole-platinum(II) complexes combined with anti-MUC1 monoclonal antibody versus monotherapy in DLD-1 and HT-29 colon cancer cells. *Translational Oncology*, *18*. https://doi.org/10.1016/j.tranon.2022.101348.

Todt, C. E., Bailey, D. C., Pressley, A. S., Orfield, S. E., Denney, R. D., Snapp, I. B., Negga, R., Bailey, A. C., Montgomery, K. M., Traynor, W. L., & Fitsanakis, V. A. (2016). Acute exposure to a Mn/Zn ethylene-bis-dithiocarbamate fungicide leads to mitochondrial dysfunction and increased reactive oxygen species production in Caenorhabditis elegans. *NeuroToxicology*, *57*, 112–120. https://doi.org/10.1016/j.neuro.2016.09.011.

Tsang, M., & Trombetta, L. (2007). The protective role of chelators and antioxidants on mancozeb-induced toxicity in rat hippocampal astrocytes. *Toxicology and Industrial Health*, *23*(8), 459–470. https://doi.org/10.1177/0748233708089039.

Turrens, J. F. (2003). Mitochondrial formation of reactive oxygen species. *Journal of Physiology*, *552*(2), 335–344. https://doi.org/10.1113/jphysiol.2003.049478

United States Geological Survey (2021). Estimated agricultural use for Mancozeb, 2018. (accessed: 1/26/23). https://water.usgs.gov/nawqa/pnsp/usage/maps/show_map.php?year=2014&map=MANCOZEB&hilo=L.

Vázquez, M., Calatayud, M., Vélez, D., & Devesa, V. (2013). Intestinal transport of methylmercury and inorganic mercury in various models of Caco-2 and HT29-MTX cells. *Toxicology*, *311*(3), 147–153. https://doi.org/10.1016/j.tox.2013.06.002.

Veeriah, S., Kautenburger, T., Habermann, N., Sauer, J., Dietrich, H., Will, F., & Pool-Zobel, B. L. (2006). Apple flavonoids inhibit growth of HT29 human colon cancer cells and modulate expression of genes involved in the biotransformation of xenobiotics. *Molecular Carcinogenesis*, *45*(3), 164–174. https://doi.org/10.1002/mc.20158.

Vij, P., & Hardej, D. (2012). Evaluation of tellurium toxicity in transformed and non-transformed human colon cells. *Environmental Toxicology and Pharmacology*, *34*(3), 768–782. https://doi.org/10.1016/j.etap.2012.09.009.

Vij, P., & Hardej, D. (2016). Alterations in antioxidant/oxidant gene expression and proteins following treatment of transformed and normal colon cells with tellurium compounds. *Environmental Toxicology and Pharmacology*, *43*, 216–224. https://doi.org/10.1016/j.etap.2016.03.009.

Wallace, K. B., & Starkov, A. A. (2000). Mitochondrial Targets of Drug Toxicity. *Annual Review of Pharmacology and Toxicology*. https://doi.org/10.1146/annurev.pharmtox.40.1.353.

Wikman-Larhed, A., & Artursson, P. (1995). Co-cultures of human intestinal goblet (HT29-H) and absorptive (Caco-2) cells for studies of drug and peptide absorption. *European Journal of Pharmaceutical Sciences*, *3*, 171–183.

Zhang, J., Fitsanakis, V. A., Gu, G., Jing, D., Ao, M., Amarnath, V., & Montine, T. J. (2003). Manganese ethylene-bis-dithiocarbamate and selective dopaminergic neurodegeneration in rat: A link through mitochondrial dysfunction. *Journal of Neurochemistry*, *84*(2), 336–346. https://doi.org/10.1046/j.1471-4159.2003.01525.x.

Vita

Name	Amanda Dhaneshwar
Baccalaureate Degree	*Bachelor of Science*, *St. John's University,* *New York* *Major: Toxicology*
Date Graduated	*May, 2015*
Other Degrees and Certificates	*Master of Science,* *St. John's University,* *New York* *Major: Toxicology*
Date Graduated	*May, 2017*